1968

Decomposition and hydrogenation studies of simple hydrocarbons on tungsten

Robert Ray Rye
Iowa State University

DECOMPOSITION AND HYDROGENATION STUDIES OF SIMPLE HYDROCARBONS ON TUNGSTEN

by

Robert Ray Rye

A Dissertation Submitted to the
Graduate Faculty in Partial Fulfillment of
The Requirements for the Degree of
DOCTOR OF PHILOSOPHY

Major Subject: Physical Chemistry

Approved:

Signature was redacted for privacy.

In Charge of Major Work

Signature was redacted for privacy.

Head of Major Department

Signature was redacted for privacy.

Dean of Graduate College

Iowa State University
Ames, Iowa

1968

TABLE OF CONTENTS

LIST OF FIGURES

LIST OF TABLES

I. INTRODUCTION

Due to the great commercial importance of catalytic surface reactions, there has been an enormous amount of research directed toward understanding these reactions. Unfortunately a great deal of this work has been concerned with kinetic studies on poorly defined surfaces. The preparation of the supported type of commercial catalysts used for most kinetic studies is "... subject to various subtle and often unknown influences that alter catalyst quality." (1) This is reflected in the large variation in the kinetic parameters tabulated by Bond (2).

Despite this extensive amount of research the hydrogenation reaction of the simplest olefin is still under debate. There have been many suggestions for the mechanism of this reaction with Rideal having suggested three (3). Basically the discussion can be separated into two types:

1) Langmuir-Hinschelwood mechanism: reaction occurs between chemisorbed hydrogen and chemisorbed ethylene.
2) Rideal-Eley mechanism: one reactant is in the chemisorbed layer and the second is in either the gas phase or a physically adsorbed layer.

Basically the problems involved in understanding the simplest catalytic reactions stem from a nearly complete lack of

knowledge concerning the surface species and surface reactions.

This investigation will be concerned with the application of ultra-high vacuum techniques and flash filament spectroscopy to the surface reactions of several simple hydrocarbons. Through the use of ultra-high vacuum and small wire samples which can be thermally cleaned one can start with essentially a metal-vacuum interface. The surface can then be dosed with a known hydrocarbon at a low temperature (95°K) where only adsorption occurs. After formation of the monolayer a flash filament spectrum can be obtained by fast controlled heating of the wire sample. The wire itself is used as a resistance thermometer and a small, rapid response mass spectrometer is used to determine the amount and composition of the products that appear in the gas phase. Thus one obtains a spectrum of partial pressure vs. temperature resulting from surface reactions. By reducing the pressure prior to flash and using short flash times, these reactions can be assigned to reactions occurring in the chemisorbed monolayer. Since the mass spectrometer is connected to the reaction cell by short, large diameter tubing, extremely fast pressure transients can be followed. In addition to the flash experiments the rapid scan capabilities allow one to study continuously reactions that occur during the formation of the first chemisorbed monolayer.

II. LITERATURE

A. Flash Filament Spectroscopy

Since a flash filament spectrometer is basically an ultra-high vacuum system containing a small metal filament, ultra-high vacuum techniques are of major importance in its use. Ultra-high vacuum is itself an active area of research with journals such as "Vacuum" and "Vacuum Science and Technology" devoted to the field. Redhead (4) has published an excellent review article covering the type of small glass system used in this work. The review by Ehrlich (5) is especially useful in that the vacuum requirements specifically for a flash filament spectrometer are discussed. In addition Ehrlich has included a listing of the various components needed for a working vacuum system along with the commercial sources. For those who like more detail a much more complete discussion of vacuum techniques in general can be found in the reference work by Dushman (6). This is undoubtedly the single most comprehensive source for vacuum technology.

The development of ultra-high vacuum and flash filament spectroscopy are intimately connected. Neither technique was possible until the ionization gauge was developed by Apker (7) in 1948. An ionization gauge is essentially an electronic tube with a filament, grid, and collector. An electron current is established between filament and grid which

ionizes gas molecules. The resulting positive ion current measured at the collector is proportional to the pressure. The relationship between the positive ion current (i^+), emission current (i^-) and pressure (P) is:

$$i^+ = i^- S_x P_x \qquad (1)$$

where S_x is the calibration factor or gauge sensitivity factor which is a function of both the gauge geometry and the gas phase composition. For this reason the sensitivity factor must be determined by calibration vs. a suitable standard such as McLeod gauge (8). This calibration is normally made by pumping the calibration system down to below the limit of the McLeod gauge and then leaking in gas of a known composition to a given final pressure. As a standard the gas normally used is nitrogen. However it is found experimentally that the ratio, r, of gauge sensitivities ($r = {}^{S}x/S_{N_2}$) is independent of the gauge geometry (6). As a result one only needs a known sensitivity factor for one gas. Tabulated values of r can then be used to convert the calibration for other gases.

This standard ionization gauge, however, is limited to pressures above 10^{-8} torr by an x-ray limit. The x-ray limit results from the production of soft x-rays from the impact of electrons on the grid. These x-rays strike the collector producing photolectrons which appear as a residual current (9). Apker in fact used the flash filament technique to get around this x-ray limit and estimate lower pressures (7). By rapidly flashing a filament of known geometrical area to a temperature

sufficient to desorb all adsorbed material, the number of adsorbed molecules can be found from the maximum pressure rise, P_m,

$$n = \frac{P_m V}{AkT} \tag{2}$$

where n is the number of molecules per cm^2, V is the volume of the system, T is the temperature of the gas after rapid equilibration with the walls and A is the surface area of the filament. If the filament is first cleaned and then allowed to adsorb gas from the ambient for a fixed period of time prior to flash, the amount of gas adsorbed during the known adsorption interval can be determined using Equation 2. From the Kinetic Theory of Gases the rate of adsorption of gases is given by

$$\frac{dn}{dt} = \frac{\alpha P}{\sqrt{2\pi mkT}} \tag{3}$$

where m is the mass of a gas molecule and α is the sticking probability or ratio of the number of molecules that adsorb to the number that arrive at the surface. For a constant pressure integration of this yields:

$$n = \frac{\alpha P t}{\sqrt{2\pi mkT}} \tag{4}$$

Thus if one adsorbs for a known period of time, t, and then flashes the filament, Equations 2 and 4 can be used to estimate the pressure, P, during the adsorption interval.

The situation however was reversed with the development by Bayard and Alpert (10) of the inverted ionization gauge. By changing the collector from a cylindrical cathode surrounding the grid to a fine wire collector in the center of a

cylindrical grid the area of the collector was reduced by orders of magnitude. Since the photoelectron current is also proportional to the area of the collector, this reduced the x-ray limit below 10^{-10} torr. Since it was now possible to know the pressure during the adsorption period interest centered around the sticking coefficient (11). And on the clean surfaces, which can be produced at these low pressures, the sticking probability of most gases is found to be generally quite high (~0.5) and to decrease with increasing coverage (11, 12, 13, 14).

However the emphasis soon shifted to the desorption process and to a study of surface states. In 1955 Ehrlich reported the detection of two peaks, α and β, in the desorption burst of nitrogen on tungsten (15). Since the filament temperature increases with time it was recognized that these peaks resulted from two binding states of nitrogen on tungsten which desorb over different temperature intervals with the α form desorbing over the lower temperature interval. Figure 1 shows a nitrogen desorption spectrum with peaks due to the α and β states. This initial report was soon followed by a more extensive report which in addition reported a third state, γ, formed only below 200°K (16). In 1958 Hickmott and Ehrlich published an extensive paper which essentially established flash filament spectroscopy in its present form (17). Since then the flash filament technique has been used extensively

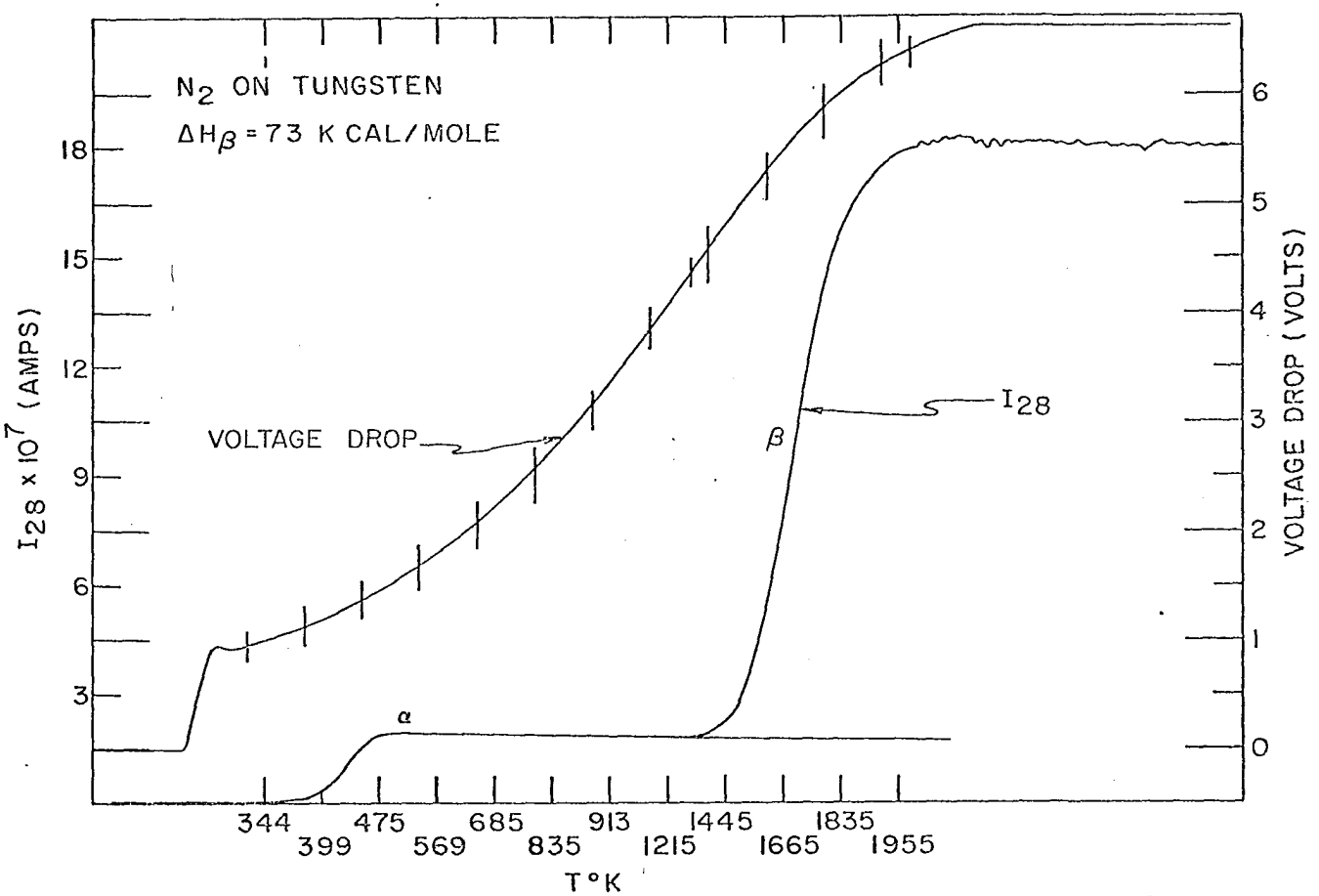

Figure 1. Flash desorption of nitrogen from tungsten dosed at 300°K

to study the different adsorption states and the kinetics of the desorption step. Hickmott and Ehrlich (17) derived a method of analyzing the desorption traces for the kinetic parameters. The basic assumption is that the desorption is governed by:

$$\frac{dn}{dt} = \upsilon_x n^x \exp\left[-\frac{\Delta H}{RT}\right]. \tag{5}$$

where n is the number of molecules per cm^2 of surface, x is the kinetic order, υ_x the frequency factor and ΔH is the activation energy of desorption. In order to integrate Equation 4 a heating rate of the form

$$\frac{1}{T} = a + bt \tag{6}$$

is used. The use of constant current to heat the filament will yield a heating rate of approximately this form. In addition to this with constant current heating the voltage drop can be used to calculate the resistance and thus the temperature as a function of time. Then using Equation 6, Equation 5 can be integrated to yield

$$\ln \frac{n_o}{n} = \frac{\upsilon_1 R}{(-\Delta Hb)} \varepsilon \exp\left[-\frac{\Delta H}{kT}\right], \quad x = 1 \tag{7a}$$

$$\frac{n_o - n}{n_o n} = \frac{\upsilon_2 R}{(-\Delta Hb)} \varepsilon \exp\left[-\frac{\Delta H}{kT}\right], \quad x = 2 \tag{7b}$$

where ε is a correction factor which can usually be approximated by 1. Thus if one plots $\ln \ln n_o/n$ and $\ln(n_o/n)\ n_o n$ vs. $1/T$

a straight line will be obtained for the correct order. From the slope one obtains the activation energy and from the intercept the frequency factor.

However the experimental data, obtained in the form of a pressure time trace, reflects the desorption from the filament as well as the sum of all leaks and pumps in the system and must be corrected for the latter effects. The mass balance in the cell is given by

$$\frac{dP}{dt} = L - \frac{S}{V}P + \left(-\frac{AkT}{V}\right)\frac{dn}{dt} \tag{8}$$

where P is the pressure, L is the sum of all leaks other than desorption from the filament, $\frac{S}{V}$ is the sum of all pumping, V is the volume of the system, A is the surface area of the filament and T is the temperature of the gas molecules after rapid equilibration with the walls. However if the filament is saturated just prior to flash and a steady state established where the total pumping in the system is balanced by the total leak into the system

$$\frac{dn}{dt} = \frac{dp}{dt} = 0 \tag{9}$$

and therefore

$$L = \frac{S}{V} P_o \tag{10}$$

where P_o is the ambient pressure just prior to flash. Equation 8 then becomes

$$-\frac{AkT}{V}\frac{dn}{dt} = \frac{d\Delta P}{dt} + \frac{S}{V}\Delta P \tag{11}$$

where ΔP is $P_{(t)} - P_o$ or the change in pressure during a flash. Equation 11 can be integrated to give

$$\frac{AkT}{v}(n_o - n) = \Delta P + \int_o^t \frac{s}{v} \Delta P \, dt \qquad (12)$$

where n_o is the total amount of adsorbed material just prior to flash. The experimental curve of pressure vs. time can then be numerically integrated following Equation 12 to correct for the amount of material lost through pumping. The pumping term, $\frac{s}{v}$, can be determined from the back side of the desorption peak. In low pumped systems where the correction in Equation 12 is not great, one has at the pressure maximum $\frac{dn}{dt} = 0$ since the surface coverage is zero. Equation 11 then becomes

$$\frac{d\Delta P}{dt} + \frac{s}{v} \Delta P = 0 \qquad (13)$$

which integrates directly to become

$$\ln \frac{\Delta P}{\Delta P_{max}} = - \frac{s}{v} t \qquad (14)$$

where ΔP_{max} is the maximum change in pressure. A log plot of $\Delta P/\Delta P_{max}$ vs. time for the backside of the peak will then yield a straight line with slope of $-\frac{s}{v}$.

Mimeault has extended the derivation of Equations 6 and 7 with no assumptions as to the form of the heating rate (18), and Mimeault and Hansen (19) have devised a numerical analysis for the case when the activation energy is a function of coverage of the form

$$\Delta H = \Delta H_o - \alpha n \tag{15}$$

where ΔH_o is the activation energy for desorption at low coverage, n is the surface coverage and α is a constant.

In using the method of analysis outlined above one must have a low pumping speed so that the pumping correction, Equation 12, is not too extensive. If this correction is too extensive erroneous results will be obtained (19). Redhead has derived a method of analysis based on very high pumping (20). Under these conditions Equation 11 implies

$$-\frac{dn}{dt} \propto \Delta P \ . \tag{16}$$

The peak maximum in the pressure spectrum will then occur when

$$\frac{d^2n}{dt^2} = \frac{d\Delta P}{dt} = 0 \ . \tag{17}$$

Redhead then differentiates Equation 5 using Equation 6 to obtain

$$\frac{\Delta H}{R} = \frac{\upsilon_1}{(-b)} \exp\left[-\frac{\Delta H}{RT_p}\right], \ x = 1 \tag{18}$$

$$\frac{\Delta H}{R} = \frac{\upsilon_2}{(-b)} \exp\left[-\frac{\Delta H}{RT_p}\right], \ x = 2 \tag{19}$$

However due to the assumptions both theoretical and experimental needed in this method of analysis, the use of this method is not as straightforward as the method devised by Hickmott and Ehrlich.

Since the nitrogen-tungsten system is a relatively simple system to study, it has been extensively studied. For this reason it is an excellent system to use for calibration purposes. The curve in Figure 1 was obtained within 20 minutes after admitting nitrogen for the first time and analyzed to yield an activation energy of 73 kcal/mole for the β peak in excellent agreement with literature values (5, 18). The β state however in highly pumped systems is found to consist of two poorly resolved peaks (21, 22, 23). Delchar and Ehrlich studied the adsorption of nitrogen on single crystal planes of tungsten (21). At 300°K the (100) and (111) planes were found to be the source of the β states while the α state was found on only the (111) plane. The (110) plane was found to be completely inactive for nitrogen adsorption.

Of the gases studied by means of the flash filament technique, hydrogen is of most interest to this investigation. Hickmott reported a sticking coefficient of 0.1 for adsorption at 77°K, and the existence of 2 binding states, α and β (24). At low coverages the β state has an activation energy of desorption of 31 kcal/mole which decreases with increasing coverage. The α state desorbs between 77°K and 194°K and fills at lowest coverage. Hickmott reports that between 273°K and 373°K, the equilibrium amount adsorbed in the β state follows a Temkin isotherm. The Temkin isotherm is

derived with the assumption of a linear decrease in heat of adsorption with coverage, Equation 15. Mimeault and Hansen were able to determine both ΔH_o and α (19). Values for ΔH_o and α of 35 kcal/mole and 28 kcal/mole/(10^{15} molecules/cm^2) were reported.

Rigby has studied the replacement of hydrogen by CO, N_2 and carbon (25). Rigby reports that adsorption of hydrogen at room temperature gives two distinct β peaks, β_1 and β_2, with the β_2 being the higher temperature form. The β_1 state is reported to be two poorly resolved peaks which Rigby considers a "split β_1 peak". The β_2 state fills at low coverages with the β_1 state filling only when the total coverage exceeds 1/30 of the amount of hydrogen required to saturate the surface at room temperature. Since nitrogen is adsorbed on only half the tungsten surface, the remainder of the surface is available for hydrogen adsorption. Mixed adsorption of both nitrogen and carbon monoxide with hydrogen led to preferential displacement of the β_2 or high temperature forms of hydrogen. However, carbonizing the filament by heating in 10^{-6} torr of propane for 5 minutes at 1900°K prior to hydrogen adsorption leads to preferential replacement of the β_1 or low temperature form of hydrogen.

The β states of hydrogen are found to exchange isotopically and have second order desorption kinetics while the α state does not isotopically exchange (19). The β states result

from either molecular adsorption or adsorption of atomic hydrogen on paired sites.

B. Hydrocarbons

There have been numerous review articles covering the catalytic reactions of hydrocarbons over the transition metals. There are several publications such as "Catalysis" and "Advances in Catalysis" devoted to reviews of the area. By far the most work has been devoted to understanding the hydrogenation of ethylene. Unfortunately most of this work has been conducted over nickel catalysis of various forms. Taylor has written an extensive review covering the use of hydrogen isotopes (26). Bond has reviewed the general area of catalysis by metals (2). Bond has since extended his review of the hydrogenation reaction through 1965 (27). Brennan has reviewed the same area in much less depth but from a different view point (28). Brennan has concentrated solely on the advances made in understanding the fundamental surface processes and ignored studies of a merely phenomenological character. Thus the two reviewers, Bond and Brennan, complement each other very nicely.

Otto Beeck summarized in 1950 the result of several years work on the hydrogenation of ethylene on evaporated metal films of Rh, Fe, Pt, Pd, Cr, Ta and W at 0°C (29). Rhodium was found to have the greatest activity with a specific rate 10^4 times that on tungsten. When the specific rate constant

is plotted vs. the crystal parameter of the metal, a smooth curve is obtained with a peak maximum at Rh with 3.75Å. When ethylene is preadsorbed on metal films, the surface is partially poisoned for hydrogenation. The rates after preadsorption of ethylene as percentages of the rates on the bare metal were Ta, 10%; W, 20%; Ni, 40%; Pt or Rh, 95%. The activation energy for hydrogenation over Rh and Ni was found to be 10.7 kcal/mole, while in the case of W the activation energy was 2.4 kcal/mole. However the information that can be gained from the activation energy without knowledge of the surface species is questionable. One has only to consider the wide range of activation energies tabulated for the reaction over nickel (2). When an equimolar gas mixture was used the initial rate was found to be 10 times faster than the final rate which was used for comparison with other metals. The initial rate was measured 20 to 30 seconds after admitting the gas mixture. When ethylene is admitted to a nickel film predosed with hydrogen the rate is immeasurably fast. However, from the results obtained by Roberts on ultra-high vacuum evaporated iridium films at 100°C, it would appear that the self hydrogenation reaction is also immeasurably fast (30). At -79°C on nickel self hydrogenation does not occur, but the hydrogenation reaction is still immeasurably fast if hydrogen is preadsorbed. The heat of adsorption of ethylene on evaporated films drops drastically with coverage ,

the value for tungsten being over 100 kcal/mole at zero coverage and dropping to ~20 kcal/mole at higher coverage. On those metals which hydrogenate both acetylene and ethylene, hydrogenation of a mixture of ethylene and acetylene leads to selective hydrogenation of acetylene.

Trapnell has followed the adsorption of ethylene on tungsten films at 0°C (31). The adsorption was complicated by the self hydrogenation of ethylene. The total adsorption at the end of the self hydrogenation reaction is reported by Trapnell to be 0.55 molecules per tungsten atom with the final surface coverage being entirely acetylenic complexes.

Kemball has studied the deuterium distribution obtained from the reaction of deuterium and ethylene on evaporated films of tungsten, nickel, rhodium and iron at -100°C (32). This low temperature was used in order to lower the rate of reaction so that the initial distribution of deuterated products could be obtained. Initial pressures of 2.7 torr of ethylene and 8.1 torr of deuterium were admitted to a reaction vessel with a volume of 180 ml. The first experimental points, however, were not taken until after approximately 7 to 13 minutes. The lowering of the temperature would also have the effect of increasing deuteration with respect to exchange. Only slight amounts of hydrogen were returned to the gas phase as evidenced by the small amounts of HD in the gas phase. A very striking difference is found

between the reactions over tungsten vs. rhodium, nickel and iron. The ratios of rate of olefin exchange to the rate of deuteration for the four metals are Fe, 2.34; Ni, 2.28; Rh, 1.02; W, 0.08. Both the rate of deuteration and exchange are the greatest over rhodium. The reaction over tungsten is almost exclusively the deuteration reaction with a maximum of only 2% d_1-ethylene found in the gas phase. Kemball reports the results as a percentage of the total amount of C_2 species in the gas phase. A major difference is also found in the distribution of deuterated ethanes. The distribution over tungsten is sharply peaked around d_2-ethane. In the case of iron, nickel and iridium much more extensive deuterium content is found in the ethane. By converting the observed deuteration rates to specific rates, Kemball was able to compare his deuteration rates at -100°C with Beeck's hydrogenation rates at 0°C (29). The ratios of the specific rates to the specific rate of rhodium are given in Table 1. Reduction of the temperature to -100°C has decreased the spread in rates by over two orders of magnitude. In addition tungsten has increased in activity relative to iron. Thus as the temperature is decreased tungsten is relatively a much better catalyst.

Since tungsten has been found to be so inactive for hydrogenation reactions, very little work has been conducted with this metal. There has been essentially no work with

Table 1. Logarithms of specific rates relative to Rh

	Rh	Ni	Fe	W
Deuteration at -100°C (32)	0.0	-0.96	-1.4	-1.3
Hydrogenation at 0°C (29)	0.0	-2.7	-3.0	-4.0

tungsten for the reaction of acetylene since Beeck (29) reported tungsten to be inactive at 23°C. Due to the lack of information it would be informative to consider a small portion of the literature covering the hydrogenation of ethylene over other metals.

Bond has a series of three papers treating the deuteration of ethylene on alumina supported Pt, Ir, Ru, Os, Pd and Rh (33, 34, 35). The catalyst was prepared by hydrogen reduction at 400°C. After admission of the reactants the reaction was allowed to go to ~5% completion where the distribution of deuterated species were reported. Numerous large tables of distribution products are reported at a variety of conditions of temperature and ethylene-hydrogen pressure ratios. Since no common conditions were used, a comparison of the results is extremely hard.

Some general observations, however, can be made of those results where hydrogen and ethylene pressures are equal. These are given in Table 2. Generally ethylene exchange becomes more pronounced as the temperature increases as shown by the

Table 2. Deuterium distributions (30, 31, 32)

Metal		Pt(25°C)	Ir(9°C)	Ru(32°C)	Os(24°C)	Pd(37°C)	Rh(-18°C)	Rh(65°C)
ethane	d_0	19.2	3.5	2.2	0	24.5	7.9	4.7
	d_1	27.2	32.0	10.4	14.3	16.1	19.7	9.2
	d_2	23.2	39.6	41.6	52.0	5.6	26.5	17.8
	d_3	10.5	12.0	2.1	8.1	1.3	8.1	1.1
	d_4	6.4	7.5	0.0	3.5	0.3	4.4	0.1
	d_5	3.1	1.7		0.7	0.1	1.8	0
	d_6	0.5	0.2		0.7	0	0.2	0
ethylene	d_1	7.4	2.9	42.8	18.2	41.5	26.2	58.7
	d_2	2.7	0.4	0.9	2.4	8.9	4.2	6.8
	d_3	0.8	0.2	0	0	1.6	0.8	1.2
	d_4	0	0		0	0.1	0.2	0.3

last two columns in Table 2. The large value of d_0 in the case of palladium and platinum may be due to incomplete removal of the hydrogen used for reduction. The general feature of the distributions is the peak in deuterated ethanes around d_2-ethane which is very pronounced in the case of osmium and ruthenium. The deuterium distribution depends on both the temperature and the relative pressures of deuterium and ethylene. If the deuterium pressure is increased relative to the ethylene pressure, deuteration is favored over ethylene exchange and the deuterium content of the ethane is increased. The amount of hydrogen exchange, however, is small with only small amounts of HD being returned to the gas phase. Increasing the temperature gives an increase in ethylene exchange over deuteration.

The greatest amount of work has been done on nickel catalysts in various forms. The work on the rest of the transition metals has at most been fragmentary. Thus there may be more hope in obtaining a coherent picture of the hydrogenation reaction on nickel. The rate falls off with time, however, the initial rate is generally accepted to be first order in hydrogen and zero order in ethylene. On nickel, as on most active transition metals, the activation energy ranges from 3.2 to 11.6 kcal/mole. Bond has compiled several tables of orders and activation energies (2). The hydrogenation rate is found to increase with temperature as

would be expected from a constant activation energy. Above a maximum temperature, Tm, the rate decreases with temperature. Sato and Miyahara have studied the pressure dependence of Tm on nickel and found an ethylene pressure dependence (36). The temperature maximum increases with ethylene pressure but not with hydrogen pressure. This, in conjunction with the increase of ethylene exchange with temperature, would suggest that olefin desorption is occurring at elevated temperatures. However the pressure dependence of Tm is used by Sato and Miyahara to support a shift in the rate limiting step from the adsorption of hydrogen to the hydrogenation of an ethyl radical at the maximum temperature.

That dissociation occurs on adsorption at 20°C is shown by the occurrence of a self-hydrogenation reaction (37). Adsorption of ethylene occurs in three phases. In the first phase instantaneous adsorption occurs which, by comparison to hydrogen adsorption at -183°C, requires 8 hydrogen sites. Jenkins and Rideal take this to imply that a considerable fraction of the surface is bare (37). Additional ethylene is adsorbed very rapidly with the production of ethane in the gas phase. At the end of the second phase the amount of ethane obtained is approximately equal to the amount of ethylene adsorbed. Admission of hydrogen at the end of phase 2 results in instantaneous adsorption of hydrogen followed by a slow hydrogenation of the residue which Jenkins

and Rideal believe to be acetylenic species bonded to two surface sites. This is in agreement with the findings of Beeck (29). Also in agreement is the fact that admission of hydrogen prior to admission of ethylene results in instantaneous hydrogenation which occurs at an immeasurably fast rate. This Jenkins and Rideal, following Beeck, take to occur through the reaction of gas phase ethylene with surface hydrogen. Jenkins and Rideal, from comparison of ethylene adsorption to low temperature hydrogen adsorption, report that in the presence of an ethylene-hydrogen mixture the surface is covered by 83.4% acetylenic species, 8.3% hydrogen as pairs, and 8.3% unoccupied sites. Heating to 170°C decomposes the surface species giving only hydrogen in the gas phase. Hydrogen, but no ethylene, could be adsorbed on the carbided surface.

Using equimolar mixtures of hydrogen and ethylene, the initial hydrogenation on Ni films was found to start with a high rate (38). With continued removal of the gas phase and admission of fresh gas samples, the rate soon reached a steady state value which was approximately the rate obtained after pretreatment of the surface with ethylene. Below the temperature maximum of 165°C the initial rate observed was

$$\frac{dP(C_2H_6)}{dt} = AP_{H_2}P^{o}_{C_2H_4} \qquad (17)$$

and at 165°C the initial rate was of the form

$$\text{Rate} = AP_{H_2} P_{C_2H_4}/(1+BP_{C_2H_4}) \qquad (20)$$

The films on which the above rate expressions and maximum temperature were obtained were first carbided by heating in ethylene for 30 minutes at 190°C. These surfaces were then found to be reproducible.

Eischens and Pliskin state that adsorption can be associative or dissociative depending on the experimental conditions (39). The variables are temperature, hydrogen pressure and the extent of hydrogen predose. Ethylene adsorbed on hydrogen covered nickel gives absorption bands characteristic of the saturated C-H stretch and weak bands due to olefinic C-H stretch. The authors, however, also report a weak H-C-H scissor vibration. Ethylene adsorption on hydrogen covered nickel at 150°C or on nickel at 35°C without a predose of hydrogen leads to a decrease in the C-H stretching band intensity. Since the addition of hydrogen brings these bonds back to the associative form, adsorption on the "clean" surface has been dissociative. Addition of hydrogen to the associative form gives absorption bands characteristic of the structure $\dot{C}H_2$-CH_3. Adsorption of acetylene, according to Eischens and Pliskin, leads to absorption bands ascribed to the ethyl radical given above. This indicates to the authors that self hydrogenation of acetylene on nickel results in the ethyl radical.

Little, et al., have studied the adsorption of acetylene and ethylene on Pd and Cu (40). Acetylene on Pd gave only olefinic C-H absorption bands which are converted to saturated species by addition of hydrogen. Adsorption of ethylene on Pd gave a mixture of both saturated and olefinic C-H stretching frequencies which is converted to the saturated species by hydrogen. Since the spectrum of the adsorbed species is identical to the spectrum of $C_{100}H_{202}$, the authors conclude that the saturated species is $H_2C_{*}-C_{*}H_2$. Little, et al. conclude that the adsorbed olefinic species could be species such as

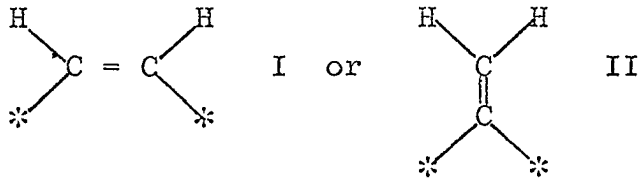

with I predominating.

The situation however is not this simple. Little has reviewed the infrared evidence for the adsorbed hydrocarbon species (41). This review consists predominantly of the work of Eischens on supported nickel and the work of Little, et al., on supported palladium. Even with this limited source, Little has compiled a table of the possible surface species which covers four pages. However, it does seem that a shift of the surface species occurs between dissociative olefinic species and saturated species.

There have been two studies of the reactions of the simple hydrocarbons in the field emission microscope. Arthur and Hansen report that the hydrocarbons are immobile on iridium below 700°K (42). Ethane partially desorbs at 100°K but a residue from adsorbed ethane does not desorb below 1000°K. From the field emission work function vs. temperature plots a two step decomposition of ethylene was inferred. A later flash filament study of the ethylene-iridium system confirmed this two step decomposition when two hydrogen peaks were obtained in the decomposition spectra (43). However two peaks were also found for acetylene on iridium. A portion of the low temperature hydrogen peak in the case of both ethylene and acetylene may be due to the use of a hot filament ionization gauge which produces hydrogen in the presence of hydrocarbons. Gardner reports that ethylene and acetylene are also immobile on tungsten and that adsorption is associative below 200°K (44). A two step decomposition of the adsorbed ethylene was inferred from the work function changes with ethylene decomposition starting at 200°K and acetylene decomposition starting at ~300°K.[1]

From radiochemical studies of ethylene adsorption Cormack, et al., have shown that regardless of the pretreatment of a catalyst a considerable portion of the adsorbed hydrocarbon species cannot be removed (45). The authors report that the following percentages of initial surface

[1]The statement, that decomposition starts at 200°K, is meant to imply that below 200°K the rate of the decomposition reaction is not appreciable.

radioactivity from adsorption of ethylene-C^{14} are not removed by hydrogenation at 20°C.

Pd (63.5); Ni (24); Rh (22.5); Ir (16); Pt (6.5)

The value for Ni is in fair agreement with the value of 20% reported by Beeck (29). However Beeck reports that on Rh 60% of the adsorbate can be removed in one minute and that 100% can be removed with long contact times.

Although the variation in crystal planes exposed to the gas phase has been suspected as a source of variation in activity, very little work has been done in this area. Beeck reported that nickel films with preferential (110) orientation are 5 times as active as unoriented films (29). Cunningham and Gwathmey report that on nickel single crystals the rates of hydrogenation show the following sequence (46).

$$(321) > (111) > (110) > (100)$$

Although the (321) plane gives the fastest rate, the self poisoning over this plane is also the most rapid.

III. EXPERIMENTAL

A. Experimental System and Components

A schematic diagram of the system is shown in Figure 2 and Figure 3 is a photograph showing the physical arrangement of the components. The rack for the vacuum system is a rectangular frame built of 1/8 inch angle iron with a single sheet of 1 inch Marinite (asbestos compost sheet) forming the top. The pumping system and gas supplies are mounted inside the frame and below the table top. Those components inside the dotted line in Figure 2 which form the working portion of the vacuum system are mounted on this Marinite sheet. In vacuum processing these components are surrounded by an oven with the Marinite top forming the base of the oven.

Since the system is designed for the study of the surface reactions of gases on metals, the vacuum system is constructed of borosilicate glass (Corning 7740) with the use of metal held to a minimum. The glass portions of the vacuum system are indicated by thick lines in Figure 2. The thin lines are used to represent electrical connections and external electronic components.

The experimental cell, shown in Figure 4, is a half liter round bottom flask containing four side arms leading to the mass spectrometer, ionization gauge, pumps, and gas supply.

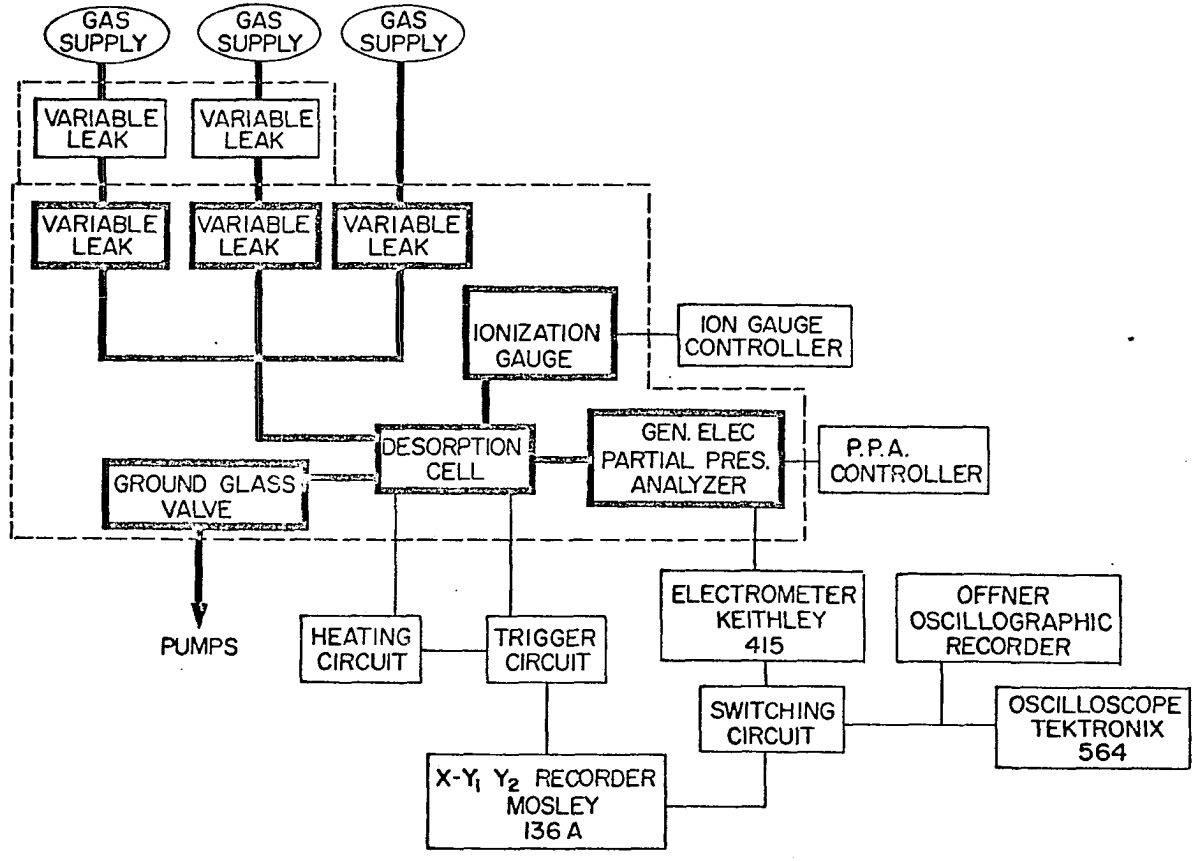

Figure 2. Schematic diagram of vacuum system with the associated electronics. The heavy lines indicate the vacuum system and the light lines indicate electrical connections. The dotted lines enclose those portions of the vacuum system which are baked

Figure 3. Flash filament spectrometer and associated electronics

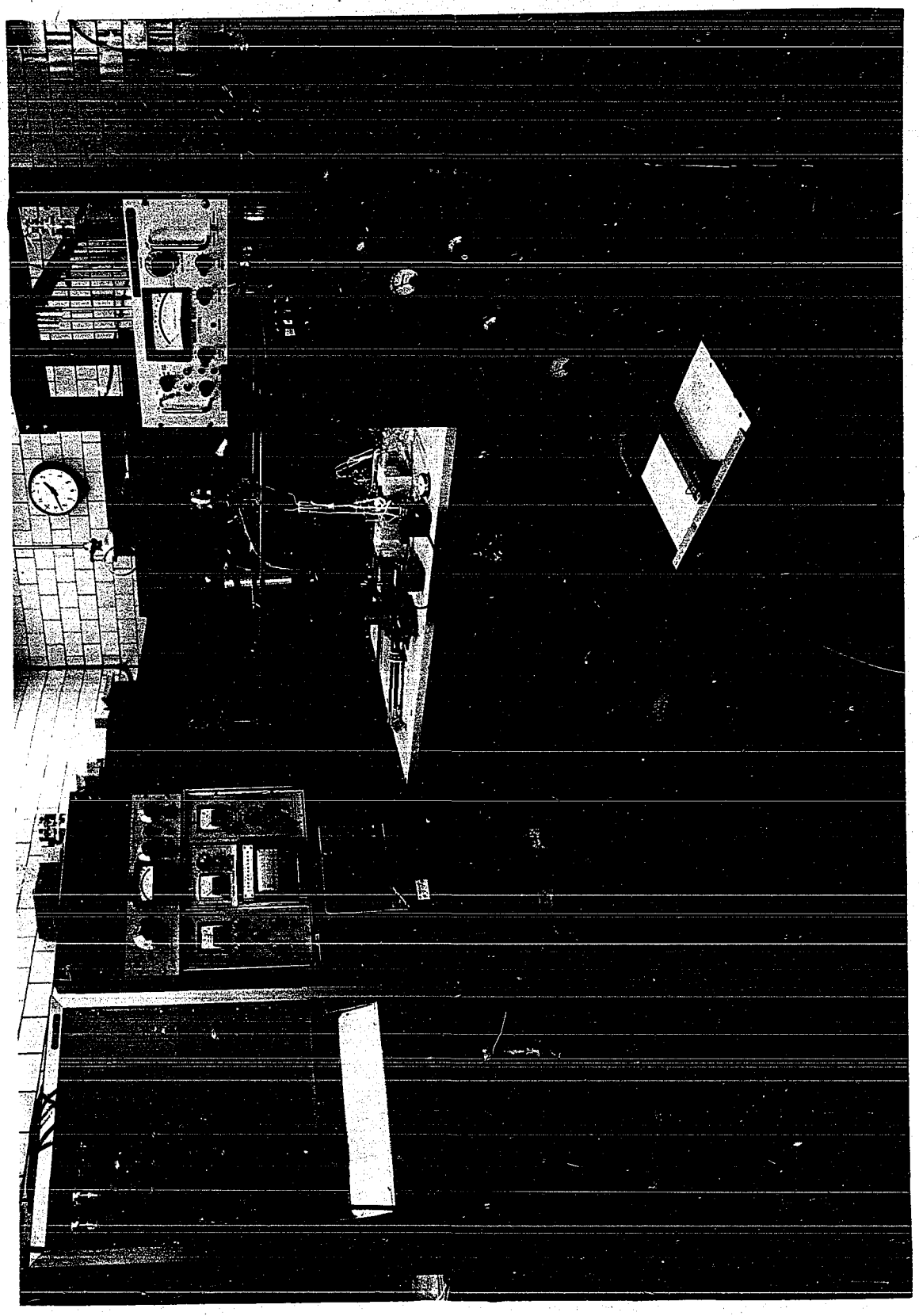

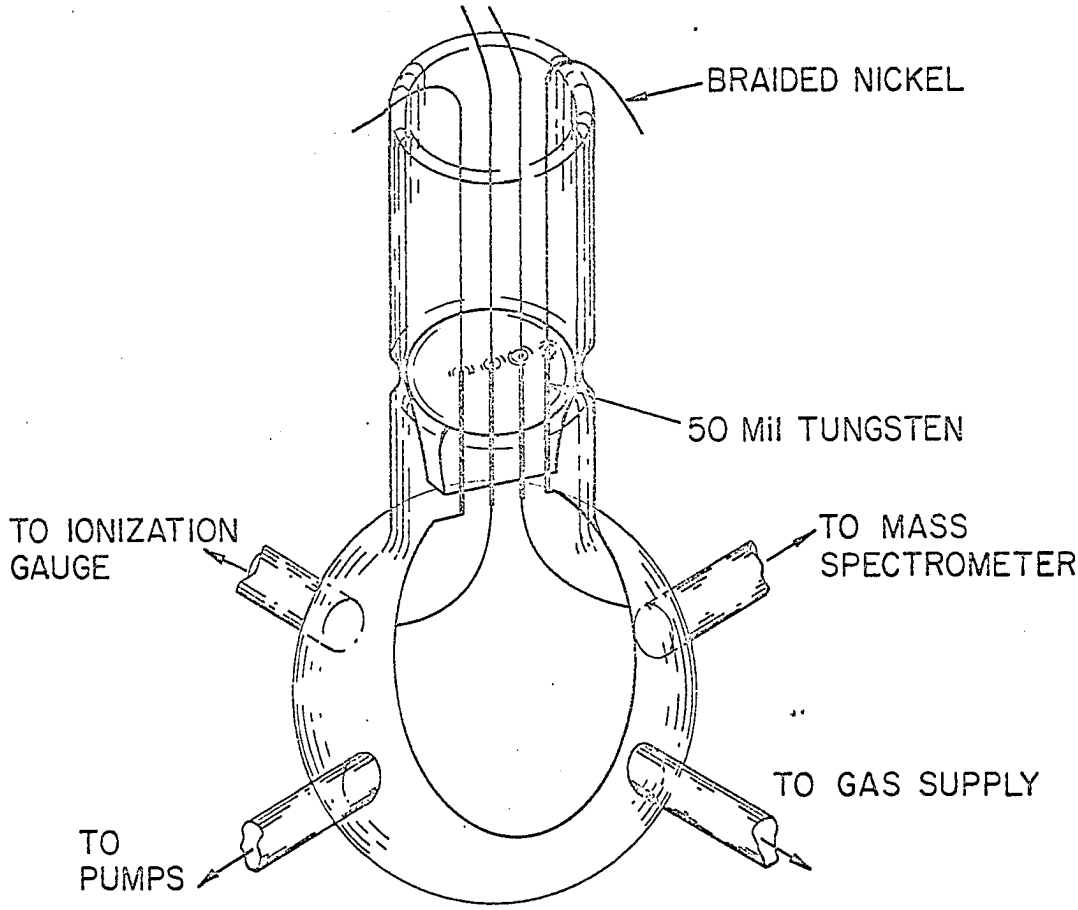

Figure 4. Sketch showing the construction of the experimental cell

With the exception of the side arm leading to the gas supply, the use of large diameter, short tubing is necessary. In a vacuum system the flow rate, Q, in torr L/sec through a constriction is given by

$$Q = F \Delta P \tag{20}$$

where F is the conductance of the constriction and ΔP is the pressure differential across the constriction (6). For a long cylindrical tube the conductance F is given approximately by (6)

$$F = 100 \frac{a^3}{l} \text{ L sec}^{-1} \tag{21}$$

where a is the radius in cm and l is the length in cm. Thus for maximum conductance the use of long thin tubing should be avoided if the measurement of a true pressure transient in the cell is to be obtained at the mass spectrometer (18). This can be illustrated by a model in which a leak (L) is turned on in the cell at time zero (i.e., the leak valve to the gas supply is opened). The mass balance in the cell would be given by

$$V_1 \frac{dP_1}{dt} = L - S_1 P_1 - F(P_1 - P_2) \tag{22}$$

where P_1 is the pressure in the cell, P_2 is the pressure in the mass spectrometer and S_1 is the pumping speed of pumps in the cell. If we neglect the slight pumping action of the mass spectrometer, the equivalent expression for the mass

spectrometer (V_2, P_2 ...) is given by

$$V_2 \frac{dP_2}{dt} = F(P_1 - P_2). \tag{23}$$

Equations 22 and 23 can be solved using Laplace transforms with the boundary condition that $P_{(t=0)} = 0$. If we assume that $V_1 = V_2 = V$ the solution is

$$P_2 = P_1 - \frac{L}{vy} e^{-dt} \sinh yt \tag{24}$$

where d and y are defined by

$$d = \frac{1}{2V} (2F + S_1) \tag{25}$$

$$y = \frac{1}{V} [F^2 + \frac{1}{4} S_1^2]^{1/2} \quad . \tag{26}$$

This is a good example of the balance between leaks and pumping. For small leaks (L) into the system the second term will be negligible for either large conductances or large pumping speeds. However, for those cases where the leak is large the second term will be appreciable unless the conductance or pumping speed is quite high. Since in quantitative experiments the loss of desorbed gas must be kept to a minimum, the conductance is the factor which is made large.

The conductance between the pumps and cell, however, must also be considered. In flash filament spectra consisting of poorly resolved multiple peaks, resolution is enhanced if high pumping is used. However, if the pumping speed of the pumps exceeds the conductance, the latter factor is limiting.

Thus since the pumping speed is needed for resolution of peaks and for reattaining a vacuum rapidly between experiments, the conductance between the cell and pumps is made large and a ground glass valve is included. The ground glass valve is then used to decrease the effective pumping by decreasing the conductance.

Sealed into the top of the experimental cell is a small dewar which is evacuated separately from the rest of the system. Sealed through the bottom of this dewar are four 50 mil tungsten electrodes. The sample filament (20 cm of 5 mil W) is spot welded to two of these. Two short segments of 2 mil tungsten are used to tap off the center ~12 cm of the sample filament for use in measuring the resistance of the center segment of the filament. The filament can be cooled by conduction by using coolants in the open portion of the dewar. The coolants used were water (≈300°K) and liquid nitrogen which gives a base temperature of ≈95°K. The dewar is evacuated separately in order to reduce the amount of cold surface seen by the vacuum system and to eliminate changes in the cold area as the liquid nitrogen level in the dewar fluctuates. Gases with normal boiling points appreciably above 95°K adsorb appreciably on glass at 95°K even to 10^{-6} torr, and the pressure in the cell will fluctuate as the nitrogen level fluctuates on this account. The major portion of both the flash

filament spectra and the hydrogenation data were obtained using a cell containing only the 4 lead dewar assembly. For flash filament spectroscopy this is an ideal arrangement. However, since it was found that the tungsten sample is completely inactive unless the surface is cleaned of all adsorbed material, the cell was modified by sealing a two lead press seal in the bottom of the cell. A tungsten ribbon (8 cm long and 0.5 cm wide) was spot welded to these leads. The cell was then placed over a hole cut in the marinite top. The ribbon and the walls surrounding the cell could then be cooled by placing a dewar containing a suitable coolant around the bottom half of the cell. For isothermal hydrogenation experiments cooling the walls as well as the leads gives better control of the temperature. For example, if the dewar is filled with liquid nitrogen (b.p. 77°K), the measured temperature of the filament is 95°K. This final temperature is a result of a balance between thermal losses through conduction down the filament and a thermal gain from radiation. The value of 95°K is the average temperature resulting from a temperature distribution along the filament (5). This will be discussed in more detail later. Since tungsten is inactive unless cleaned, either the filament or ribbon can be used with no interference from the other by simply cleaning only the one to be used for experiments. However only the filament is used for flash filament spectra. The

use of resistance thermometry necessary for flash filament spectroscopy is unreliable when applied to thin tungsten ribbons (47).

Two types of ionization gauges were used with this system for total pressure measurements: (1) a standard Westinghouse 5966 gauge (48), and (2) a modified Bayard-Alpert gauge developed by Redhead (49) and marketed by Electron Technology, Inc. The 5966 gauge has been a standard in vacuum work for a number of years but employs hot tungsten filaments as a source of electrons for ionization. This gauge is supplied with 1/4 inch nonex tubulation. For increased conduction this is replaced with 1 inch Pyrex tubing for sealing to the vacuum system. The E.T.I. gauge is a more expensive gauge, however E.T.I. will supply these gauges with the modifications desired by the user. For our uses this gauge was supplied with two thoria coated tungsten filaments for low temperature operation. The gauge itself is contained inside a half liter round bulb with the inner walls coated with stannous oxide as a grounding shield, and the internal metal structure is constructed entirely of tungsten.

All decomposition and hydrogenation data were taken with the mass spectrometer. The mass spectrometer was a 90° magnetic deflection type developed by Davis and Vanderslice (50). Ionization is by electron bombardment with the

resulting positive ions separated by either magnetic or electrostatic selection. The collector is a 10-stage electron multiplier with a gain of approximately 10^5 to 10^6. With the multiplication from the electron multiplier the mass spectrometer is capable of detecting partial pressures as low as 10^{-13} torr. Adjacent mass peaks up to mass 90 can be separated. In the electrostatic mode of operation the mass spectrometer is capable of very rapid scans. Repetitive scans over 10 amu can be taken every 0.1 seconds. However, in the rapid scan mode, especially at low pressures, the number of ions collected during each scan is small. At a pressure of 10^{-10} torr and scan rates of 0.1 sec/scan the number of ions collected during each scan is at most 100. Therefore for more accurate flash filament spectra, the mass spectrometer is used to follow only one mass species.

The output from the multiplier is connected to a high speed electrometer for amplification. After this final amplification the output signal is large enough to be safely switched without electrical pick-up problems. The amplified signal can then be switched to either the x-y recorder or to a high speed recording system consisting of an oscilloscope and a direct writing oscillographic recorder. The x-y recorder is used for recording slow mass scans or partial pressure spectra, and the high speed system is used for recording high speed mass scans.

The sample gases are separated from the working area by a bank of UHV variable leak valves. The hydrogen supply is a hydrogen diffuser consisting of a palladium tube connected to the vacuum system. By surrounding the palladium tube with hydrogen, diffusion of hydrogen through the palladium will establish a pressure of hydrogen inside the tube. Since the tube can be easily cleared of hydrogen by the reverse process, the hydrogen supply is used on the gas line having the single variable leak in Figure 2. For other gases the gas supply is contained in ampoules having break off tips. These gases are mounted on those gas lines having two variable leaks in series. The variable leaks inside the large area enclosed by the dotted line are mounted on top of the Marinite top and those inside the small area are mounted below the table top. With this arrangement the entire system up to the break-off tips can be pumped to a hard vacuum. The leak valves are then closed and the break-off tip opened by using a glass enclosed iron slug. By using two valves in series it is possible to bake periodically the working portion of the vacuum system without replacing the gas ampoules each time. The variable leaks are bakeable to 450°C, but they must be baked in the fully open position. With two valves in series, the gas supply can be sealed off and the dosing valves mounted on top of the table opened for baking.

The pumps have not been included in Figure 2 since two types of pumping systems were used: mercury diffusion pumps and an ion pump. The mercury pumping system consists of two, two stage pumps in series separated from the system by two liquid nitrogen cold traps in series. The diffusion pump is backed by a rotary forepump separated from the diffusion pumps by a liquid nitrogen cold trap. This trap is used to maintain the forepump free of mercury and the diffusion pumps free of oil from the forepump. The first of the cold traps following the diffusion pumps is used to protect the system from mercury and the second trap is a pumping trap. An ion pump is basically a variation of a Penning type ionization gauge consisting of a ring anode and two cathode plates with a magnetic field coaxial with the ring anode. With the anode operated at a high positive potential (5000 V) electrons are admitted from the cathodes by a field emission process and forced into a spiral path by the strong magnetic field. This increases the path length and results in a high probability of ionization of gas molecules. The positive ions formed in this process then bombard the cathode. Due to the high energy of the impacting positive ions, these ions are buried in the cathodes and at the same time sputter cathode material. The pumping action of the ion pump then results from both burying the positive ions in the cathode and gettering of neutral gas molecules on the freshly sputtered

films. The complete pumping system consists of a rotary pump, diffusion pump, cold trap and the ion pump. A 1 inch UHV valve is used to separate the ion pump and system from the mercury pump system which is only used as a roughing system when first starting up. Although the ion pump can be started at a pressure of 10^{-3} torr, extended operation at high pressure will decrease its life. After roughing to a pressure of 10^{-6} torr with the mercury pump system, the vacuum system is sealed off with the 1 inch valve and the mercury pumps shut down. From then on all pumping is done with the ion pump in a completely closed system. An additional feature of the ion pump is that since it is basically a Penning type ionization gauge, the pump current can be calibrated for pressure.

B. Ultra High Vacuum Processing

Since vacuums of at least 10^{-10} torr are necessary in order to study the interaction of a sample gas with a clean metal surface, a consideration of ultra-high vacuum (UHV) techniques is necessary. From Equation 22 it can be seen that the ultimate vacuum will be governed by a balance between the sum of all leaks in the system and the sum of all pumping. At steady state where $\frac{dP}{dt} = 0$ and $P_1 = P_2$ the pressure is

$$P_0 = \frac{LV}{S} \tag{27}$$

In practice one is limited to a finite pumping speed $(\frac{S}{V})$ so the ultimate vacuum is governed by the magnitude of the actual

or virtual leaks into the system (4). The attainment of UHV then becomes a problem of elimination of all possible leaks. Dushman (6) has included a large section on methods of detecting actual leaks to the atmosphere. As a general practice all glass seals should be tested with a tesla spark coil. If any small pin holes are present the spark will preferentially go to these pin holes and indicate the leak. The spark will in addition punch holes in any weak points in the glass such as bubbles or thin spots. For smaller leaks the mass spectrometer can be used in conjunction with a fine stream of helium or hydrogen. A leak in the glass will be indicated by an increase in the partial pressure of the test gas in the system. Virtual leaks due to outgassing of walls or metal parts inside the system etc. are much greater problems. For this reason all metal parts in the vacuum system must be vigorously outgassed at as high a temperature as possible. The main limiting factor in reaching vacuums below 10^{-8} torr is the re-evolution of water adsorbed on the glass walls (51). For this reason the region enclosed by dotted lines in the schematic of the vacuum system, Figure 2, is surrounded by an oven and baked to 350°C. In practice the system is first pumped as low as possible and then baked out for 24 hours. The system is brought back to room temperature and all internal metal parts outgassed by electron bombardment. Ionization gauges are outgassed using 1500 V on the grid and an emission current of 150 ma between filament and grid. The mass

spectrometer is outgassed using 500 V on the grid and an emission current of 100 ma between filament and grid. Following this the system is baked for a second time at 350°C. During this final bake the filament and ionization gauge are outgassed periodically. After removal of the oven the leak valves are closed as soon as the valves have cooled sufficiently to replace the drivers. With this treatment the pressure should reach 10^{-10} torr within a few hours.

Bake out procedures for mercury pumped and ion pumped systems differ slightly. Before the mercury pumps are started, the cold traps and glass tubing of the pumping system are baked up to the throat of the last mercury pump with only the rotary pump in operation. Following this the mercury pumps are started and the first cold trap filled with liquid nitrogen. From then on the baking cycle is the same with the final trap being baked along with the working portion of the vacuum system. In the case of the ion pumped system, the first bake out and outgassing is conducted with the mercury pump roughing system. The ion pump is baked along with the working portion of the vacuum system. The mercury system is then sealed off and the final bake conducted with only the ion pump operating.

C. Calibration

Although the development of UHV was opened up by the development of the Bayard-Alpert ionization gauge (10), UHV

pressure measurements are still limited in accuracy. The gauge does not measure pressure as such, but gas density. The relationship between ion current and pressure, Equation 1, is determined empirically by calibration against a manometer such as a McLeod gauge (8). The calibration factor, s, in Equation 1 is a function both of the gauge geometry and the composition of the gas. In addition ionization gauges can act both as a source and as a pump for gases (6). The pumping-action is greater for active gases such as hydrogen and hydrocarbons.

Since the ratio of gauge sensitivity factors is found to be only a function of the type of gases, one only needs know a calibration for a known gas such as nitrogen (6). The gauge sensitivity for other gases can then be taken from tabulated values of the ration S_x/S_{N_2}. Experimentally it is found that with ethylene flowing into a highly pumped system with the mass spectrometer monitoring mass 28, the major peak in the cracking pattern of ethylene, the ionization gauge yields the following relationship when momentarily turned on

$$P_{N_2} = a\ i^+_{28} \qquad (28)$$

The factor a ranges between 3 and 7 and the pressure P_{N_2} is the indicated gauge pressure when set for a nitrogen sensitivity. Only the initial reading is taken since this minimizes the effect of both gauge pumping and gauge outgassing (6). From Equation 1 this could be converted to hydrocarbon pressure by using the ratios of the sensitivities.

$$i_{28}^{+} = \frac{1}{a} \frac{S_E}{S_{N_2}} P_E \qquad (29)$$

Due to the extensive fragmentation of hydrocarbons no accurate sensitivity values for hydrocarbons are known, however, Santeler, et al., report a range of values from 3 to 10 for hydrocarbons (52). If we compare the authors' values of S for argon and hydrocarbons with the value of S for argon and nitrogen determined for the W5966 gauge by Schulz (48), the ratio of S_{N_2}/S_E falls in the range of 2 to 9. Then with the experimental value of a, Equation 29 becomes

$$i_{28}^{+} \simeq P_E \qquad (30)$$

To a fair approximation (i.e., within a factor of 3) the mass 28 ion current (amps) from the mass spectrometer is equal to the ethylene pressure (torr).

The filament is heated to obtain flash filament spectra by passing through the filament a fixed constant current supplied by a constant current generator similar to the one used by Mimeault (18). Through the use of sensing leads shown in Figure 4, the voltage drop across the center segment of the filament can be continuously monitored. Thus one has a continuous measure of the resistance of this center segment and with a prior calibration a continuous measure of temperature. In order to obtain this prior calibration the calibration system shown in Figure 5 was designed. The lower portion was constructed of Vycor and connected to the upper Pyrex portion by a standard taper joint. Ceramic to metal vacuum feed

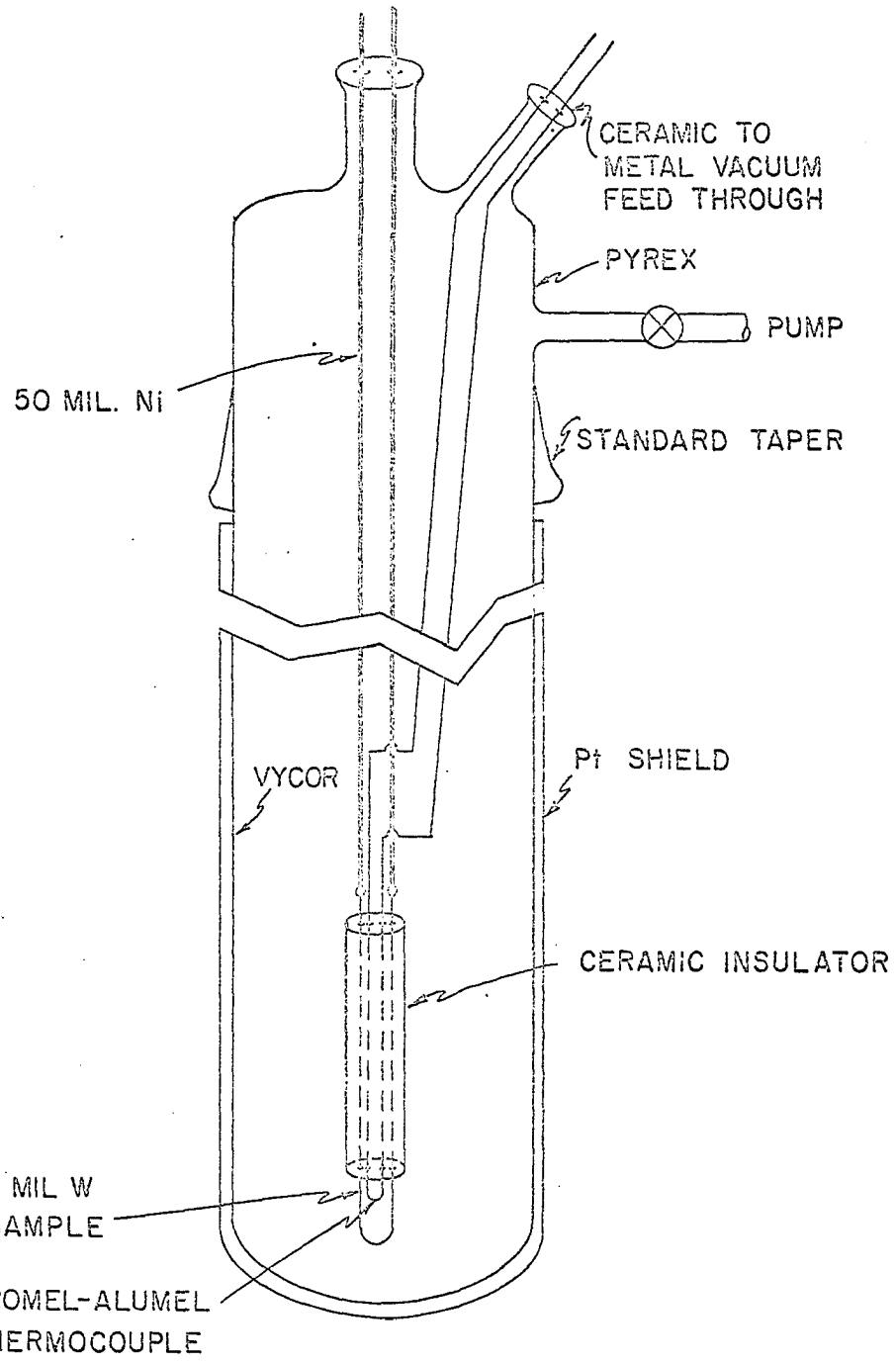

Figure 5. Cell used for resistance vs. temperature calibration

throughs mounted on Kovar to glass seals were used to carry heavy 50 mil Ni leads and a chromel-alumel thermocouple into the calibration system. A 5 mil tungsten sample was threaded into two holes of a 4 hole ceramic insulator and spot welded to the Ni electrodes. The chromel-alumel thermocouple was threaded through the other set of holes and the junction spot welded. The complete lower Vycor section was then surrounded with a Pt heat shield and placed in a Marshall tube furnace capable of reaching 1000°C. The temperature of the furnace was controlled to within 2°C with a Brown Electronic temperature controller. After equilibration at a given temperature setting, the temperature of the ceramic insulator containing the sample filament was measured with the chromel-alumel thermocouple and Rubicon Instrument potentiometer.

With the above calibration system a temperature vs. resistance calibration for tungsten was obtained from room temperature to 1000°C, as shown in Figure 6 along with the data from previous calibrations below 300°K (18, 53). The ordinate, R/R_{295}, is independent of the physical dimensions of the sample. Below 620°K the data are well represented by

$$T = 239 \frac{R}{R_{295}} + 55 \qquad (31)$$

With this equation one then needs to determine the resistance of the sample filament at one temperature from which the resistance of the filament at 295°K can be calculated. In practice this is done by filling the dewar in Figure 4 with

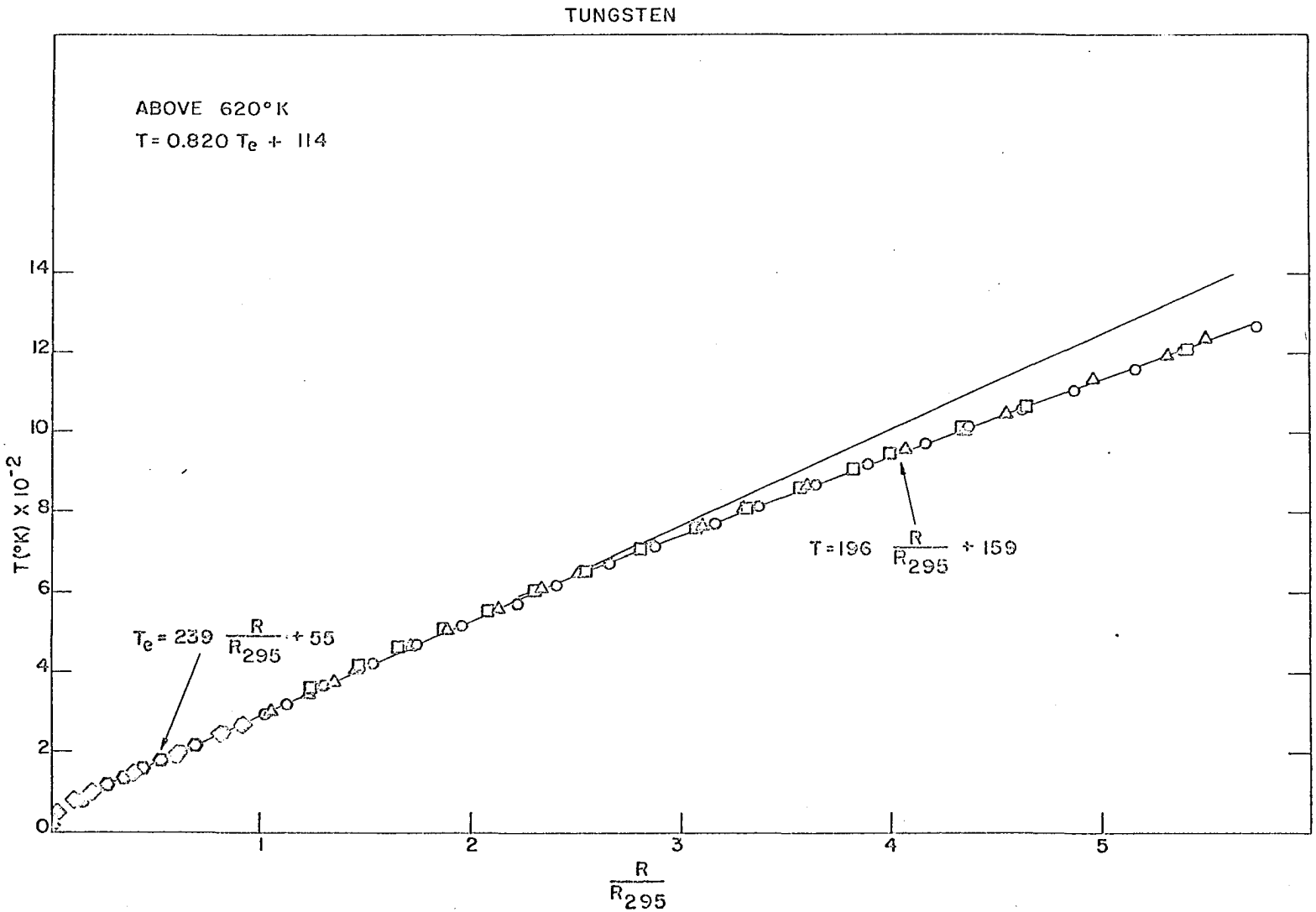

Figure 6. Resistance ratios vs. temperature for tungsten. ○, △, □ this calibration; □ Reference 53; ⬡ Reference 18

water at room temperature. Since R_{295} is known and the filament is heated with a known constant current (I), Equation 31 becomes

$$T = \left[\frac{239}{R_{295}I}\right] V_f + 55 \qquad (32)$$

and the voltage drop, V_f, can be used directly for a measurement of the filament temperature.

Above 620°K a break occurs in the calibration of resistance vs. temperature for which a correction must be made using the equation given in Figure 6. With the hydrocarbon, however, this was not found necessary since reactions occurring during a flash are essentially complete below 620°K. In practice the filament voltage drop is monitored both by the trigger circuit for temperature control and a recorder for temperature measurement. As shown in Figure 2 the heating circuit and trigger circuit are electrically connected. When the filament voltage reaches a predetermined value the relay in the trigger circuit closes and switches the filament heating current from the filament to an internal dummy load limiting the maximum temperature reached by the filament.

In flash filament spectroscopy the assumption is made that the temperature is uniform over the entire length of the filament. Ehrlich has experimentally shown this to be not quite true (54). Under steady state conditions the temperature distribution assumes an approximate parabolic form with the ends of the filament where they are spot welded

to the electrodes being at the temperature of the coolant used in the dewar, and the center of the filament being at a maximum temperature greater than the temperature of the ends. The distribution results from an energy loss through conduction of heat along the filament and out the ends. At very high temperatures, where radiation losses become an appreciable part of the total energy loss, the distribution becomes flatter, but the distribution still is parabolic.

During a flash, however, the experimental temperature distribution is significantly more uniform with only the segment at the very ends of the filament being appreciably different from the temperature of the major portion of the filament. For temperatures of the center of the filament less than 370°K, Ehrlich finds the nonuniformities to be negligible. In addition the major error in the average temperature during a flash comes from including the small portion of the filament at the very ends. By using sensing leads the measured temperature corresponds to the major portion of the center of the filament where the distribution is quite uniform and excludes the cold ends of the filament. Although in these experiments a heating rate slower than Ehrlich's was used, the sample filament was a factor of 2 smaller in diameter and nonuniformities in the temperature distribution across the center segment of the filament were quite small below ~400°K.

D. Experimental Techniques

Flash decomposition of a hydrocarbon monolayer yields hydrogen in the gas phase and a carbon residue on the surface. In order to run more than one experiment on a clean surface this residue must be removed. Heating the filament in an ambient of hydrogen is ineffective for this purpose and in addition forms considerable amounts of water from the reaction of the atomic hydrogen with the oxygen in the glass walls (55). This is highly detrimental to the operation of an UHV system and is to be avoided. Cleaning in an ambient of oxygen is quite effective in removing carbon and was used periodically. This however also leads to a transport of tungsten oxide to the walls and for this reason is used sparingly. The simplest method is a brute force method in which the surface is thermally cleaned between each experiment. This has involved using an unregulated auxiliary power supply for cleaning purposes. The regulated power supply used for heating the filament does not supply sufficient power for cleaning. The power setting which gives a reproducibly clean surface was then found experimentally. Although the temperature of the filament during cleaning was not accurately known, a pyrometer estimate placed it above 3000°K.

Since such drastic conditions are required for cleaning and decomposition of the unsaturated hydrocarbons occurs at such a low temperature, the normal procedure used in flash

filament spectroscopy must be modified when studying hydrocarbons. It has been standard practice to hold the filament at a temperature above which desorption is complete while establishing a steady state pressure of the sample gas. The filament is then turned off and adsorption starts as soon as the filament starts to cool. However decomposition of hydrocarbons occurs during cooling, the surface is contaminated before the intended dosing temperature is reached, and this method is therefore unsatisfactory. With the exception of NO (56), however, this method appears adequate for the study of simple diatomic molecules. That this procedure is not adequate for the study of hydrocarbons can be seen from a consideration of the cooling rate of the filament, Figure 7, after high temperature cleaning. This curve was obtained by switching in a small monitoring current automatically as the cleaning current was switched off. After high temperature cleaning it takes 2.5 minutes to reach the base temperature. If hydrocarbons were present a wide range of both surface and gas phase products would be produced during this period.

For this reason the filament was cleaned in a vacuum and cooled for two minutes prior to admitting the sample gas. In order to be able to cool for two minutes and not have the filament covered to an appreciable extent with the background gases (predominantly CO), the pressure must be held in the low 10^{-10} torr range during the cleaning process. At 2×10^{-10} torr only 1 percent of the surface

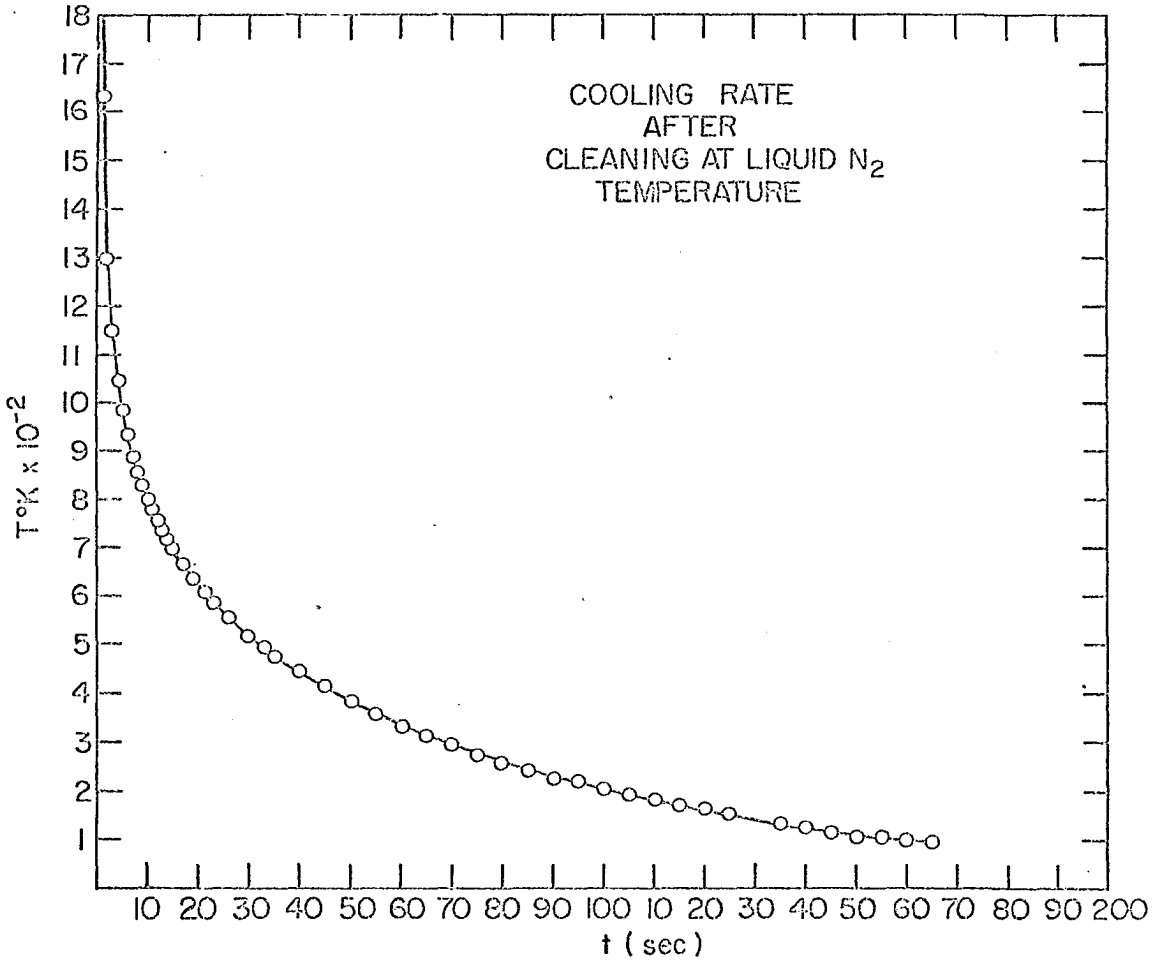

Figure 7. Cooling rate after high temperature cleaning with dewar filled with liquid nitrogen

can be covered during this cooling period. Following this cooling period the variable leak is opened and the sample gas admitted to the cell. In order to reduce contamination from adsorption of background gases, the filament should be dosed as soon as the filament temperature drops below 200°K.

In the usual flash filament experiment only the chemisorption reaction occurs during the dosing period, but this is not the case with hydrocarbons. For this reason the ambient gas composition was monitored constantly using the fast scan mode of the mass spectrometer and an oscilloscope display of the output signal. The masses from 24 to 32 amu were scanned for this purpose. This mass region contains the major mass peaks of ethylene, acetylene and ethane, Figure 8 (57), in addition to the major peak of CO, mass 28. Since the ionization gauge also contains a high area hot filament which cracks hydrocarbons to an appreciable extent, only the mass spectrometer is operated during experiments. The mass spectrometer is equipped with a very small thoria coated iridium filament which when operated in a highly pumped system produced only a slight increase in hydrogen pressure. Hydrogen is the major gas phase product of hydrocarbon decomposition reactions on the hot filaments.

For flash filament decomposition spectra adsorption was conducted at 95°K (liquid nitrogen bath) where in all cases the only species observed in the gas phase is the sample gas. After formation of the chemisorbed monolayer, the filament

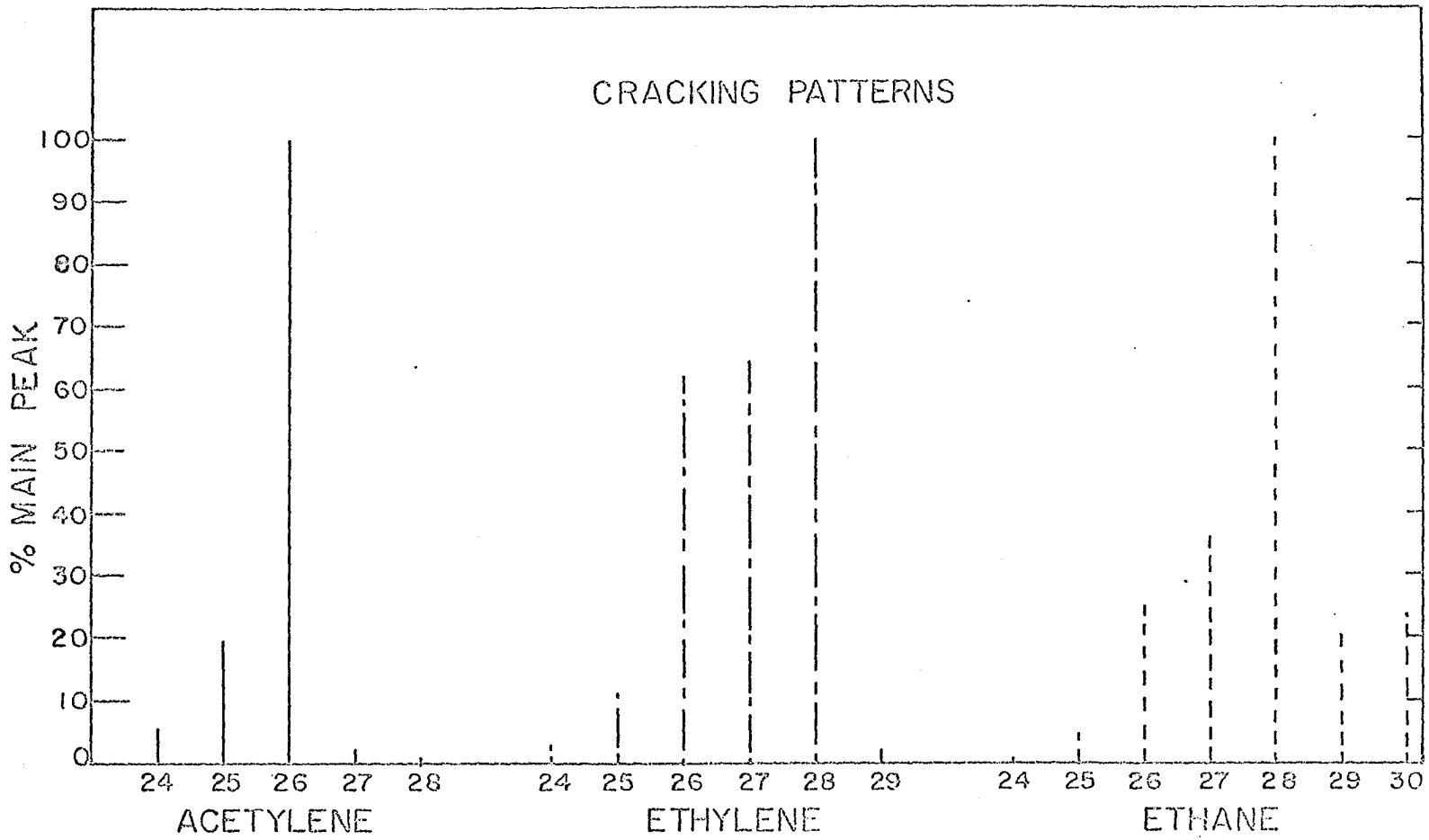

Figure 8. Cracking patterns of acetylene, ethylene and ethane reported in Reference 55

was flashed using a low heating current (0.5 amps) which heated the filament from 95°K to 1000°K in ~ 20 seconds. This slow heating rate was used in conjunction with maximum pumping for maximum resolution of multiple peaks (5).

IV. RESULTS

A. Flash Filament Spectroscopy

Since the predominant product obtained from the flash decomposition of hydrocarbons is hydrogen, hydrogen desorption spectra were obtained under the same conditions used in the hydrocarbon experiments. The flash desorption spectrum resulting from a saturated dose of hydrogen on tungsten at 95°K is shown in Figure 9. In addition this curve illustrates the form of the data in a flash filament experiment. Both the filament voltage drop (curve B) and the mass 2 ion current from the mass spectrometer (curve A) are recorded simultaneously on a two pen x-y recorder with a common time axis. The temperatures in Figure 9 were calculated from the voltage drop using Equation 32. In the desorption spectrum there are three distinct peaks which following common terminology have been designated α, β_1 and β_2 (24, 25). Desorption of the α form occurs as soon as the filament is heated. The β_1 and β_2 forms are more tightly bound to the surface with the peak maxima occurring at 390°K and 570°K. However there are also reproducible breaks at 200°K and 320°K. These points of detail are superimposed on desorption that is continuous from 95°K to above 800°K.

At lower coverages adsorption is preferential in the more tightly bound β_2 state as shown in Figure 10. Curve B is a normalized plot of the high coverage desorption spectrum

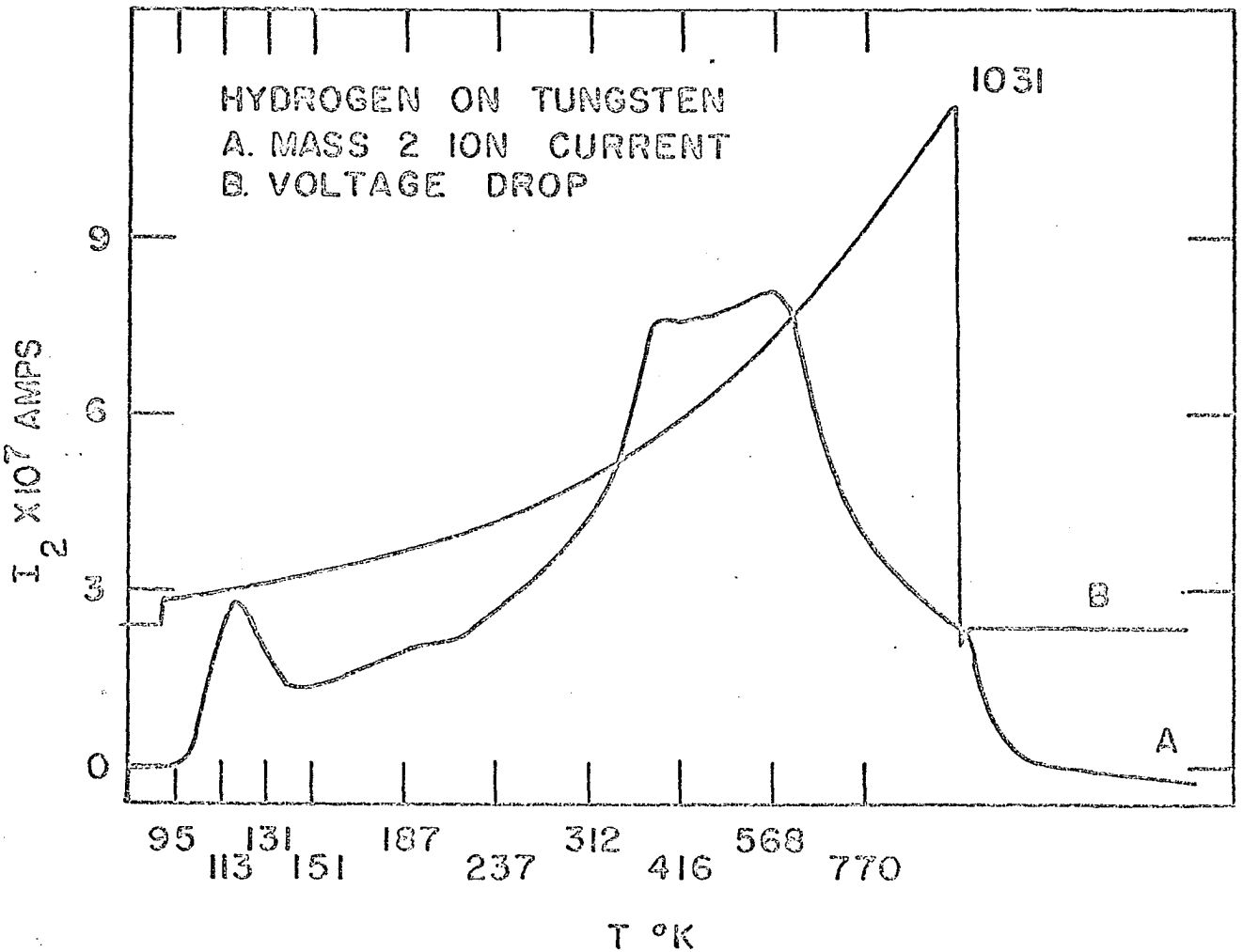

Figure 9. Hydrogen desorption spectrum: Curve A, mass 2 ion current; Curve B, filament voltage drop

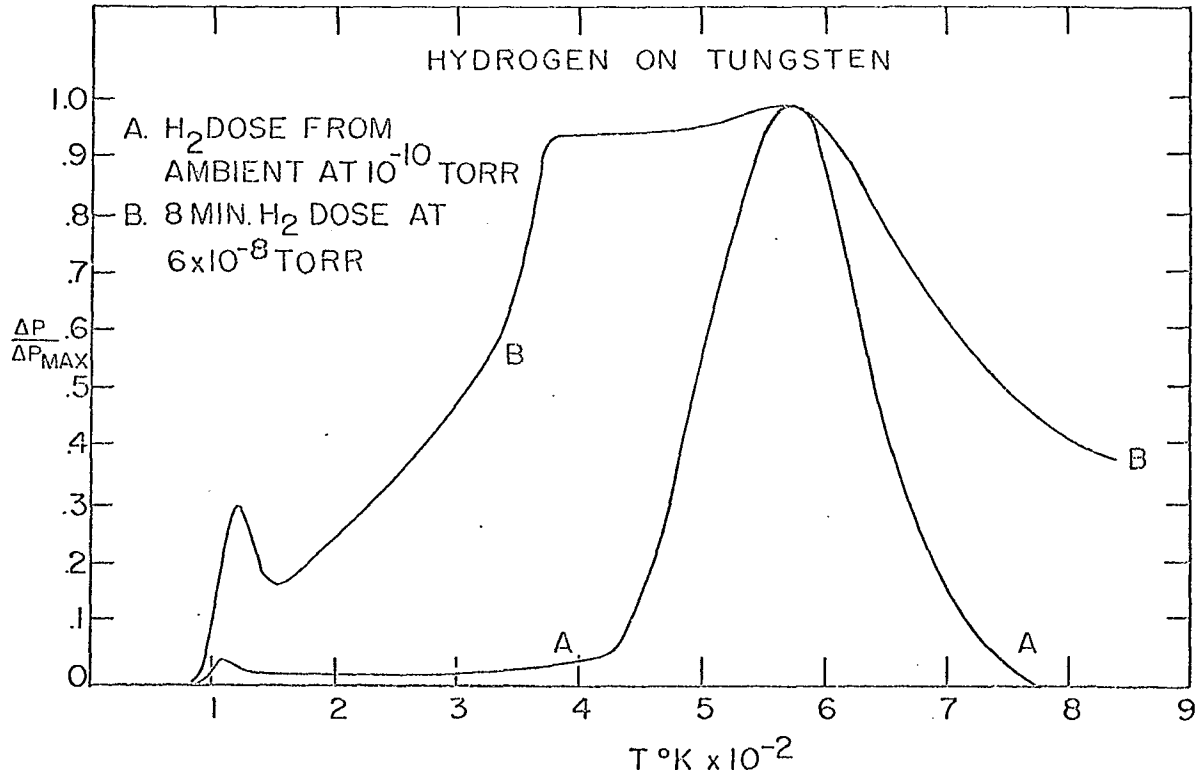

Figure 10. Normalized hydrogen desorption spectra for a heavy dose of hydrogen, Curve B, and a light dose of hydrogen, Curve A

resulting from an 8 min dose of hydrogen from the background ambient at a total pressure of 1×10^{-10} torr. The background at this pressure is composed nearly entirely of hydrogen and carbon monoxide with carbon monoxide predominating. As such this represents an extremely light dose with the β_2 peak of curve B being 200 times greater than the β_2 peak of curve A.

The hydrogen spectrum resulting from the flash decomposition of an ethylene monolayer formed at 95°K is shown in Figure 11. A two peak spectrum is obtained with the low temperature peak (300°K) designated β_1 and the high temperature peak (450°K) designated β_2. If the filament temperature is below 200°K before ethylene is admitted, the two peaks contain approximately equal amounts of hydrogen. If the filament temperature is still above 200°K when ethylene is admitted, decomposition will occur during the initial portions of the adsorption period with the result that the β_2 peak will be larger than the β_1. Due to the dosing procedure this occurs quite frequently. Following high temperature cleaning opening of the valve is started at that point in the cooling period where it is estimated that the filament will be below 200°K when the valve opens.

This is seen in Figure 12. The difference between adsorption on a clean surface, curve A, and adsorption on a contaminated surface is also shown in this figure. Immediately following curve A the filament was cooled back to 95°K and redosed with ethylene on the carbon residue remaining

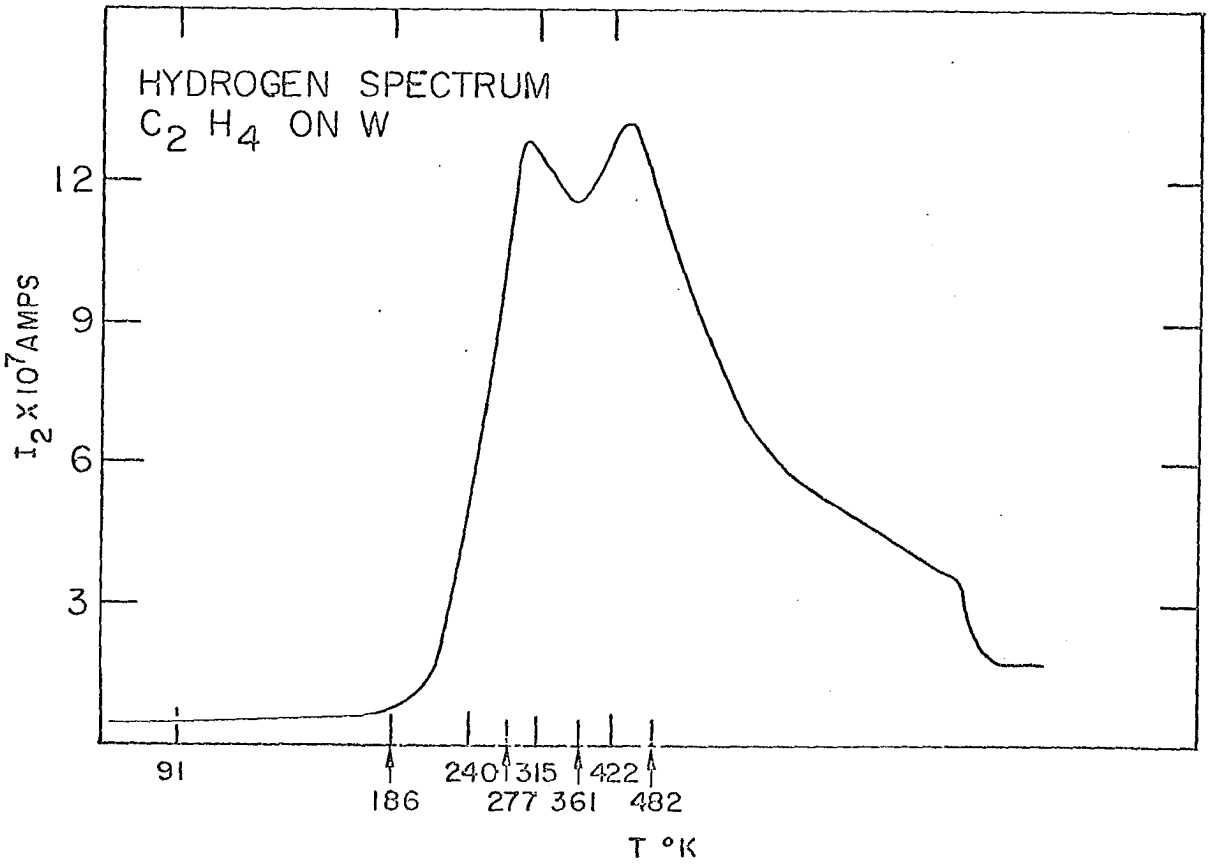

Figure 11. Hydrogen partial pressure spectrum resulting from the flash decomposition of an ethylene monolayer formed at 95°K

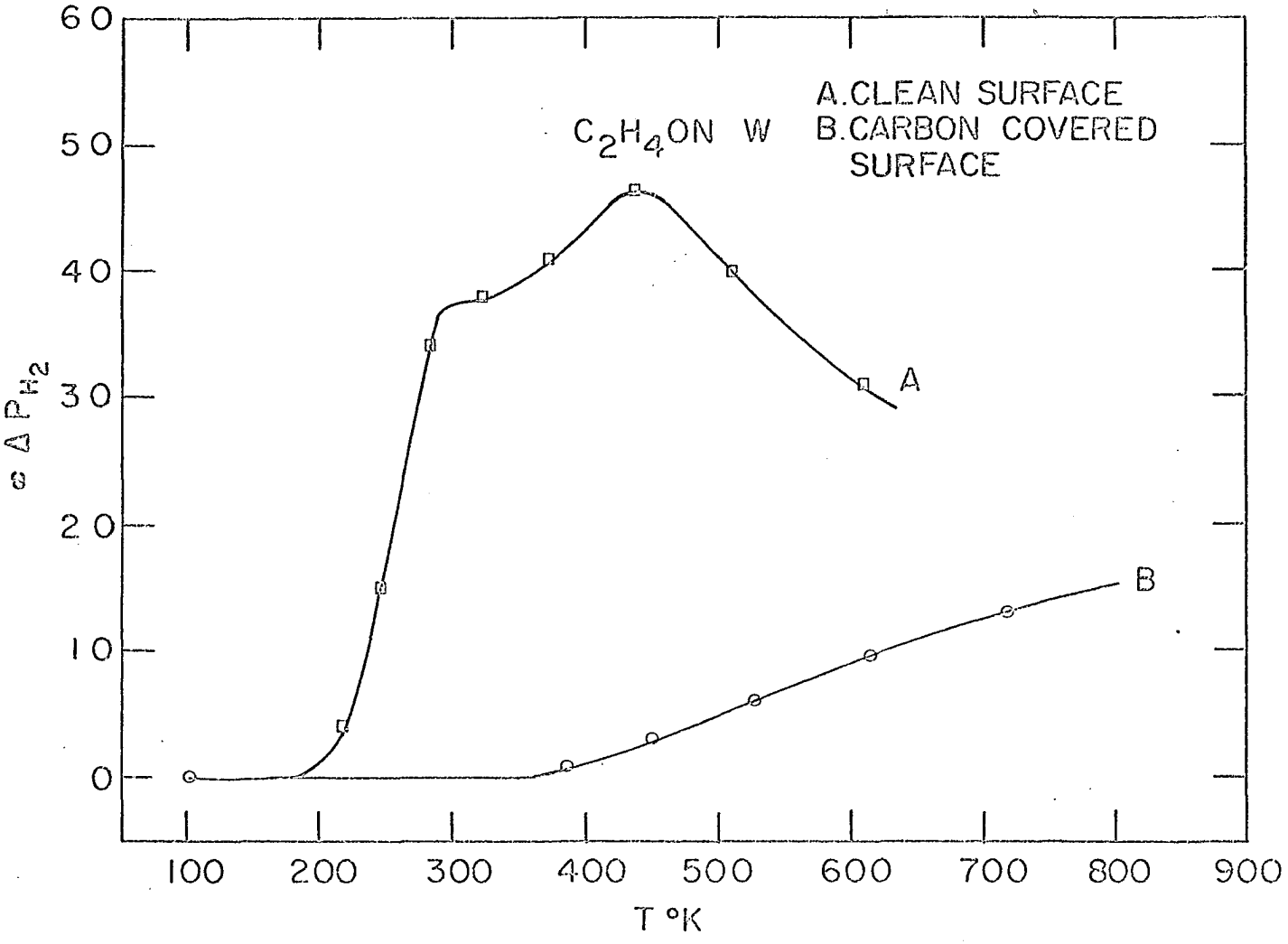

Figure 12. Hydrogen partial pressure spectra: Curve A, ethylene adsorption on a clean surface; Curve B, ethylene adsorption on the residue remaining after the flash giving Curve A

from the previous flash decomposition. Flashing the filament then to 1000°K resulted in curve B. The detail in the decomposition spectrum resulting from adsorption on a clean surface is completely reproducible. If the surface is not cleaned prior to adsorption, however, nonreproducible curves similar to B are obtained.

The differences between hydrogen spectra resulting from hydrogen adsorption and from ethylene adsorption can be seen from Figure 13 where the two normalized curves are shown. In the hydrogen spectrum resulting from mixed adsorption of ethylene and hydrogen details of both curves can be seen. Figure 14 results on flashing after a saturated dose of hydrogen followed by a light dose of ethylene. In the hydrogen spectrum one has the α peak of hydrogen and the β_1 and β_2 peaks of ethylene. In addition there is a peak at about 620°K similar to the β_2 hydrogen peak but shifted approximately 50° higher in temperature. If the surface is saturated with hydrogen and then heavily dosed with ethylene, the hydrogen is displaced and one has essentially an ethylene spectrum. In Figure 15 the surface was first dosed for 5 min with $2\text{x}10^{-6}$ amps (~$1\text{x}10^{-6}$ torr) of hydrogen. Ethylene was then admitted to $4\text{x}10^{-7}$ amps (~$4\text{x}10^{-7}$ torr) and dosed for 8 min. After closing the ethylene leak the filament was allowed to stand for an additional 2 min in the hydrogen ambient prior to flash. The resulting hydrogen spectrum is identical to the spectrum of ethylene. The factor of 5 difference between the

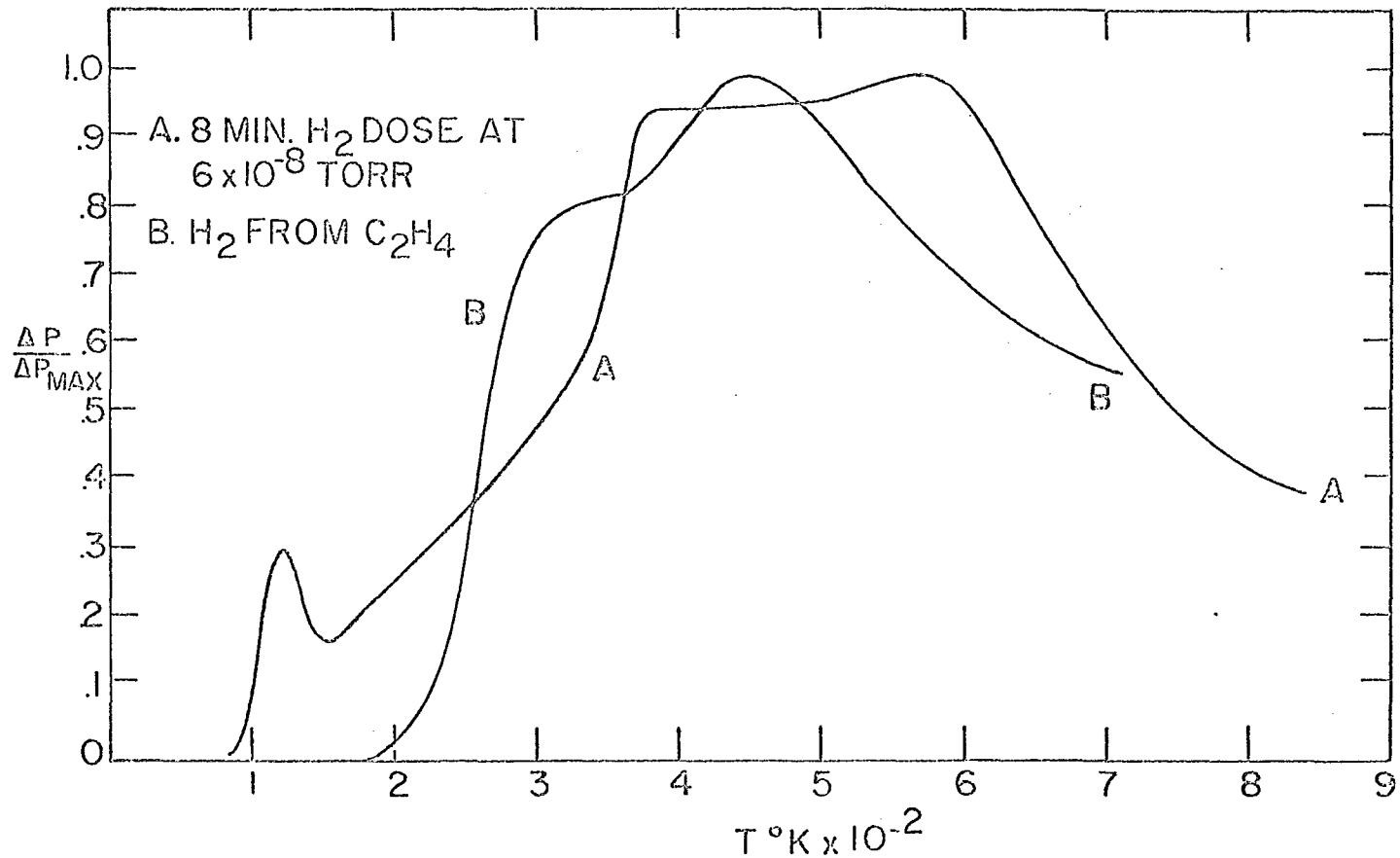

Figure 13. Hydrogen spectra resulting from a monolayer dose of hydrogen, Curve A, and ethylene, Curve B

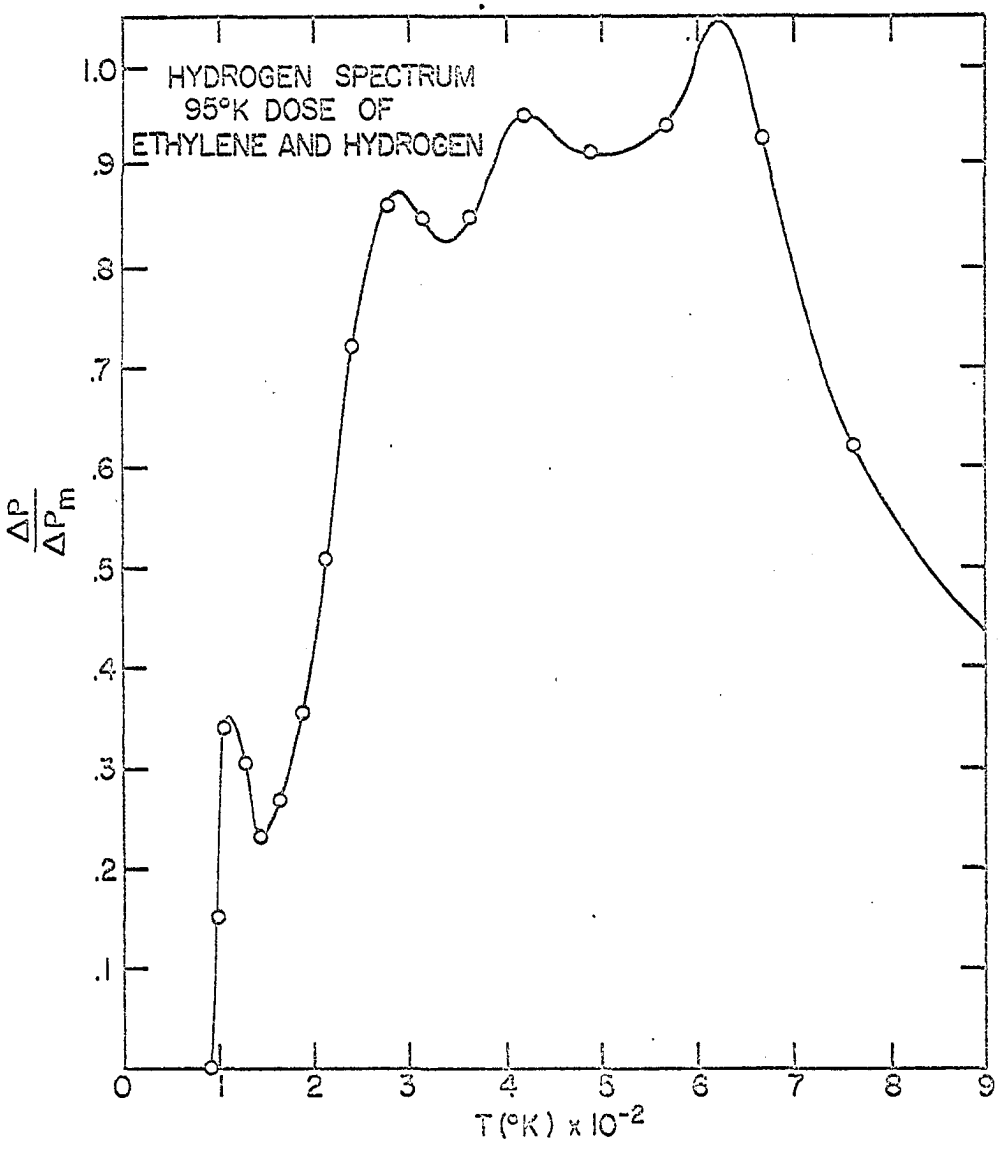

Figure 14. Normalized hydrogen spectrum resulting from a heavy dose of hydrogen at 95°K followed by a light dose of ethylene

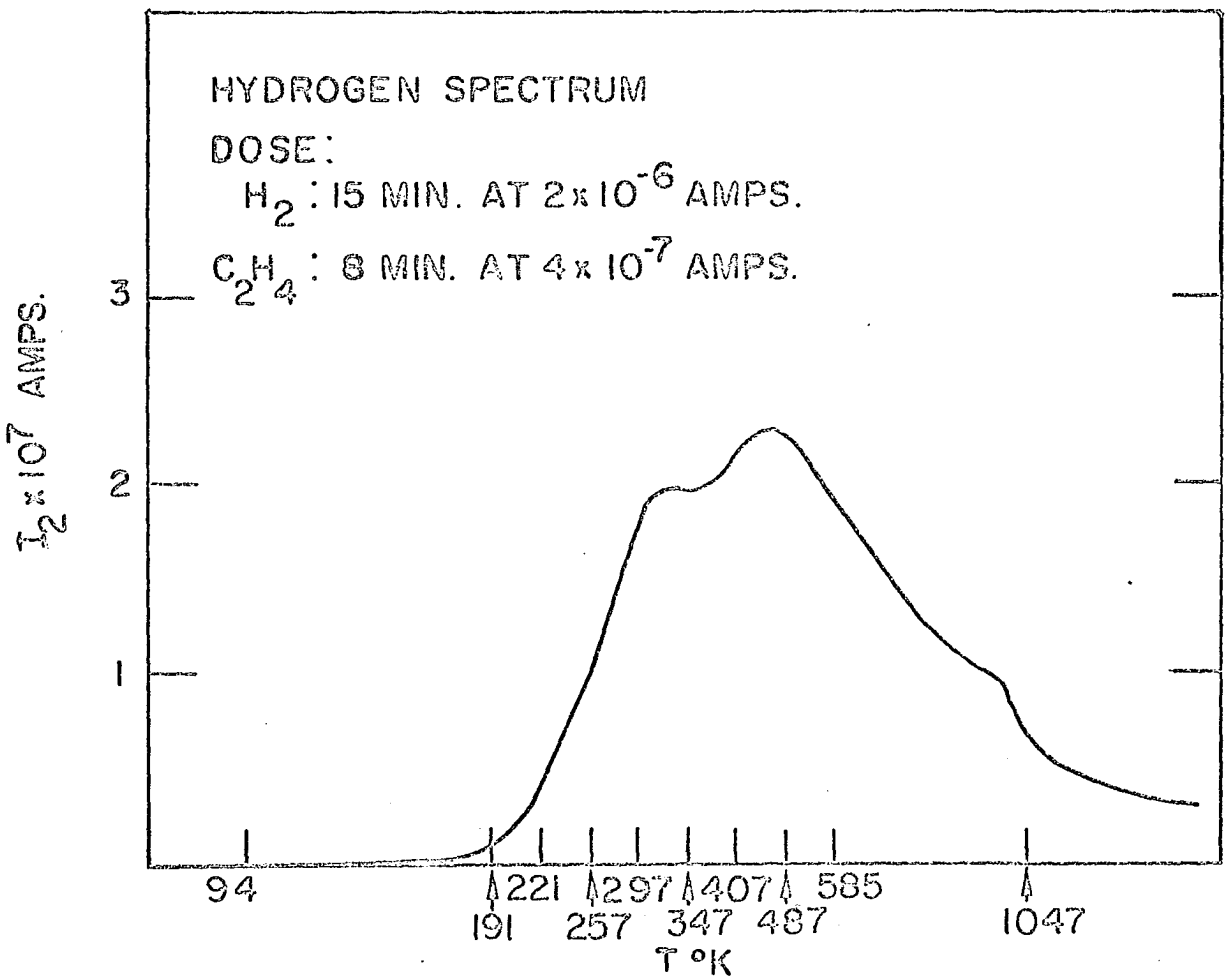

Figure 15. Hydrogen spectra resulting from a heavy dose of hydrogen at 95°K followed by a heavy dose of ethylene

maximum pressure burst in Figures 11 and 15 results from the use of two different mass spectrometer tubes. Since the detector is an electron multiplier, there can be large differences in gain between tubes. Where comparisons are made between pressure bursts, spectra taken on the same mass spectrometer are used. For those cases where only the relative position of the peaks is important, the gain is not important and the spectra are given in terms of either normalized or relative pressure.

The ethylene monolayer can be partially decomposed as shown in Figure 16. Instead of heating continuously to 1000°K, heating was interrupted at 300°K and the filament cooled back to 95°K. This resulted in the removal of the β_1 peak. Adsorption was then continued in the ethylene ambient for a period equal to the first and the filament was then flashed to 1000°K resulting in just the β_2 peak. Partially decomposing the ethylene monolayer does not open any new sites for ethylene adsorption. Removal of the β_1 peak does not open any new sites for hydrogen adsorption either; for admitting hydrogen, after removal of the β_1 peak, to a pressure of 10^{-6} torr also only results in the β_2 peak. Adsorption at 300°K, Figure 17, will accomplish the same purpose as flashing to 300°K. In this case the partial dehydrogenation occurs during the formation of the hydrocarbon monolayer.

The major product obtained from the decomposition of an ethylene monolayer is hydrogen leaving a residue of carbon on

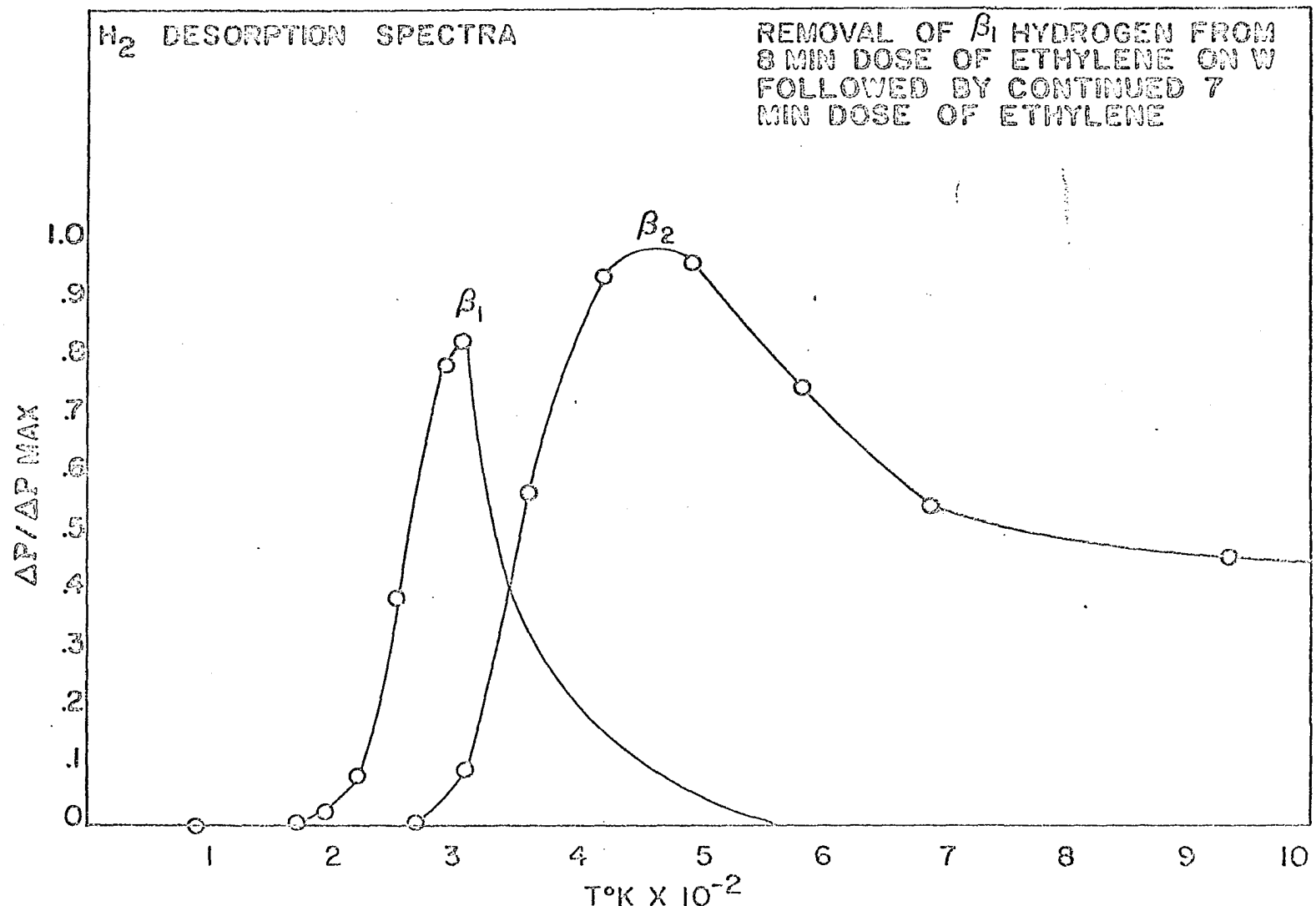

Figure 16. Hydrogen spectra resulting from flashing an ethylene monolayer to 300°K to remove the β_1 peak. This was followed by a second adsorption interval and a flash to 1000°K which gives the β_2 peak

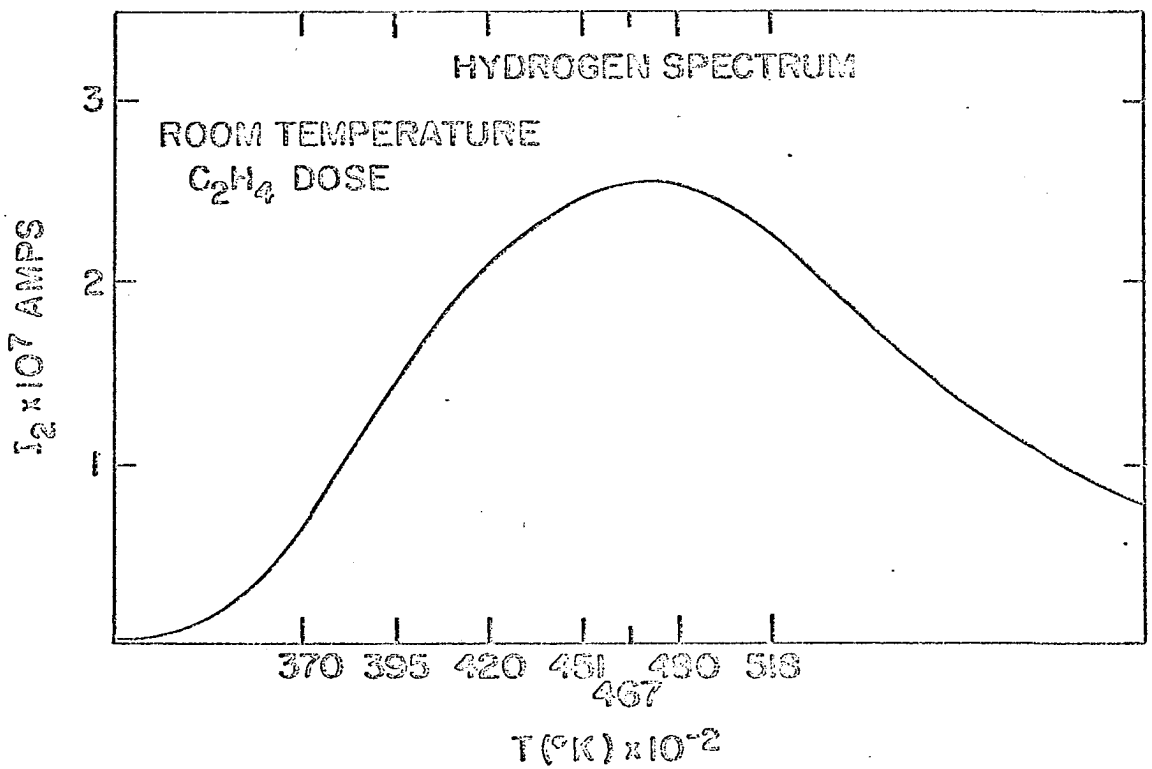

Figure 17. Hydrogen partial pressure spectrum resulting from a room temperature dose of ethylene

on the surface. An important minor product, however, is ethane resulting from a self hydrogenation reaction during the flash. Figure 18 is the spectrum obtained by monitoring the mass 30 ion current during a flash. The mass 30 ion current is directly proportional to the ethane partial pressure as can be seen from the cracking patterns of the hydrocarbons, Figure 8. The largest mass species found in the cracking pattern of ethylene is a small isotope peak at mass 29. Of the three hydrocarbons the mass 30 peak is unique to ethane. The production of ethane during a flash starts above 160°K with the maximum rate occurring at 250°K. The amount of ethane produced during a flash is only a few percent of the hydrogen produced. From the cracking pattern of ethane the maximum change in the mass 28 ion current is 3.6×10^{-9} amps. This is roughly a factor of 10^2 less than the amount of hydrogen. Since the amount of ethane produced during a flash is so small, the valve to the pumps is closed just prior to the flash in order to minimize the loss of ethane. After formation of the ethylene monolayer at 95°K, the reaction is nearly independent of the ambient. A change in the hydrogen pressure over 4 orders of magnitude has no effect on the mass 30 spectra and a factor of 200 increase in the ethylene pressure yields only a factor of 3 increase in the ethane pressure burst.

The hydrogen decomposition spectrum resulting from a 95°K dose of acetylene is shown in Figure 19. Decomposition

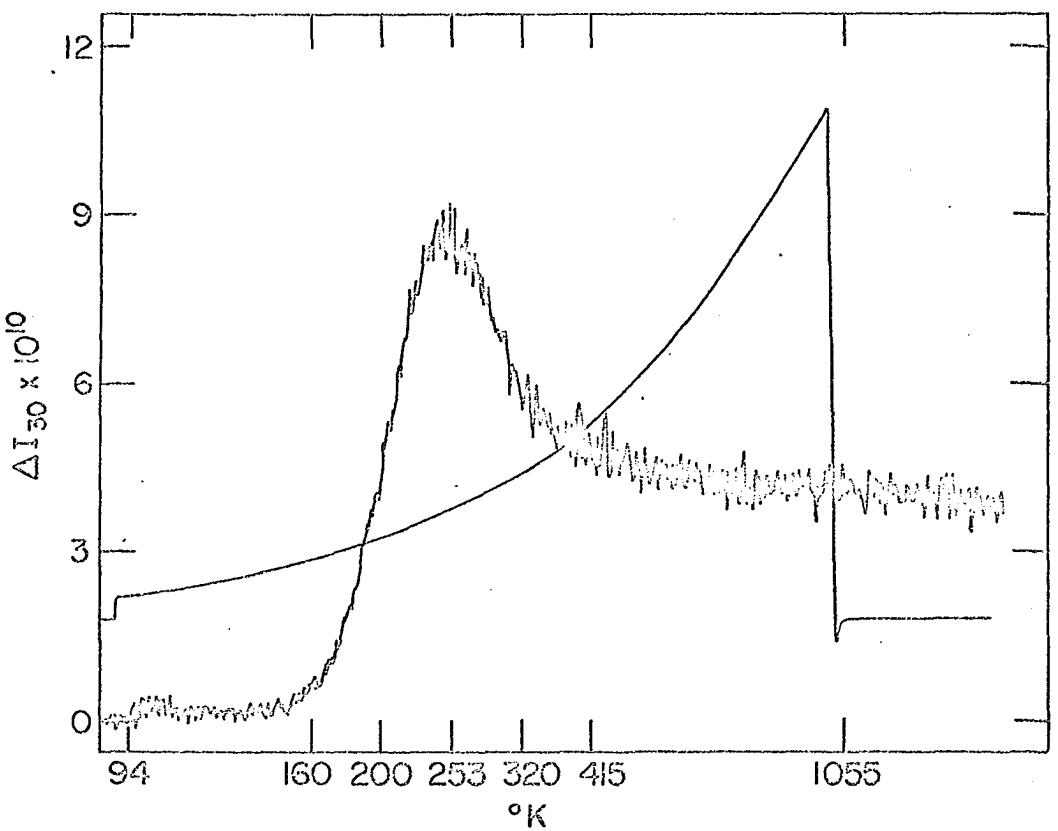

Figure 18. Mass 30 partial pressure spectrum resulting from the decomposition of an ethylene monolayer formed at 95°K. The mass 30 ion current is directly proportional to ethane pressure

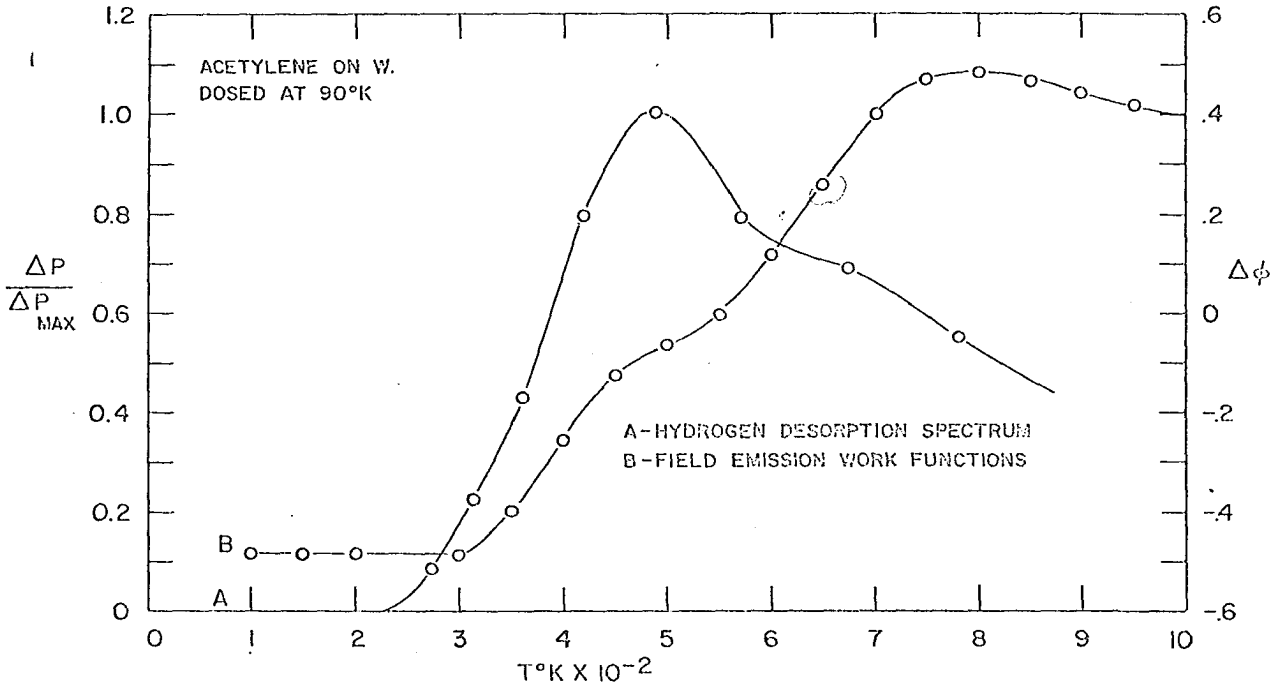

Figure 19. Normalized hydrogen spectrum resulting from a 95°K dose of acetylene on W, Curve A. Curve B is the field emission work function plot from Reference 44. The right hand scale is associated with Curve B

of acetylene, like ethylene, results in a hydrogen spectrum. However, acetylene gives only a single peak at 470°K with decomposition starting at 250°K. This single peak is quite similar to the β_2 peak of ethylene. Both the β_2 ethylene peak of Figure 16 and the acetylene peak of Figure 19 are shown in Figure 20 as normalized plots and it is evident that they are substantially coincident. There is equally good agreement between the amounts of hydrogen contained in the two peaks. The acetylene spectrum, Figure 21, and the ethylene spectrum, Figure 11, were taken under identical conditions. In both cases the maximum hydrogen pressure burst is 1.35×10^{-6} amps.

Figures 22 and 23 contain the flash decomposition spectra resulting from ethylene and acetylene on iridium at 95°K (43). Although the same two peak structures for ethylene is obtained, the hydrogen resulting from the decomposition is not observed in the gas phase until 400°K. This detail is quite clear in total pressure spectrum obtained with an ionization gauge. The partial pressure spectra, however, were obtained using an omegatron mass spectrometer with a sensitivity of $\sim 10^{-5}$ amps/torr. This necessitated the measurement of extremely low level signals with associated slow response. For this reason there is considerable loss of detail in the partial pressure spectra. The acetylene spectrum also contains two hydrogen peaks, the β_1 peak appears only as a shoulder on the much larger β_2 peak. The β_1 peak in the

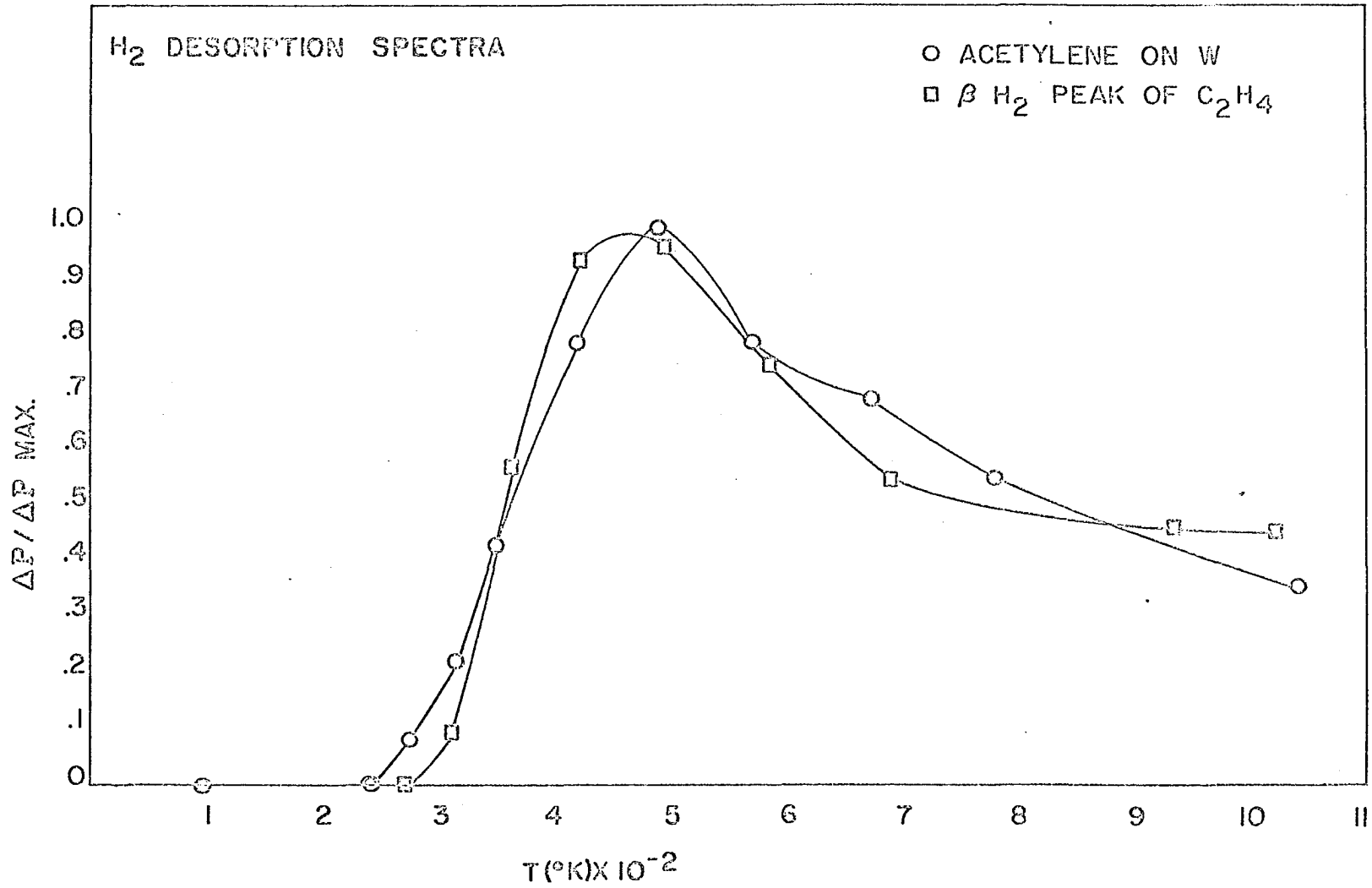

Figure 20. Normalized hydrogen spectra from Figures 16 and 19

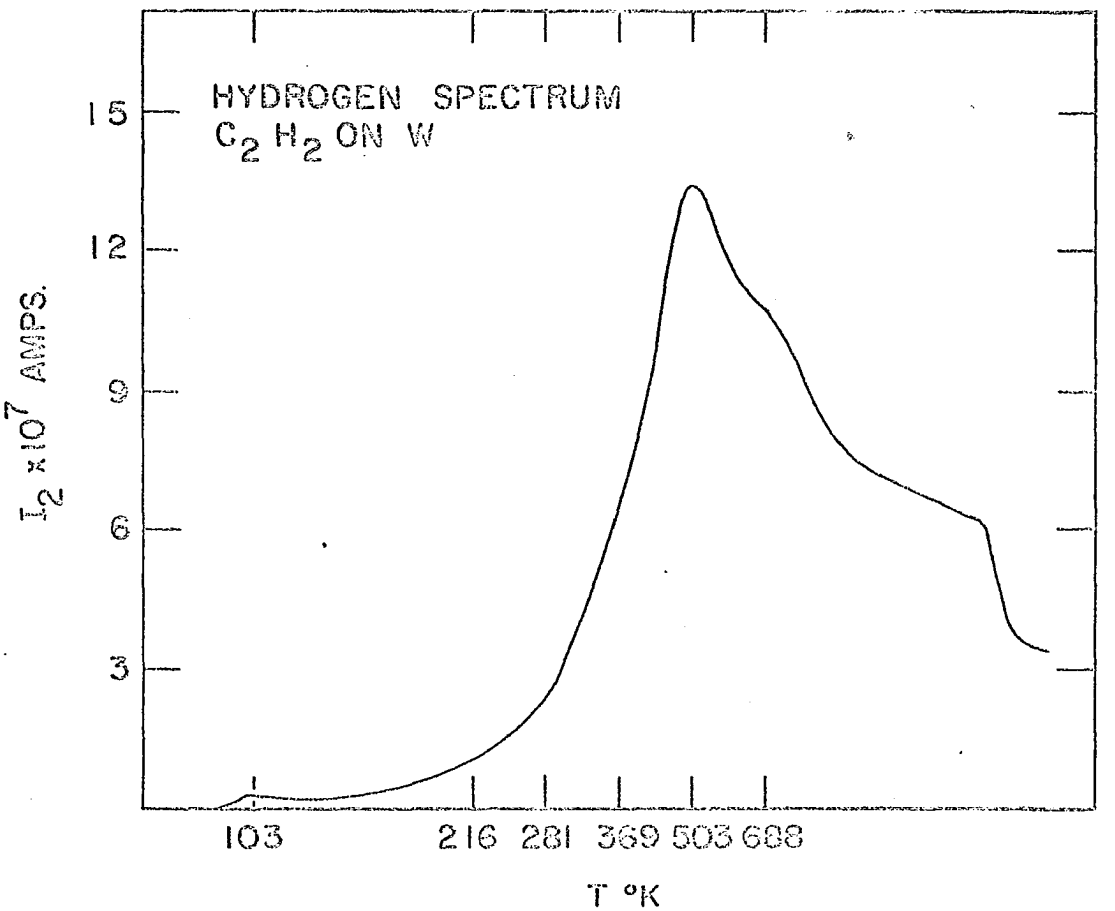

Figure 21. Hydrogen spectrum resulting from a 95°K dose of acetylene on tungsten

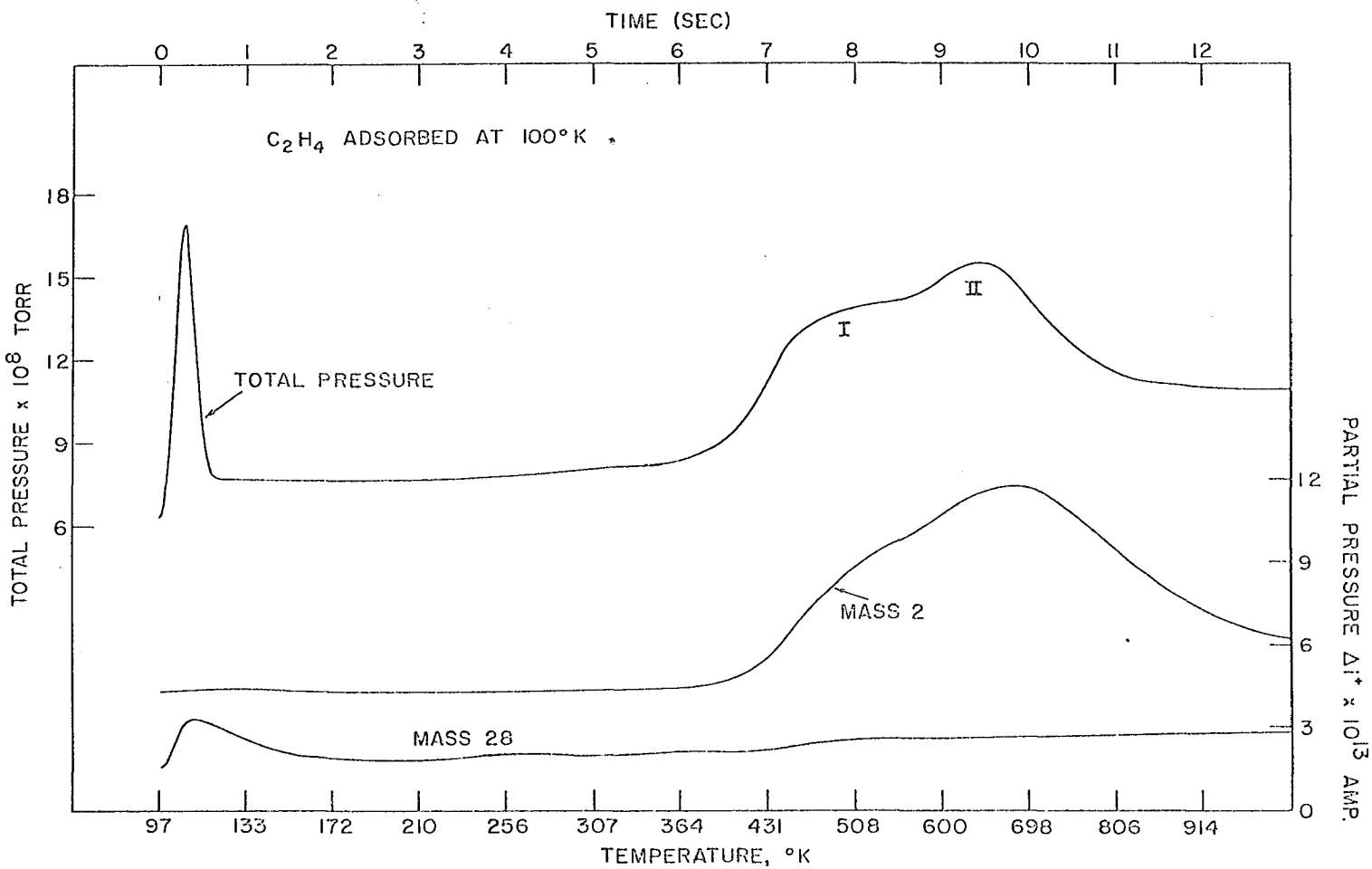

Figure 22. Total and partial pressure spectra resulting from a dose of ethylene on iridium at 95°K

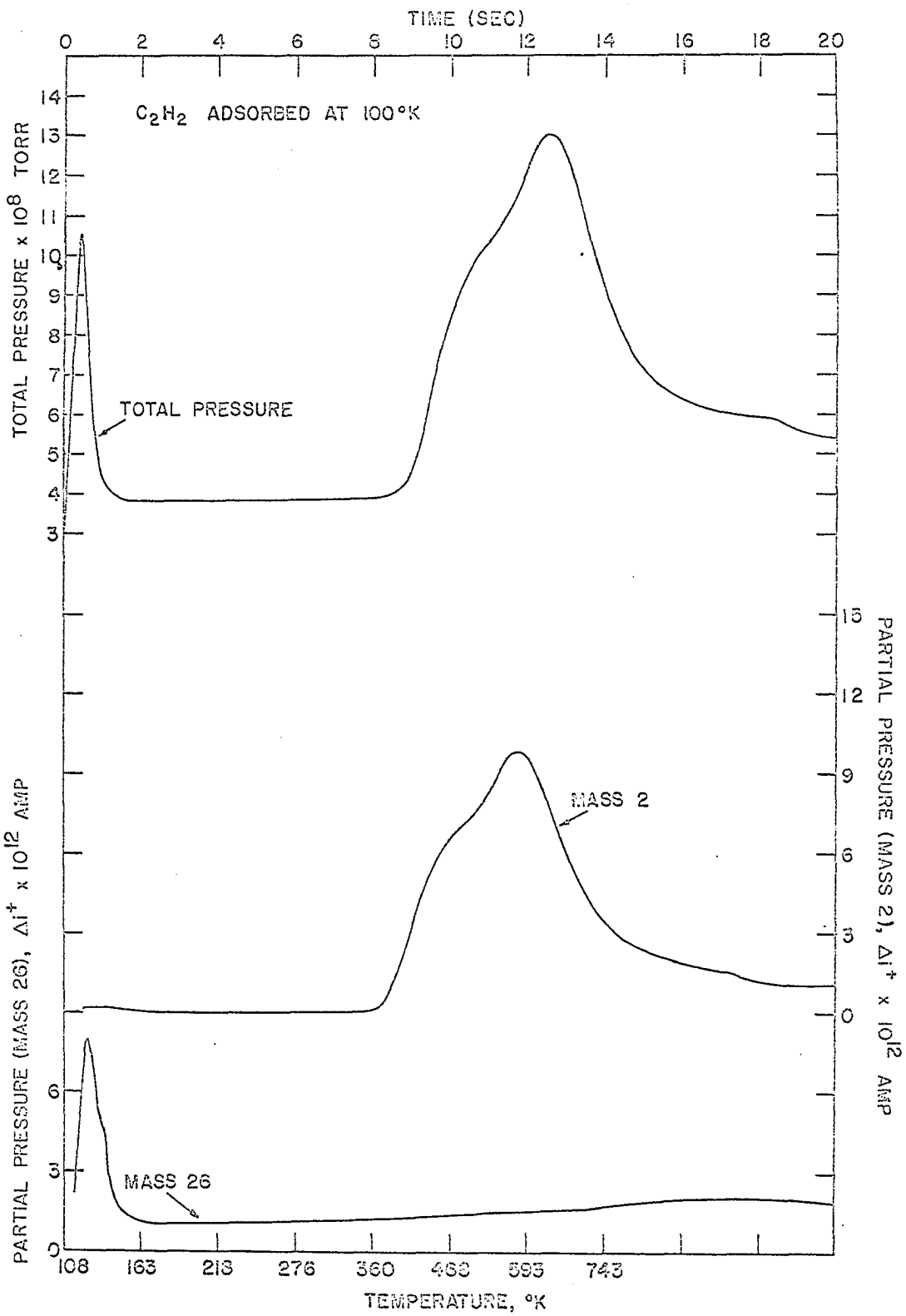

Figure 23. Total and partial pressure spectra resulting from a dose of acetylene on iridium at 95°K

acetylene spectrum is undoubtedly due to hydrogen contamination. These early experiments were conducted in the presence of a hot tungsten filament ionization gauge. As a result the ambient during a adsorption interval contained a high percentage of hydrogen. The desorption of this hydrogen, Figure 24 (19) at low coverage would occur over the temperature interval corresponding to the β_1 peak of ethylene.

The most stable surface species on tungsten result from the adsorption of ethane and methane. The flash filament spectra of both of these are shown in Figure 25. The maximum rate of the decomposition reaction does not occur until 670°K in both cases. There is a difference, however, in the low temperature detail. This detail can be seen better in Figure 26 where the ethane and methane spectra have been replotted as normalized curves on a linear temperature scale. In the methane spectrum there is a small shoulder occurring between 350°K and 500°K which is about 15 percent of the main peak at 670°K. Between 200°K and 300°K there is a small shoulder and between 300°K and 450°K there is a second partially resolved shoulder in the ethane spectrum. The temperature ranges for the two shoulders in the ethane spectrum are nearly identical to the temperature range for decomposition of ethylene on tungsten.

Figure 24. Hydrogen desorption spectra resulting from hydrogen dosed on iridium for increasing coverages at liquid nitrogen temperature. Curves are offset vertically for clarity

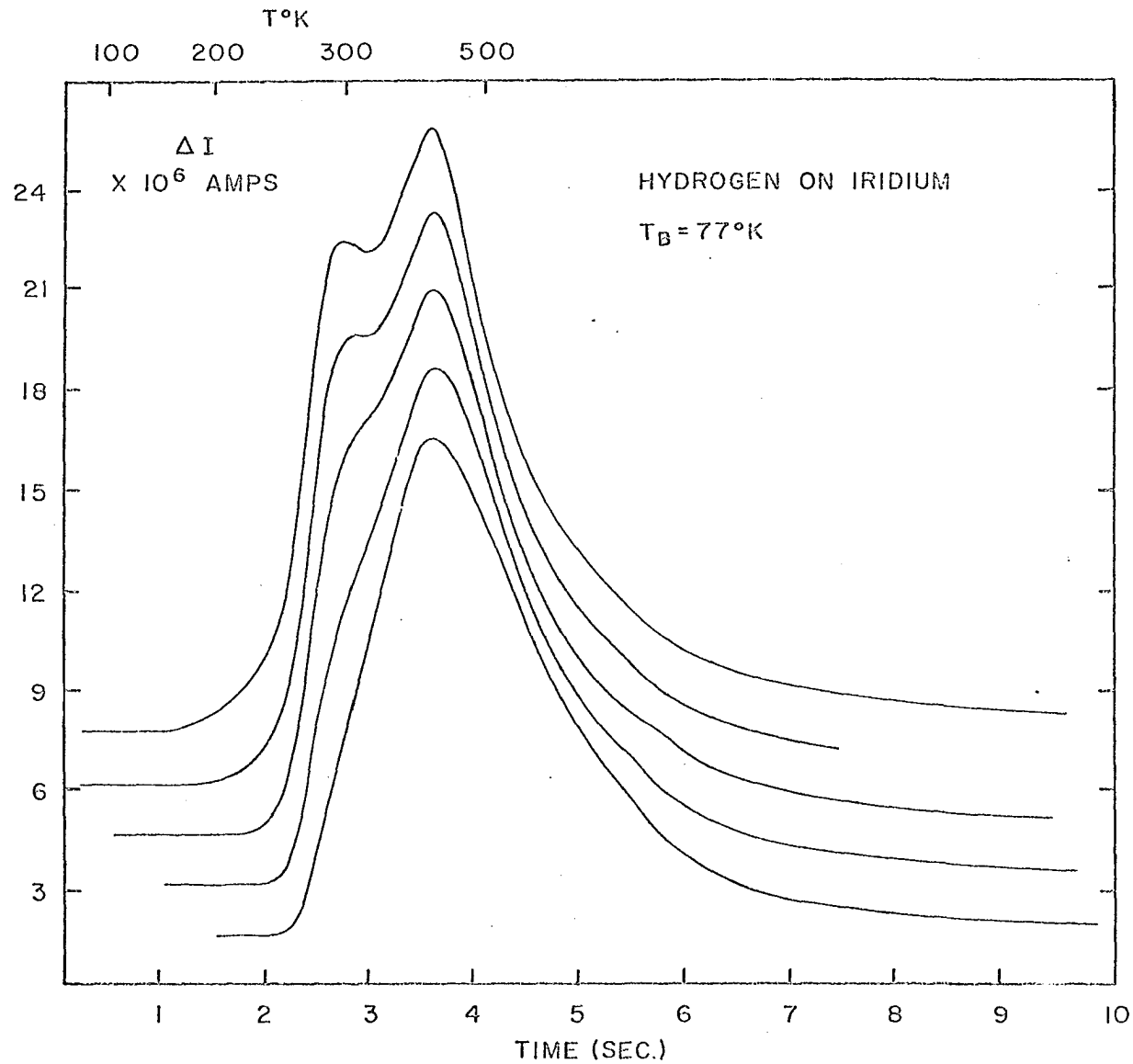
T°K
100
200
300
500
ΔI
X 10^6 AMPS
HYDROGEN ON IRIDIUM
T_B = 77°K
24
21
18
15
12
9
6
3
1
2
3
4
5
6
7
8
9
10
TIME (SEC.)

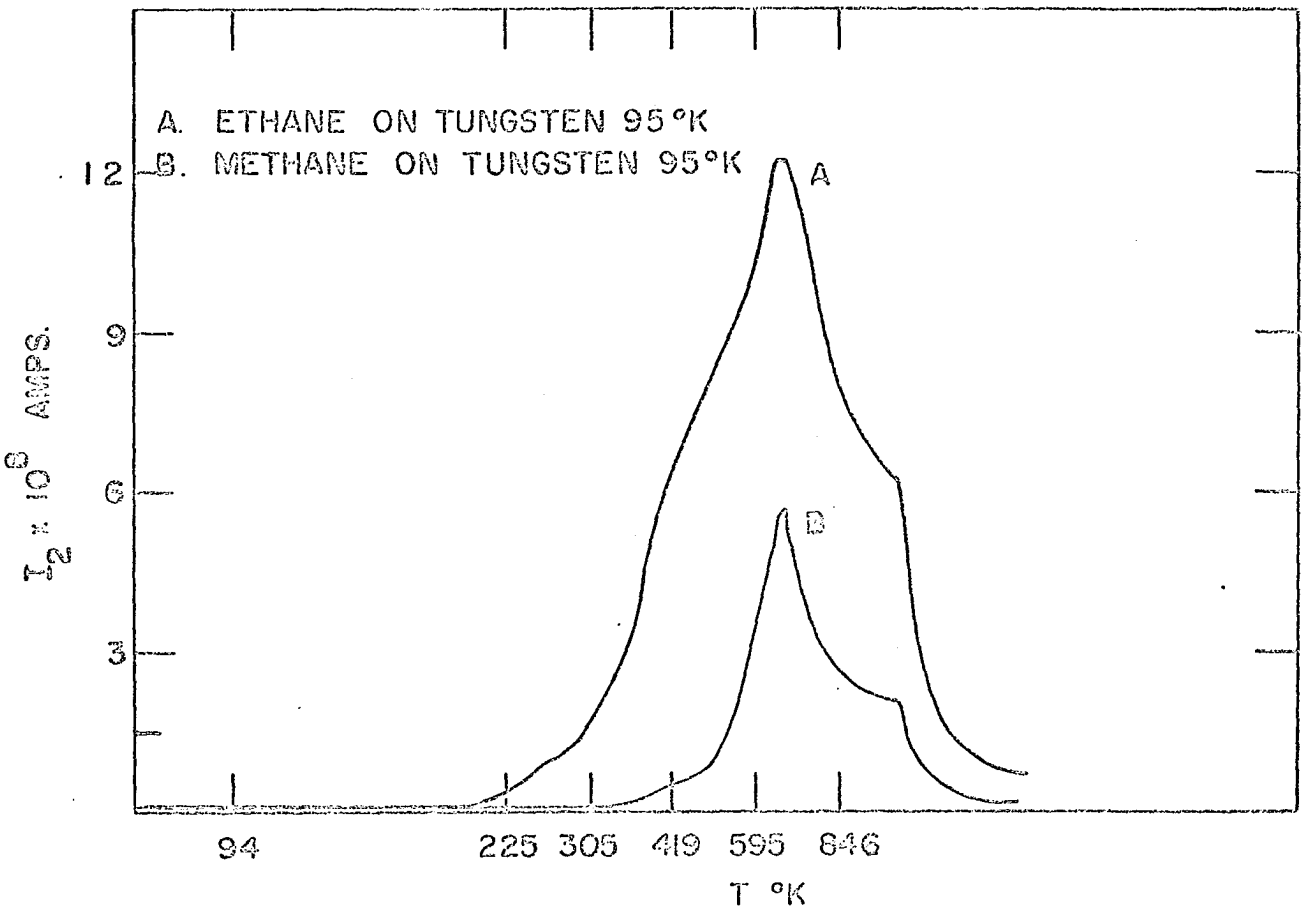

Figure 25. Hydrogen spectra resulting from the adsorption of methane, Curve B, and ethane, Curve A, at 95°K

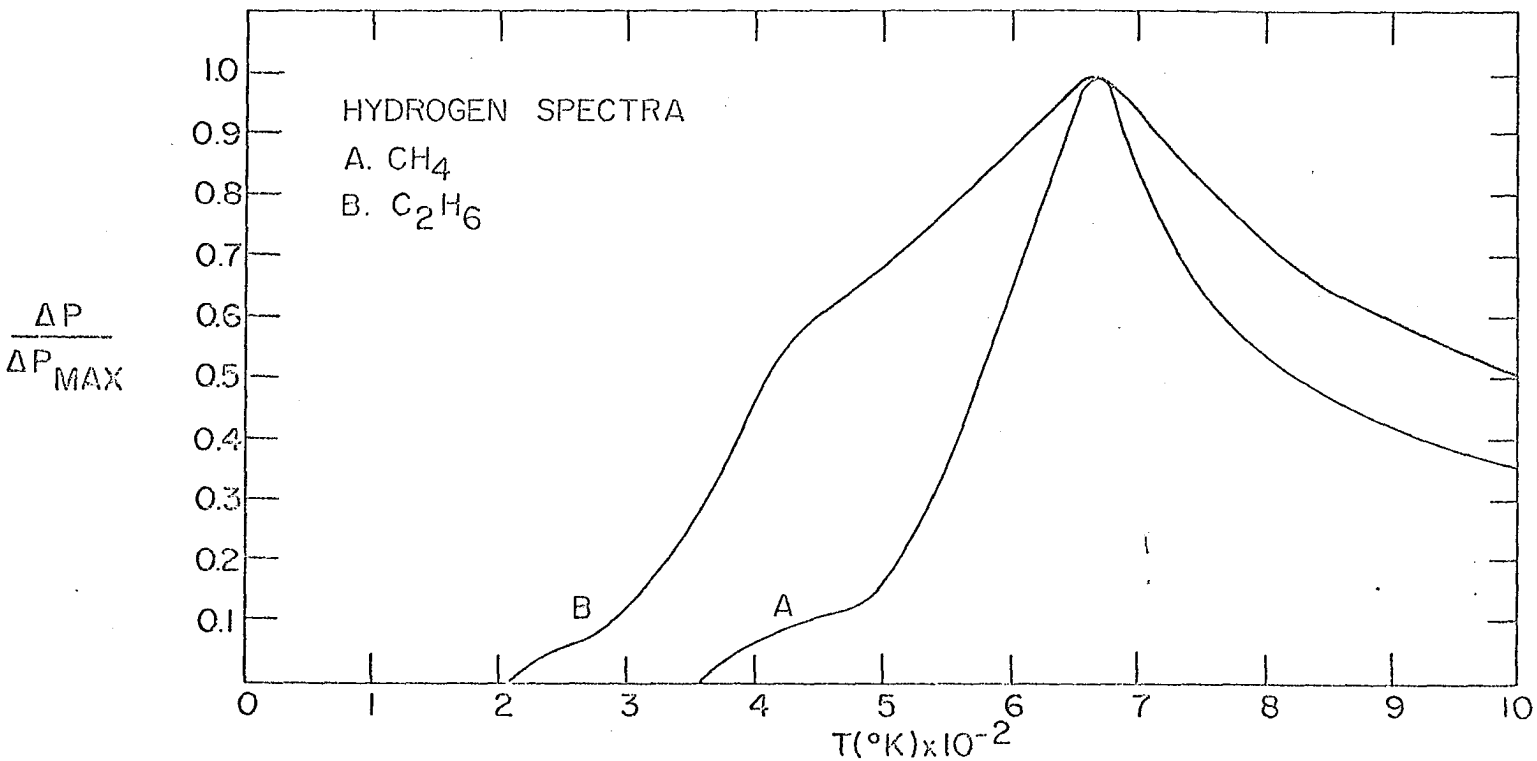

Figure 26. Normalized hydrogen spectra of methane, Curve A, and ethane, Curve B

B. Hydrogenation

If ethylene is admitted to the cell with the filament at 95°K the only reaction that occurs is chemisorption of ethylene, and the only species that is observed in the gas phase is ethylene. If the filament is predosed with hydrogen at 95°K, admission of ethylene leads to the displacement of the adsorbed hydrogen and chemisorption of ethylene. However, with filament predosed with hydrogen at 300°K admission of ethylene leads essentially to instantaneous hydrogenation. A clean surface is critical for this reaction. Regardless of the temperature of the filament, no hydrogenation is observed unless the filament has been previously cleaned of all surface species such as carbon or carbon monoxide.

The results of such a rapid hydrogenation experiment at 300°K are shown in Figure 27. The filament was cleaned at a pressure of 10^{-10} torr and allowed to cool. The valve to the pumps was then closed creating a closed system with very little pumping. A pressure of 1×10^{-6} torr of hydrogen was established in the cell saturating the surface with hydrogen. The leak to the ethylene supply was then manually opened and the partial pressure of hydrocarbon monitored continuously using the rapid scan mode of the mass spectrometer. The amplified output of the mass spectrometer was recorded on the high speed oscillographic recorder. The insert in the lower right hand corner of Figure 27 contains a short segment of the recorder mass scans taken from 61

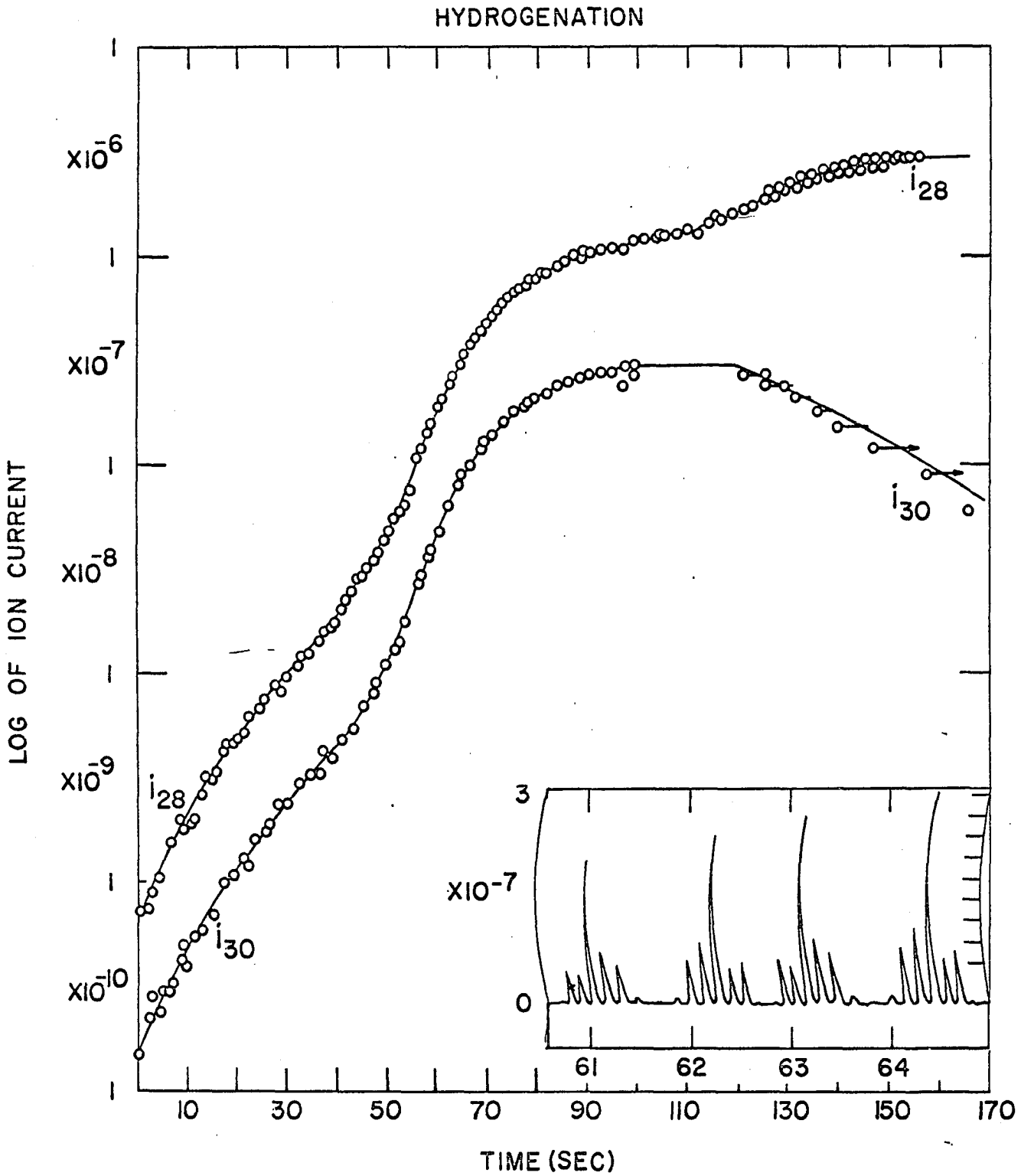

Figure 27. Mass spectrometer ion currents obtained for the hydrogenation reaction occurring during the formation of the first hydrocarbon monolayer. Interpretation of this is given in the text and in Figure 28

to 64 seconds after admitting ethylene. Mass scans covering the mass range from 24 to 31 amu were recorded in order to include the major mass peaks of acetylene, ethylene and ethane, Figure 8. From the mass scans at 62 and 63 seconds the experimental cracking patterns were calculated and these are shown in Table 3 along with cracking pattern of ethane reported in the API tables (57). From the cracking patterns it is apparent that at this point the ambient is approximately 100% ethane with no appreciable amounts of ethylene in the gas phase.

In order to determine the relative amounts of ethylene and ethane in the gas phase one need only consider the mass 28 and mass 30 ion currents. This can be seen from a consideration of the cracking patterns in Figure 8. Both ethylene and ethane have their major peaks at mass 28. However, since the mass 30 peak is unique to the ethane, the mass 30 ion current can be used to calculate the contribution in the mass 28 ion current due to ethane. For 100 percent ethane the ratio $i_{30}^{+}:i_{28}^{+}$ should be 0.26 and should decrease for increasing ethylene content. Thus only these ion currents were plotted in Figure 27. From this figure it is obvious that starting at time zero when the first increase in hydrocarbon partial pressure is observed, the ambient is composed predominantly of ethane. As the hydrocarbon partial pressure increases the ambient is predominantly ethane until the pressure reaches $1x10^{-6}$ torr. At this point the mass 30

Table 3. Experimental cracking patterns calculated from the data in Figure 27 and literature values

Mass	62 sec	63 sec	API tables (57)
31	2.0	2.2	0.5
30	26.4	25.2	26.2
29	22.5	22.0	21.7
28	100	100	100
27	36.2	36.2	33.3
26	26.9	27.5	23.0
25	4.8	5.5	4.15

ion current goes through a maximum and the mass 28 ion current continues to increase. If the valve to the pump is opened sweeping out the ambient and then closed again, the subsequent increase in pressure is due entirely to ethylene. Thus there is an extremely fast hydrogenation reaction occurring during the formation of the first hydrocarbon monolayer. However there is an equally fast poisoning of the surface for hydrogenation. If the filament is flashed after the surface poisons, the β_2 peak of ethylene, Figure 17, is obtained.

The same reaction has been run at a minimum temperature of 195°K by completely surrounding the cell with powdered Dry Ice. The same initial rapid reaction is observed. However, if the valve to the pump is opened sweeping out the ambient and then closed again, rapid hydrogenation activity continues. At 195°K the reaction does not poison

after the formation of the first monolayer. By periodically opening the valve to sweep out the ambient this reaction has been observed for as long as two hours.

The data in Figure 27 can be converted to ethane and ethylene pressures. Using the mass 30 ion current and the cracking pattern of ethane, the mass 28 ion current due to ethane is given by

$$i^{+}_{28(C_2H_6)} = 0.26\ i^{+}_{30} \tag{33}$$

Subtraction of this from the observed mass 28 ion current then gives the contribution due to ethylene. Assuming that Equation 30 holds for both ethylene and ethane, the data in Figure 27 were converted to Figure 28. Only after the hydrogenation reaction poisons is an appreciable amount of ethylene observed. During the initial portions of the reaction there is ethylene present in the gas phase. However, the amount is quite small and there is a large amount of scatter in the points. Only those points which could be used for a smooth curve were included in Figure 28. Since the reaction is occurring in a nearly closed system the approximate maximum amount of ethane produced during the reaction can be calculated. From the ideal gas law the number of molecules produced is

$$N = \frac{P_m V}{kT} \tag{34}$$

where P_m is the maximum ethane pressure (1.2×10^{-6} torr), V is the volume of the system ($\approx$1L), k is Boltzman's constant

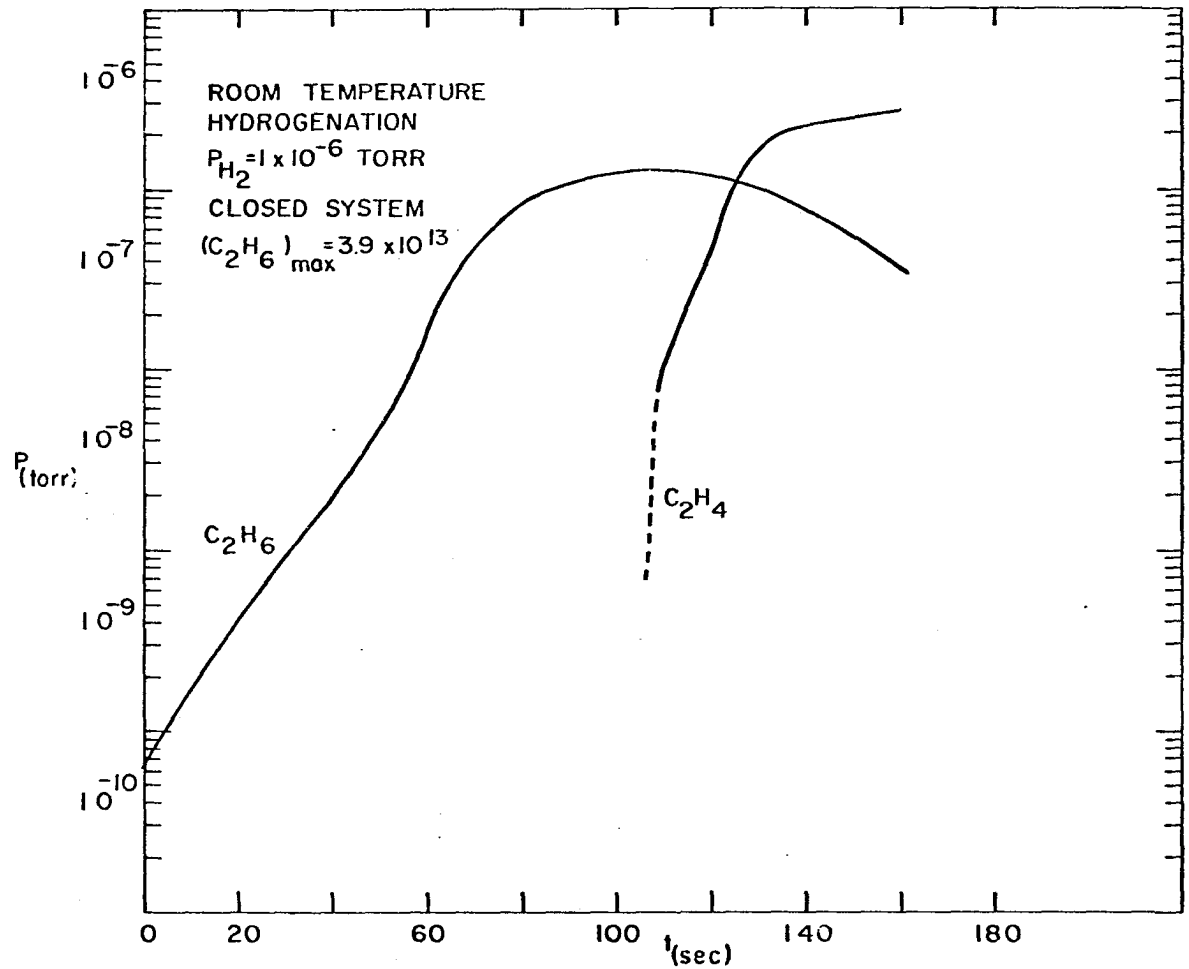

Figure 28. The experimental data in Figure 27 converted to pressures

and T is the temperature (300°K). If we assume the average density of ethylene sites to be $\frac{1}{2}N_w$ where N_w is the surface density of tungsten atoms ($1x10^{15}$ atoms/cm^2), the number of ethane molecules produced per ethylene site, Θ_c, can be defined as

$$\Theta_c = \frac{P_m V}{N_w A k T} \qquad (35)$$

where A is the geometrical area of the filament (0.8 cm^2). Since the maximum pressure of ethane obtained in Figure 28 is $1.2x10^{-6}$ torr, Θ_c is approximately 0.1.

An equally fast self hydrogenation reaction is observed when only ethylene is admitted to the clean surface at 300°K. However in this case the hydrogen is supplied by the surface decomposition reaction, and as a result there is an induction period where ethylene is observed in the gas phase. This is seen in Figure 29. The conditions for this reaction are the same as those leading to Figure 27 with the exception that no hydrogen is present in the gas phase. In this case no ethane is observed in the gas phase until the pressure has reached $1x10^{-8}$ torr at 18 sec. Ethane can be detected at this point with the first measurable amounts occurring at 19 sec. Self hydrogenation is extremely rapid after this point, but just as in the hydrogenation case the reaction poisons extremely rapidly.

The ethane and ethylene pressures corresponding to these ion currents are shown plotted in Figure 30. In the self

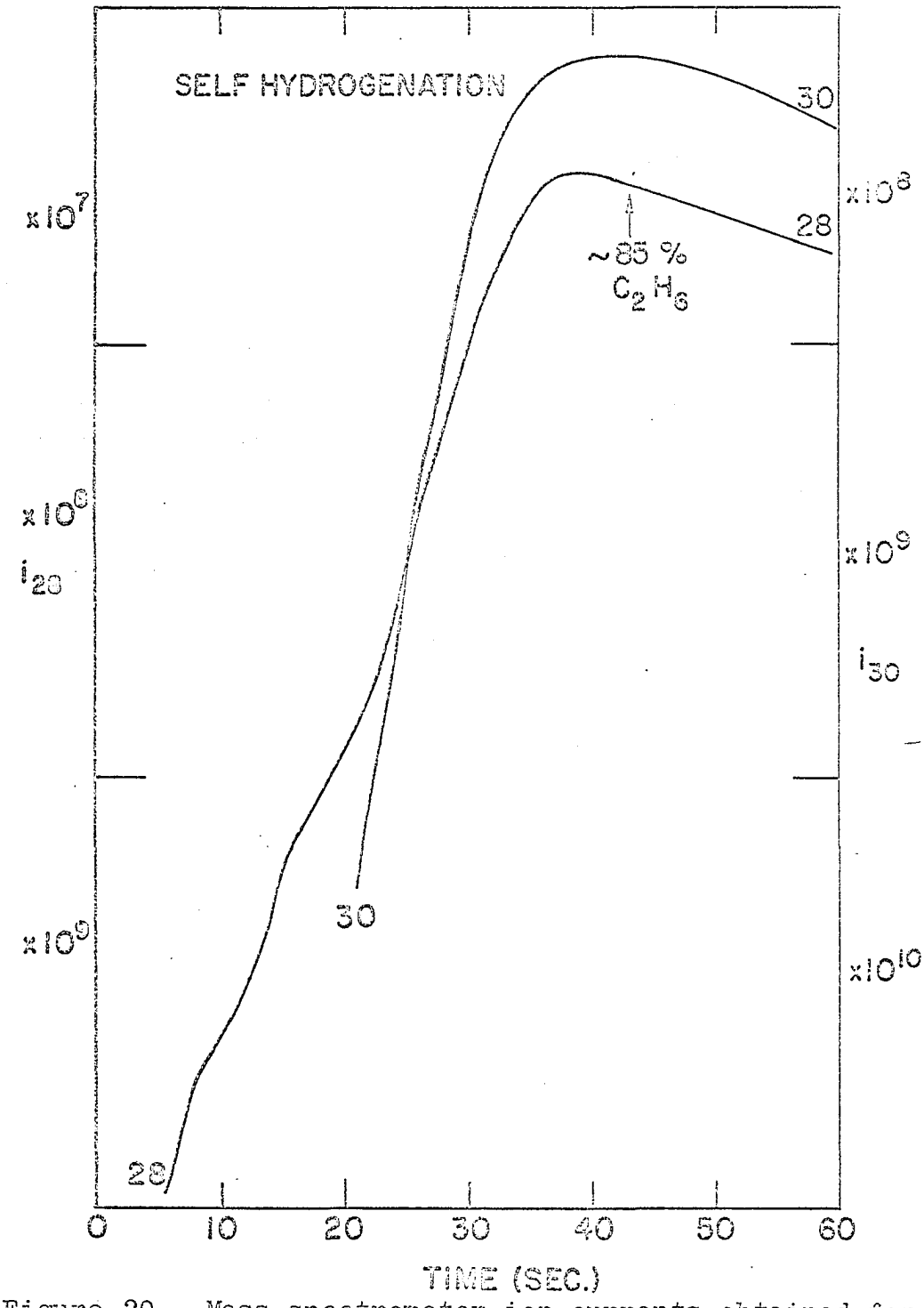

Figure 29. Mass spectrometer ion currents obtained for the self hydrogenation reaction occurring during the formation of the first hydrocarbon monolayer. Interpretation of this curve is given in the text

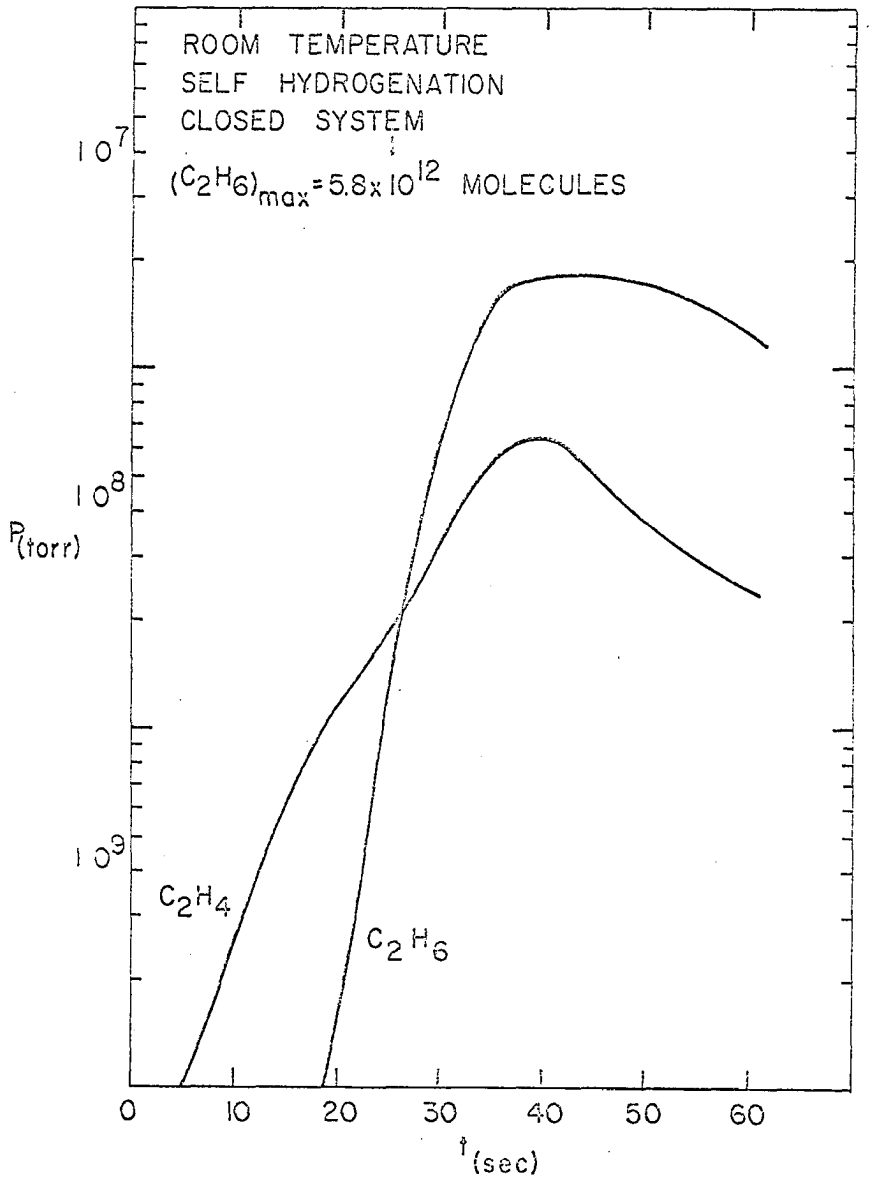

Figure 30. The experimental data in Figure 29 converted to pressure

hydrogenation case there is an appreciable quantity of ethylene in the gas phase throughout the reaction with a maximum percentage of ethane in the gas phase of only 85 percent. The maximum in the ethylene pressure in this case results from decreasing the leak at the maximum and is artificial. In separate experiments the ethylene pressure was allowed to increase past this point with a maximum still being obtained in the ethane pressure. The value of Θ_c using Equation 35 is 0.015 for the self hydrogenation case, i.e. the amount of ethane produced corresponds to 0.015 of an ethylene monolayer.

Since there is an induction period in the self hydrogenation reaction, the approximate surface coverage at the point where self hydrogenation becomes appreciable can be determined. The mass 30 ion current in Figure 29 was plotted on a linear scale from time zero to 18 seconds as shown in Figure 31. If we assume the sticking coefficient of ethylene on tungsten to be one, the number of molecules on the surface at 18 seconds can be calculated from the integrated form of Equation 3

$$n_{(C_2H_4)} = (2\pi mkT)^{-1/2} \int_o^t P(t)\, dt \qquad (36)$$

If we again assume that there are $5x10^{14}$ surface ethylene sites per cm^2 and evaluate the constant factors in Equation 36, the ethylene surface coverage, Θ_E(Θ_E = n/no. of sites/cm^2) becomes

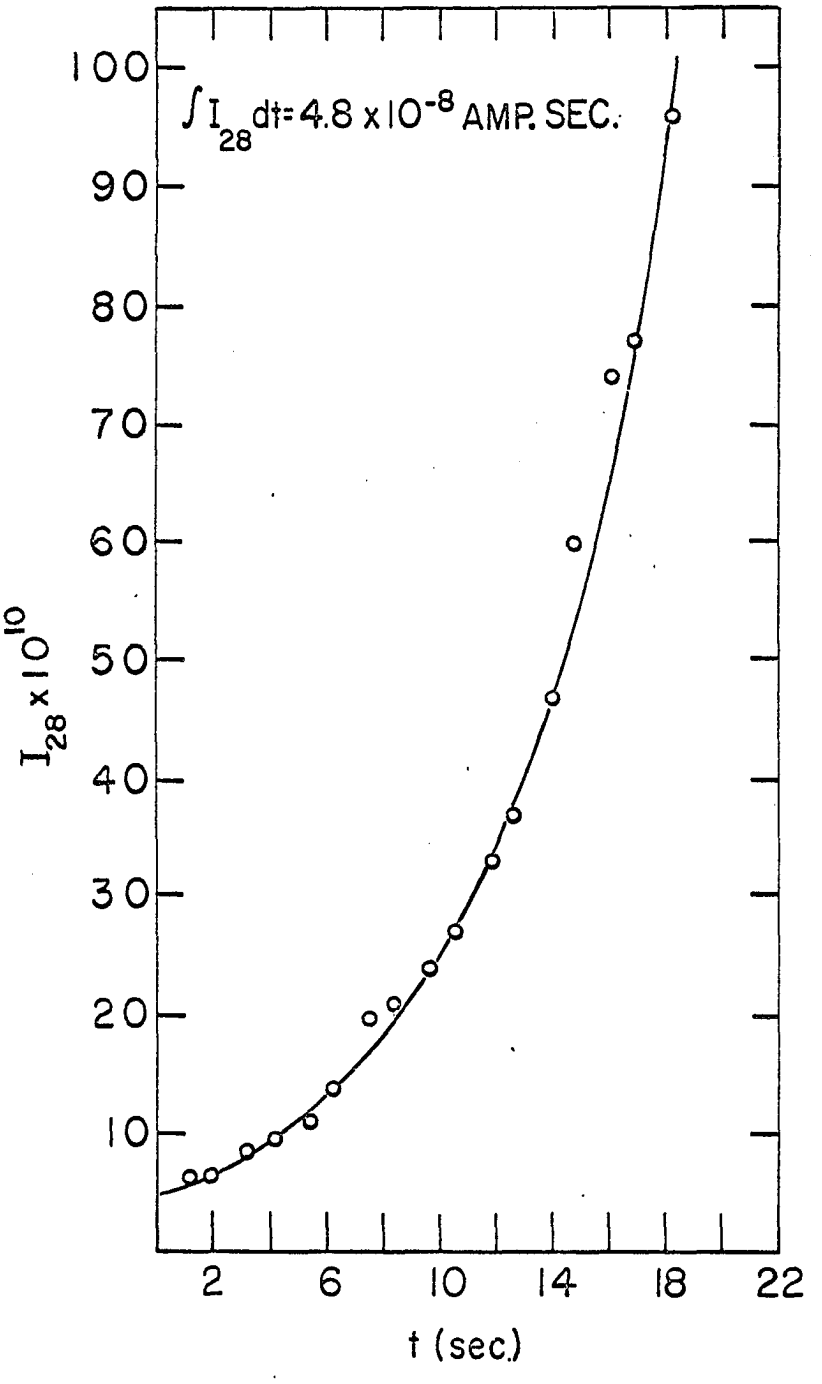

Figure 31. Increase in mass 28 ion current from Figure 30 from time zero when ethylene is first observed in the gas phase until self hydrogenation starts at 18 seconds

$$\theta_E = 7.6 \times 10^5 \int_o^t P(t)\, dt \qquad (37)$$

With the assumption that the 28 ion current is approximately the pressure, this integration has been performed by measuring the area under the curve in Figure 31. The resultant surface coverage at the point where self hydrogenation starts is approximately 3.7×10^{-3} monolayers.

V. DISCUSSION

A. Hydrogen

The major product obtained in the gas phase from the decomposition of a hydrocarbon monolayer is hydrogen. Only trace amounts of hydrocarbon species are obtained. Thus the major reason for obtaining hydrogen desorption spectra is to distinguish between hydrogen coming from the surface and hydrogen coming from the decomposition of surface hydrocarbon species.

The hydrogen desorption spectrum, Figure 9, contains three distinct peaks resulting from three forms of surface hydrogen. The two high temperature peaks β_1 and β_2 (25) and the low temperature form, α (24), have been reported previously. The α form does not isotopically exchange and results from the adsorption of either molecular hydrogen or atomic hydrogen on paired sites (19). The β forms isotopically exchange and have second order kinetics indicating that the β forms result from atomic adsorption (19, 24).

In addition to the above states breaks are observed in the P vs. T curve at 200°K and 320°K. This suggests two additional states for a total of five surface states for hydrogen on tungsten. Sachtler, et al. (58) observed a qualitatively similar set of low temperature surface states in their field emission studies of hydrogen on tungsten, provided dosing was conducted below the temperature at which

hydrogen is mobile on tungsten, ~170° (58,59). These features, however, were not found if dosing was conducted at higher temperatures, or if dosing was conducted at low temperature and the ambient hydrogen pumped away. This suggests that the adatom distribution obtained on low temperature dosing is a weak, non-equilibrium one, and that some of the adatoms may desorb while others migrate to more favorable sites as the temperature is increased during a flash. The time scale in a flash, however, is sufficiently short that temperature substantially greater than 170°K are required for appreciable migration, so that this weak non-equilibrium distribution is evident in the desorption spectrum. At extremely low coverages, Figure 10, the β_2 state is the first to fill at 95°K and is the most stable form of hydrogen on tungsten (25). The reported values of 31 to 35 Kcal/mole for the heat of desorption of hydrogen on tungsten at low coverages (19,24) corresponds to this hydrogen state.

The main features of interest in the hydrogen spectrum for catalytic hydrogenation reactions are the two β states. These appear to be two distinct atomic states. The question as to the source of the two different surface states has not as yet been resolved. In general there are two groups of models for the different hydrogen states (60). The first group has its basis in the topography of a metal surface. A metal has a distribution of metal planes consisting of metal atoms with different spacings and varying degrees of

coordination to other metal atoms. Becker states that the nucleus of the hydrogen adatom is undoubtedly below the electronic surface state (61). The hydrogen adatom however, forms a resonating σ-bond to tungsten atoms with the strength of the bond being determined by the degree of coordination of the tungsten atom to tungsten nearest neighbors. Ehrlich has shown that the three adsorption states of nitrogen on tungsten are structure sensitive (21). The second group is essentially quantum mechanical with the different states being characterised as due to different bond types. Toya (62) interprets the adsorption of hydrogen in terms of two types of bonds, r and s. The r-type bond is a resonance of the form M-H, M^--H^+ and M^+-H^- with the plane of the hydrogens above the surface. The s-type involves solution of hydrogen as protons in the metal near the surface. From this model Toya is able to calculate heats of adsorption for hydrogen on nickel of 3.0 ev/atom and 2.5 ev/atom for the r and s type of adsorption. The value of 3.0 ev/atom is in fair agreement with the heat of adsorption of 30 Kcal/mole for the adsorption of hydrogen on nickel films at low coverage (29).

Although the topography of the surface undoubtedly is of importance in the adsorption of larger molecules and especially those that form two point attachment to the surface, one would expect that due to the small size of hydrogen, solution should play a part in its adsorption. Solution has been reported to occur during flash filament experiments (63). If the β_1

and β_2 states on tungsten are equivalent to the s and r states calculated by Toya, displacement of the β_2 species would be expected by those species which form stronger σ-bonds to the surface. Rigby finds the β_2 species is preferentially displaced by CO and N_2 while the β_1 species is preferentially displaced by carbon (25), and in the present study the β_2 species is displaced by ethylene. In the present study nothing can be said concerning the lower temperature form of hydrogen since the hydrogen from the decomposition of ethylene occurs over the same temperature interval. Carbon monoxide adsorbs by forming σ-bonds to the surface (36,64) while carbon may be present on the surface in intersitial positions (65). The limiting factor in the cleaning of a tungsten surface through oxygen treatment is the interstitial diffusion of carbon to the surface (65,66).

B. Flash Decomposition of Ethylene and Acetylene

If adsorption of ethylene and acetylene is carried out at sufficiently low temperature, chemisorption is associative and probably occurs through opening of the unsaturated bond to form carbon-metal σ-bonds.

$$C_2H_4(g) \rightarrow \overset{*}{C}H_2\text{-}\overset{*}{C}H_2 \qquad (38)$$

$$C_2H_2(g) \rightarrow \overset{*}{C}H\text{=}\overset{*}{C}H \qquad (39)$$

Following common practice the stars are used to represent bonding to the surface. Adsorption at 95°K, as in this study, does give associative adsorption on tungsten. This

can be seen from Figure 32 where the field emission work function plot for the decomposition of ethylene (44) is shown superimposed on the normalized hydrogen decomposition spectrum. The work function is flat below 200°K indicating that there have been no changes on the surface below 200°K other than the chemisorption of ethylene which gives the large drop in work function. Above 200°K the detail in the surface work functions is reflected in the flash filament spectrum. This same parallel between the surface work function and flash filament spectrum is seen in the case of acetylene, Figure 19. As a result of low temperature associative adsorption side effects such as self hydrogenation are eliminated.

The surface hydrocarbon species are shown in Equations 38 and 39 as σ-bonded to surface metal atoms. This has been generally the most widely accepted bonding model for the adsorption of unsaturated molecules (37,40,64,67). However, recently a π-complex mode of adsorption represented by

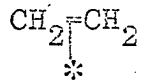

has been preposed (68,69). The case for π-complex adsorption is based mainly on analogy to the olefinic complexes of transition metals which are catalytically active in the liquid phase (70). However the infrared spectrum of the associative form of ethylene on Pd has been shown to be identical to the infrared spectrum of $C_{100}H_{202}$ (40) which indicates that in the associative form chemisorbed ethylene consists of methylene groups.

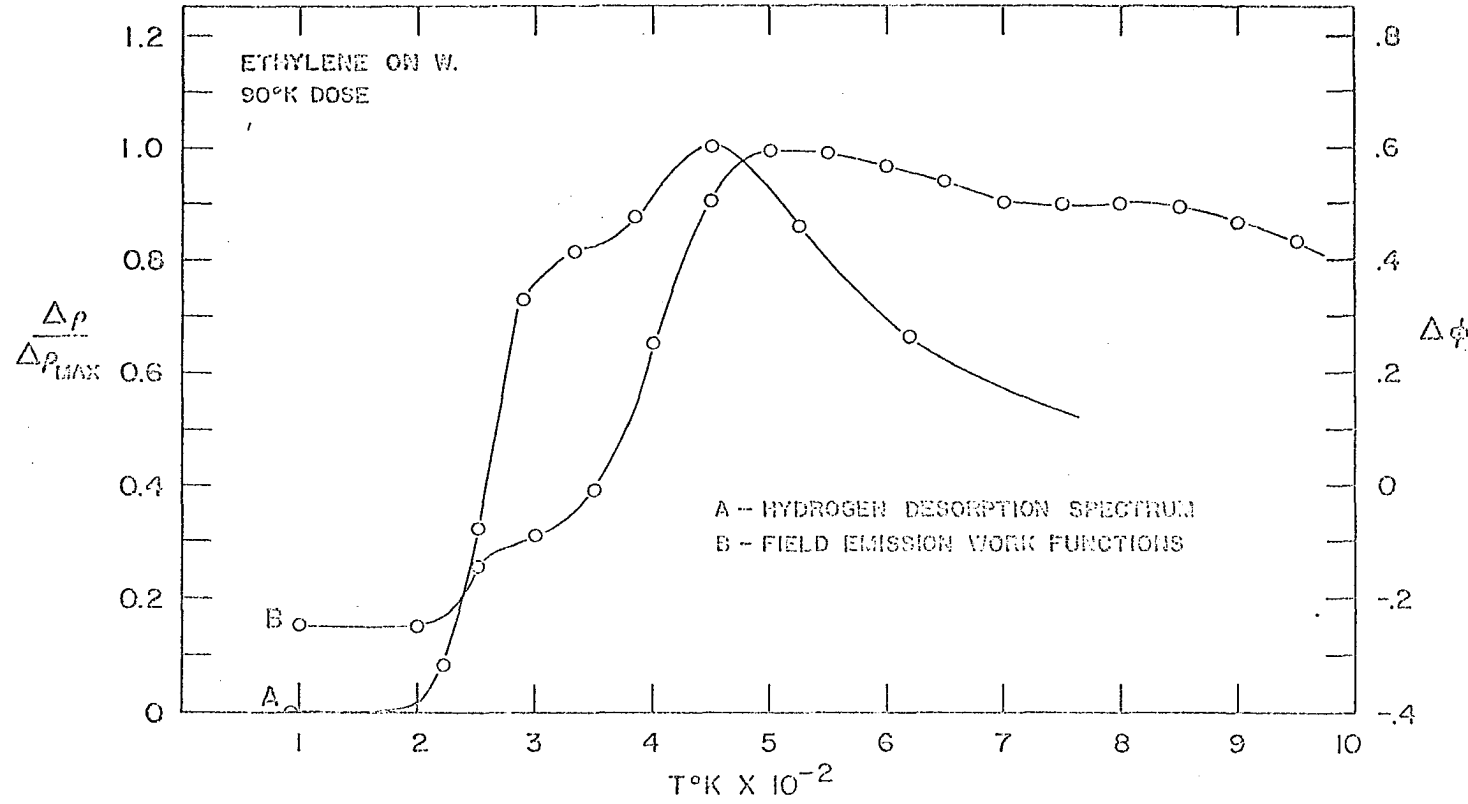

Figure 32. Hydrogen spectrum resulting from a monolayer of ethylene on tungsten formed at 95°K, Curve A. Curve B is the field emission work function curve for the decomposition of an ethylene monolayer (44). The right hand scale is associated with Curve B

Gardner found from field emission migration studies that the (110) plane of tungsten does not act as an area of high site density for ethylene (44). From this Gardner rules out a π-complex since this bonding mode apparently requires that the highest site density occur on the most dense planes. Migration studies of benzene on tungsten, however, seem to indicate π-bonding to the surface (71). The migration boundary of benzene is straight indicating no site preference as expected from a π-bonded benzene.

The flash filament decomposition spectrum of ethylene on tungsten is given in Figure 11. From the ratio of the peak heights the simplest interpretation for this spectrum is a two step dehydrogenation of the adsorbed ethylene to give the two hydrogen peaks, β_1 and β_2, in the gas phase. The symbols β_1 and β_2 refer respectively to the low and high temperature peaks. Starting at 200°K the loss of the first mole of hydrogen occurs leaving a residue with the stoichiometry of acetylene.

$$\overset{*}{C}H_2\text{-}\overset{*}{C}H_2 \xrightarrow{>200^\circ} \overset{*}{C}H{=}\overset{*}{C}H + 2\overset{*}{H} \qquad (40)$$

Continued heating above ~300°K results in the hydrogenation of the acetylenic species leaving a residue of carbon on the surface.

$$\overset{*}{C}H{=}\overset{*}{C}H \rightarrow (\overset{**}{C}_2) + 2\overset{*}{H} \qquad (41)$$

The hydrogen is written as σ-bonded to the surface. However, the residence time of hydrogen on the surface is short, with

the decomposition of the surface hydrocarbon and not the desorption of hydrogen being the rate limiting step for appearance of H_2 in the gas phase. Coverage experiments with mixtures of hydrogen and ethylene show that the high temperature forms of hydrogen are displaced by ethylene. This would be expected from the relative heats of adsorption of hydrogen and ethylene (29). During a flash the surface sites available to hydrogen are low energy sites from which hydrogen immediately desorbs. The cleaning process may well involve diffusion of carbon into the bulk as well as vaporization of the carbon. The temperature at which the filament is cleaned would decompose and vaporize any carbides formed (72). However, periodic cleaning in an oxygen ambient leads to the production of CO for as long as 24 hours. Only after the carbon content of the filament is depleted does the production of CO cease (65,66). The surface, however, can be cleaned by simply flashing rapidly to the cleaning temperature. The ethylene desorption spectra obtained after cleaning in oxygen are identical to the spectra obtained after thermal cleaning.

Reactions 40 and 41, however, do represent the overall stoichiometry of the decomposition reactions of ethylene and acetylene dosed at 95°K. Comparison of Figures 11 and 21, ethylene and acetylene decomposition spectra obtained following identical adsorption conditions, show that approximately the same amount of hydrogen is contained in the single

acetylene peak and the β_2 peak of ethylene. Figure 20 which is a superposition of the normalized acetylene curve and the normalized β_2 peak of ethylene remaining after removal of the β_1 peak also emphasises the close agreement between the two in terms of surface stability. For a monolayer formed at 95°K one has the same number of surface sites for both acetylene and ethylene. This could be just a frozen structure due to adsorption at 95°K. However the hydrogen decomposition spectrum from a room temperature dose of ethylene, Figure 17, also is in agreement with the acetylenic peak from a 95°K dose of ethylene or acetylene. From the hydrogen decomposition spectra ethylene and acetylene appear to occupy the same number of surface sites, and the simplest interpretation is that they occupy the same surface sites.

The spectrum resulting from the flash decomposition of ethylene on iridium, Figure 22, shows the same two peak structure resulting from a two step decomposition reaction. The major difference between the spectra obtained on iridium and tungsten is the temperature at which decomposition starts: 400°K in the case of iridium vs. 200°K in the case of tungsten. Thus the associative form of ethylene is stabilized to a greater extent on iridium than on tungsten.

The surface structures for diadsorbed ethylene and acetylene are shown in Figure 33. Due to free rotation around the C-C single bond ethylene is able to accommodate on a wide range of available spacings (44). On short metal-

Figure 33. Surface geometry of adsorbed ethylene and acetylene. Top row: "trans" adsorption across long spacings. Bottom row: "Cis" ethylene adsorption across short spacings and adsorbed acetylene

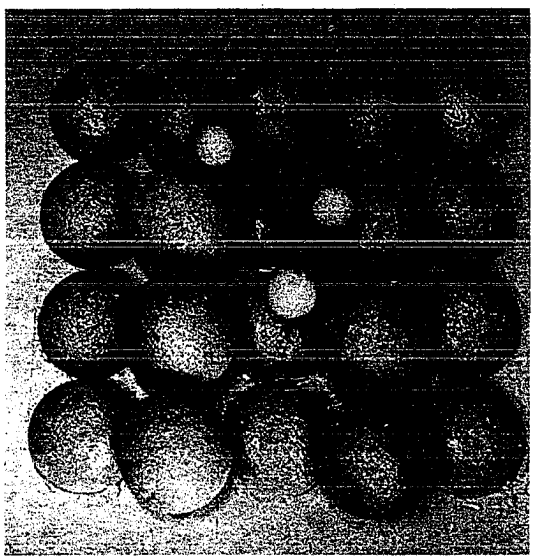

"trans" adsorbed ethylene

top view

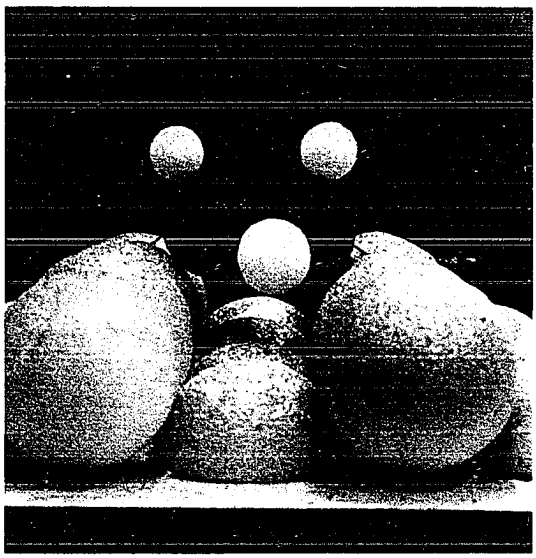

"trans" adsorbed ethylene

side view

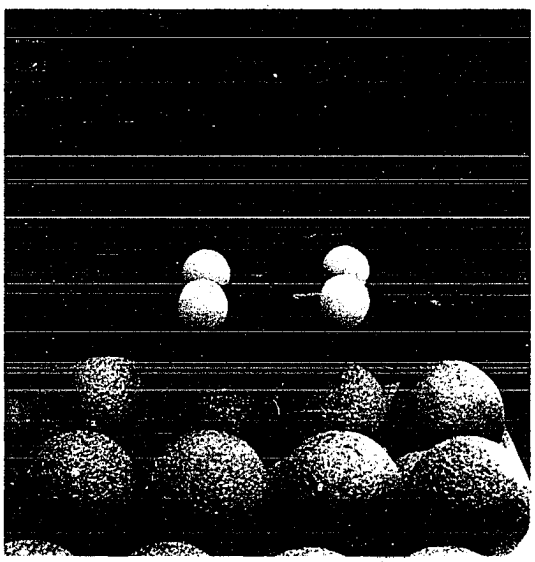

"cis" adsorbed ethylene

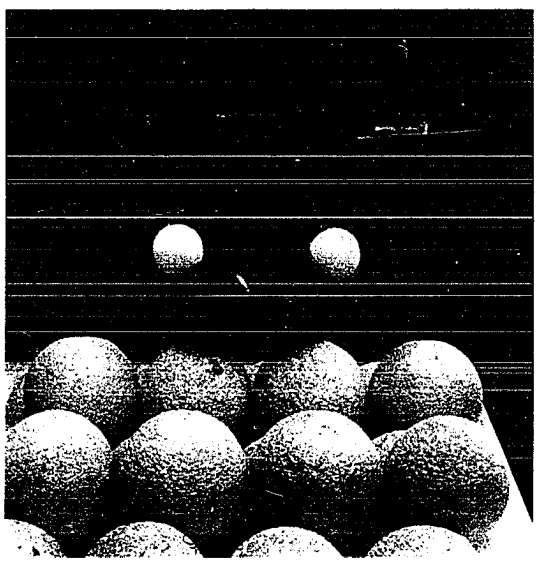

adsorbed acetylene

metal spacings ethylene can adsorb in the cis-configuration where the carbon and metal atoms are in the same plane and the hydrogen atoms are fully eclipsed. On long spacings ethylene could adsorb in the trans-configuration. From the geometrical representation in Figure 34 the optimum metal-metal distance would be given by

$$d_{M-M} = d_{CC} + 2d_{C-M} \sin (\gamma - 90°) \qquad (42)$$

where γ would be 120° for acetylene and 109° for ethylene in the fully eclipsed form. For purposes of calculation the following values for metallic and covalent radii were used (73): carbon single bond, 0.772Å; carbon double bond, 0.667Å; tungsten, 1.304Å. From Equation 42 the optimum metal distance for adsorption of acetylene without strain is 3.41Å. Since the metallic radii of the transition metals change only slightly this distance will be a good approximation for the fcc and bcc transition metals. For ethylene the optimum metal-metal distance in the eclipsed form is 2.89Å.

One must now consider two cases for ethylene decomposition: (1) the available spacings are $>$ 2.89Å and (2) the available spacings are $\leq$ 2.89Å. For this consideration we will assume that the surface dehydrogenation of the adsorbed ethylene occurs through the formation of a transition state complex with surface metal atoms. If we consider just one carbon and one hydrogen this transition state can be depicted as follows

Geometrical model for hydrocarbon adsorption
γ = 109° for ethylene, 120° for acetylene.

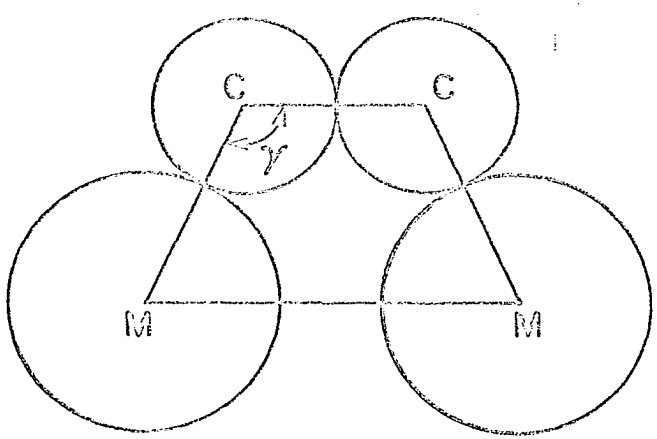

Figure 34. Geometrical model used to calculate the optimum metal-metal distances for adsorption of ethylene and acetylene

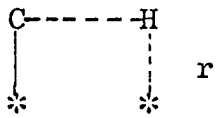

with small values of r aiding formation of the transition state.

For the first case where the available spacings are >2.89Å, ethylene is able to bond across these long spacings by rotating about the carbon-carbon bond. This would give the "trans" species shown in Figure 33 with two of the ethylene hydrogens directed down into the trough between rows of surface atoms in the extreme case and a small value of r. This structure would be favorable for the decomposition of surface ethylene. For the second case, where the available spacings are $\leq$ 2.89Å, ethylene would bond in the eclipsed form if angular strain is not too great. In this configuration the hydrogens would be equally far removed from the surface decreasing the probability for formation of the transition state, and favoring the associative adsorption of ethylene.

Figure 35 gives the surface topography for a representative bcc metal (W) and a fcc metal (Rh). Only the (100), and (110) and (111) planes are shown since the higher index planes will be composed of the same and longer spacings. For the bcc metals there is only one spacing on these three planes which would fit case 2. From the foregoing one would expect a greater probability of ethylene decomposition on bcc metals such as tungsten. The fcc metals, however, are rich in the short spacings. All three planes contain

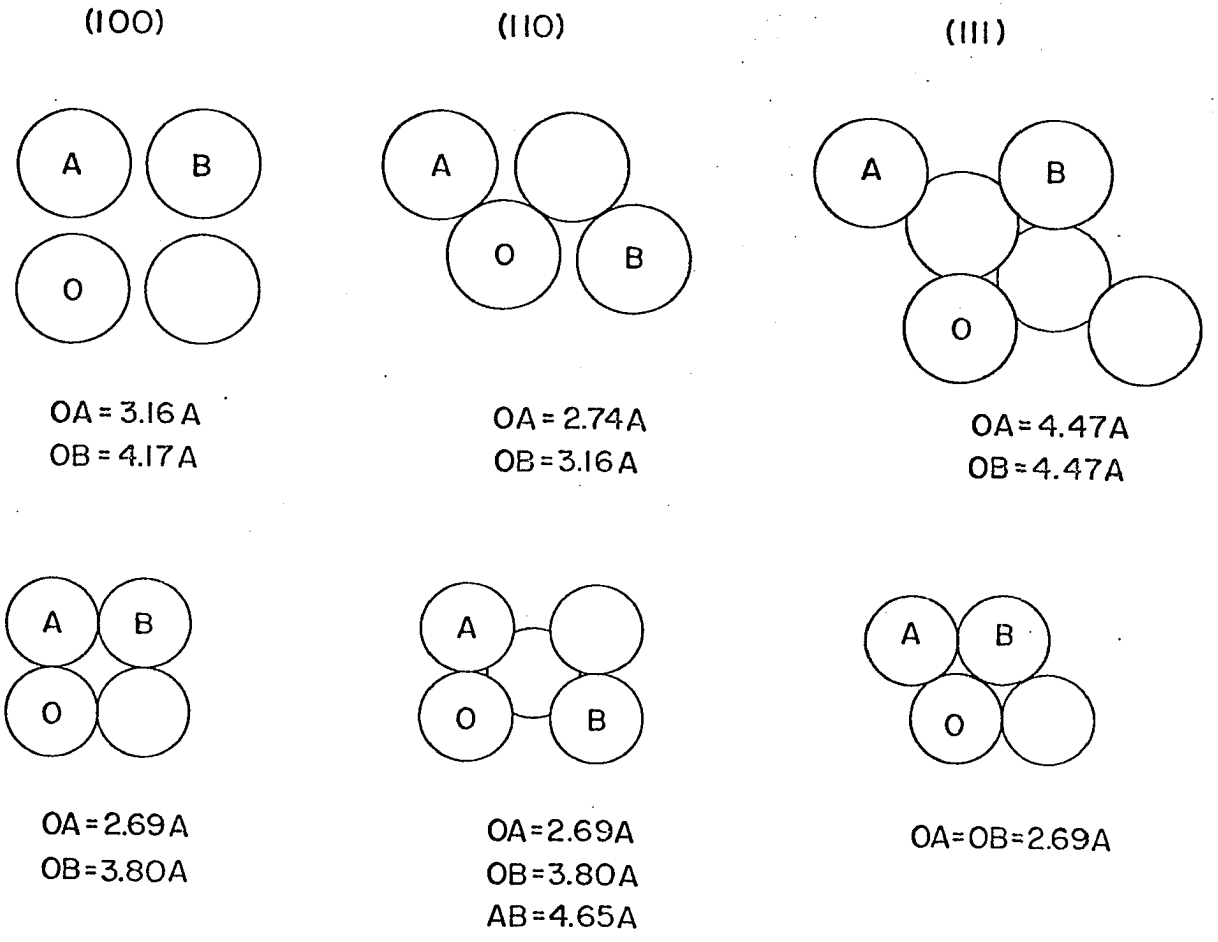

Figure 35. Spacings and geometry for the three low index planes of tungsten (top row) a bcc metal and of rhodium (bottom row) a fcc metal. The figures below each plane are the metal-metal distances available on that plane

spacings less than the minimum distance of 2.89Å for ethylene, and the 2.69Å spacings of rhodium would allow adsorption of ethylene with only 3° of strain. In the case of the fcc metals ethylene adsorption should be preferentially associative. The experimental evidence for the decomposition of ethylene on tungsten (bcc) and iridium (fcc) is in agreement with the above observations. Ethylene decomposes on W at 200°K, Figure 11, and on iridium at 400°K, Figure 22.

C. Flash Decomposition of Ethane and Methane

According to Bond there is no question but that the initial step in the adsorption of a saturated hydrocarbon is a dissociative process in which a carbon-hydrogen σ-bond is broken (2). In the case of methane the adsorption reaction would be

$$CH_{4(g)} \rightarrow \overset{*}{C}H_3 + \overset{*}{H} \qquad (43)$$

Exchange experiments which yield predominately CH_3D on tungsten at 423°K (74) strongly indicate a surface methyl group. In the flash filament spectrum, Figure 25, the low temperature shoulder results from the desorption of surface hydrogen and the high temperature peak at 670°K results from the decomposition of the methyl group.

The initial step in the adsorption of ethane also occurs through the breaking of a carbon-hydrogen bond to give

$$C_2H_{6(g)} \rightarrow \overset{*}{C}H_2\text{-}CH_3 + \overset{*}{H}. \qquad (44)$$

However, in the early portions of the formation of the chemisorbed monolayer when the adsorbed ethyl group has bare surface available, a second reaction with the surface is possible.

$$\overset{*}{C}H_2\text{-}CH_3 \longrightarrow \overset{*}{C}H_2\text{-}\overset{*}{C}H_2 + 2\overset{*}{H} \qquad (45)$$

For adsorption below 200°K where decomposition of ethylene does not occur, the surface species would be ethyl radicals resulting from reaction 44 and adsorbed ethylene resulting from reaction 45. The subsequent flash decomposition spectrum should then be a composite resulting from the decomposition of the ethylene and ethyl groups. In the decomposition spectrum of adsorbed ethane, Figure 25 or 26, the two low temperature shoulders are assigned to ethylene and the high temperature peak is assigned to the decomposition of the ethyl group.

Kemball reports that on tungsten deuterium exchange experiments below 400°K give predominantly d_1-ethane but are complicated by cracking of ethane to methane above 400°K (75). At 450°K on tungsten a 12 to 1 hydrogen-ethane mixture gives 100 percent methane (76). However, hydrocracking reactions on metals are accompanied by rapid poisoning of the surface due to the formation of carbon deposits (2). From the flash decomposition spectrum, the decomposition of surface ethyl group is appreciable somewhat above 400°K. The temperature at which decomposition starts cannot be estimated with any accuracy due to interference from the decomposition of surface ethylene.

If we assume that the rate limiting step in the decomposition of both the surface methyl and ethyl groups is the removal of the first hydrogen from the carbon atom bonded to the surface, one can explain the above results and the decomposition of ethane and methane. The analogy here is to the decreasing bond dissociation energies in the sequence $CH_3 > CH_2 > CH$ (77). Thus if sufficient energy is present to remove one hydrogen from $-CH_3$, the removal of the remainder will be fast.

$$\overset{*}{C}H_3 \xrightarrow{\text{slow}} \overset{*}{C}H_2 + \tfrac{1}{2}H_2\uparrow \xrightarrow{\text{fast}} (C) + H_2\uparrow \qquad (46)$$

The surface is of course an active participant in the removal of the hydrogen. If the rate limiting step in the decomposition of the ethyl radical is also the removal of the first hydrogen, the loss of the second again will be fast. However, during the decomposition the second carbon will be forming a transition state with the surface

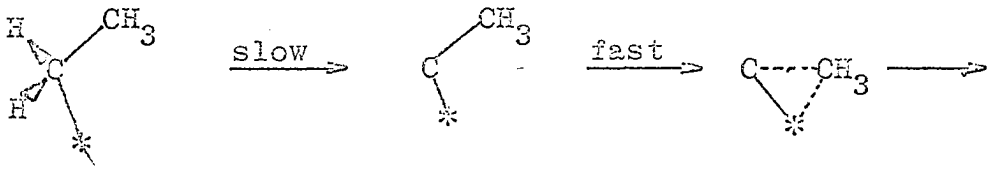

$$(C) + \overset{CH_3}{\underset{|}{\overset{*}{}}} \qquad (47)$$

with the carbon atom left from rupture of the carbon-carbon bond going into solution either in the interface or in the bulk. In a flash experiment, since the temperature is rising continually, the resultant methyl group would also rapidly decompose.

As a result of the same rate limiting step in the decomposition of both the ethyl and methyl groups, the spectra in both cases should consist of a single hydrogen peak occurring over the same temperature interval. If a large excess of hydrogen is present, as in hydrocracking experiments, the transition state in 47 would be very liable to attack by surface hydrogen. This would result in the production of one methane molecule and one surface carbon for each ethane molecule, accounting for both the hydrocracking of ethane over tungsten (76) and the rapid carbiding of the surface (2). In addition, since we know that adsorbed ethylene irreversibly decomposes above 200°K, the surface species would be the acetylenic residue from reaction 38 and the frozen in ethyl group from reaction 44. The only active surface species would be the ethyl group and deuteration experiments would give predominantly d_1-ethane as observed by Kemball (75).

D. Hydrogenation and Self Hydrogenation

On clean tungsten both hydrogenation, Figure 28, and self hydrogenation, Figure 30, are immeasurably fast at 300°K during the formation of the first hydrocarbon monolayer. This instantaneous hydrogenation of ethylene has been observed previously on tungsten and other metals (29,30,37) and has been used as experimental evidence for the Rideal-Eley type mechanisms where the formation of ethane results from a reaction between gaseous ethylene and chemisorbed hydrogen. Beeck interpreted this fast reaction as occurring between

gaseous ethylene and chemisorbed hydrogen on adjacent sites (29). Beeck points out, however, that ethylene competes strongly with hydrogen for surface sites vacated by impact hydrogenation, so that eventually a certain rate of hydrogenation of chemisorbed ethylene will be necessary to maintain hydrogen sites for impact hydrogenation. Jenkins and Rideal (38) are also in favor of an impact hydrogenation step but with a modification to account for deuterium experiments in which ethylene exchange is observed.

However, on the basis of the self hydrogenation reaction which is equally fast, order of magnitude calculations can be used to negate a Rideal-Eley (RE) type mechanism, and to support a Langmuir-Hinschelwood mechanism involving a reaction between chemisorbed species. If we first assume a RE type mechanism where hydrogenation occurs through the collision of a gaseous ethylene molecule with hydrogen on paired sites, the maximum rate should be the rate of ethylene arrival at the surface multiplied by the probability of impacting two hydrogen atoms on arrival. The ethylene impact rate per cm^2 follows from kinetic theory:

$$\text{Impact rate} = \frac{P_{(C_2H_4)}}{\sqrt{2\pi mkT}} \qquad (48)$$

If every impact produced an ethane molecule the rate of change of ethane pressure would be

$$\frac{dP(C_2H_6)}{dt} = \frac{kT}{V} \frac{P(C_2H_4)}{\sqrt{2\pi mkT}} \tag{49}$$

Then using compatible units and the experimental volume of 1L the maximum rate becomes

$$\frac{dP(C_2H_6)}{dt} = 12P(C_2H_4) \tag{50}$$

At the point where self hydrogenation becomes appreciable the hydrogen surface coverage is at most 0.04 monolayer. The probability of an ethylene molecule hitting two sites both occupied with hydrogen would then be $(0.04)^2$. Equation 50 then becomes

$$\frac{dP(C_2H_6)}{dt} \simeq 12\ (0.04)^2\ P(C_2H_4) \tag{51}$$

The pressure at the point in Figure 30 where self hydrogenation becomes appreciable is $1x10^{-8}$ torr which, when inserted Equation 51, gives as the upper limit for the rate of hydrogenation

$$\frac{dP(C_2H_6)}{dt} \simeq 1.9x10^{-10} \text{ torr/sec.} \tag{52}$$

Since the observed rate is obviously greater than this, Figure 30, a Rideal-Eley type mechanism involving gaseous ethylene picking up two hydrogens from the surface cannot account for it.

A Langmuir-Hinshelwood type surface reaction, in which the ethylene molecule is allowed to adsorb and then be

hydrogenated as a result of a collision between a highly mobile hydrogen adatom (59,60) and immobile adsorbed ethylene, can account for the observed rate. If we assume such a model, the number of effective collisions of hydrogen with ethylene can be formulated using a two dimensional collision theory model. A mobile hydrogen atom will sweep out an area of the surface given by

$$\text{area/sec} = vr \tag{53}$$

where v is the hydrogen velocity and r is the collision cross section for a collision between hydrogen and ethylene. There are N_W tungsten sites/cm^2 and we will assume that two are required for each ethylene and one for each hydrogen adatom. The total number of collisions, z, then becomes

$$z = \frac{1}{2}\,\Theta_H \Theta_E N_W^2\, v\, r \tag{54}$$

where Θ_E and Θ_H are the ethylene and hydrogen surface coverages. Let $\Delta H^{\ddagger}$ be the energy barrier a collision must overcome for reaction. Then the number of ethane molecules produced per cm^2 per sec should be

$$\frac{d(C_2H_6)}{dt} = \frac{1}{2}\,\Theta_H\,\Theta_E\, v\, r \exp\left(-\frac{\Delta H^{\ddagger}}{RT}\right) \tag{55}$$

The activation energy for hydrogen diffusion is given as 9.5 kcal/mole at intermediate coverages (60). The velocity of a surface hydrogen is then given by

$$v = d\upsilon \exp\left(-\frac{\Delta H_d}{RT}\right) \tag{56}$$

where d is the jump length and υ is the jump frequency.

Equation 55 then becomes

$$\frac{d(C_2H_6)}{dt} = \frac{1}{2}\,\Theta_H\,\Theta_E\,N_w^2\,d\,\upsilon\,r\,\exp\left[-\frac{\Delta H^{\ddagger} + \Delta H_d}{RT}\right] \quad (57)$$

If Beeck's (29) activation energy of 2.4 kcal/mole for the hydrogenation of ethylene on tungsten and Gomer's (59) activation energy of 9.5 kcal/mole for surface diffusion of hydrogen are used, Equation 57 can be simplified assuming the following values:

$N_w = 1\text{x}10^{15}\ cm^{-2}$, $d = 2\text{Å}$, $\upsilon = 1\text{x}10^{13}\ sec^{-1}$, $r = 4\text{Å}$, $T = 300°K$

$$\frac{dN(C_2H_6)}{dt} = \Theta_E\,\Theta_H\,\text{x}10^{19} \quad (58)$$

Then using the ethylene coverage of 0.04 at the point in Figure 30 where self hydrogenation starts and assuming 99% decomposition, the rate by Equation 58 would still be $1\text{x}10^{14}$ molecules/sec/cm^2. Since this corresponds to 0.2 monolayers/sec, the experimental results are easily understandable in terms of a Langmuir-Hinshelwood mechanism.

In spite of such an unusually low activation energy the rate of ethylene hydrogenation on tungsten is unusually low. This low long term rate is, of course, due to the irreversible ethylene decomposition reaction. The rate is low due to low concentration terms in Equation 58. In the fast hydrogenation experiment, the initial hydrogen concentration was one and the initial reaction therefore fast. However as the pressure of ethylene increased, ethylene displaced the hydrogen, and since the decomposition reaction is also rapid, this caused a rapid decrease in both the associative ethylene and hydrogen

coverages. This decomposition is even more a factor in the self hydrogenation reaction, Figure 30. In this case the initial reaction is ethylene decomposition and is the predominant reaction until the hydrogen coverage reaches the point where an incoming ethylene molecule has agreater probability of hydrogenation than of decomposition.

For these initial rapid reactions it is necessary to ask whether the reaction is occurring on other metal parts or on a thin film laid down during the cleaning procedures, and whether the pressure measured by the mass spectrometer is the true cell pressure. Both the rapid hydrogenation and flash decomposition reactions of ethylene require an initially clean surface. On a surface covered with the residue from a previous experiment conducted above 200°K no hydrogenation activity was observed. If the filament is not previously cleaned, adsorption of ethylene occurs, but, as shown in Figure 12, nonreproducible spectra are obtained. If the filament is cleaned and then cooled to 95°K, no hydrogenation is observed. Since the filament is cooled by conduction through the leads, the major portion of the cell is not affected and remains at approximately room temperature. Thus the reactions do occur on the filament.

The question of a pressure differential is essentially a response problem which can be answered by use of Equation 24. For the hydrogenation experiments in a closed system with an initially clean filament, the adsorption pumping of this filament is by far the major pumping term. From Equation 3, the

maximum pumping speed of this filament is

$$S_1 = \frac{1}{V}\frac{AkT}{\sqrt{2\pi mkT}} \tag{59}$$

Evaluating this for the 1L system and a surface area of 1 cm^2 gives a maximum pumping speed of 12 L/sec. Since the mass spectrometer is separated from the cell by 19 cm of 1 inch tubing, the conductance of this tubing, using Equation 21, is 11L/sec. Using these values, Equation 24 becomes

$$P_2 = P_1 - 4Lx10^{-2} \exp(-4.5t) \tag{60}$$

The maximum leak rate can be estimated from the maximum pressure reached at the end of a hydrogenation experiment. From Equation 10 this maximum leak rate is

$$L = \frac{S_o}{V} P_o \tag{61}$$

where $\frac{S_o}{V}$ is the natural pumping of the system isolated from the pumps after the filament is saturated and P_o is the maximum pressure. Using $1x10^{-6}$ torr for the maximum pressure, Equation 60 becomes

$$P_2 = P_1 - 4S_o x10^{-8} \exp(-4.5t) \tag{62}$$

Since the pumping term, S_o, is between 0.01 and 0.1 L/sec, the second term is negligible on a time scale of seconds and pressure equilibration between the cell and mass spectrometer is essentially instantaneous.

Since conductance is no problem, the system (mass spectrometer and cell) can be treated as one volume, V. The change in ethylene pressure (P_1) during the initial portion

of the fast reaction can be written as:

$$V \frac{dP_1}{dt} = L - S_1 P_1 \tag{63}$$

where L is the ethylene leak and S_1 is the pumping by the filament. Equation 63 can be integrated to give

$$P_1 = \frac{L}{VS_1} \left[1 - \exp (-S_1 t) \right] \tag{64}$$

If for an approximation we assume that each ethylene molecule that hits the surface is hydrogenated, the sum of ethylene and ethane pressure must be equal to the total leak into the system

$$(P_1 + P_2)V = Lt \tag{65}$$

From Equations 64 and 65 the ethane pressure is given by

$$P_2 = \frac{L}{VS_1} \left[S_1 t - 1 + \exp (-S_1 t) \right] \tag{66}$$

However, since S_1 has a value of 12 sec^{-1} we can neglect the exponential terms in comparison to one. Equations 64 and 66 then become

$$P_1 = \frac{L}{VS_1} \tag{67}$$

$$P_2 = \frac{L}{VS_1} \left[S_1 t - 1 \right] \tag{68}$$

This is a fair approximation for the very early portions of the hydrogenation reaction. The ethylene pressure (P_1) should hold steady at a low value determined by a balance between the leak into the system and the pumping speed of the filament while the ethane pressure (P_2) increases with

time. When the hydrogen is exhausted the ethane production should cease and the ethylene pressure should then increase with time. In converting the data in Figure 27 to Figure 28 a small ethylene maximum was found between 0 and 50 seconds. However since the percentage was small the scatter in the points was quite large and these points were not included in Figure 28. However this simple model does give the same general features as the experimental data.

That the hydrogenation reaction occurs in the chemisorbed monolayer is supported by the self hydrogenation obtained during a flash, Figure 18. The self hydrogenation starts at ~160°K where hydrogen is mobile on tungsten (59,60) and reaches a maximum rate at 250°K where decomposition of ethylene is appreciable. The self hydrogenation is independent of both the hydrogen and ethylene pressure present during a flash. The lower temperature limit for hydrogenation on tungsten is not due to an activation energy for the hydrogenation step but, an activation energy for mobility of hydrogen. The procedure used by Kemball in low temperature experiments was to cool his films to 153°K before admitting a gas mixture (32). After waiting a few minutes for the gas mixtures to flow into the mass spectrometer, the film was warmed to 173°K and readings taken. Although it is not stated, this must imply, in agreement with flash filament results, that no reaction occurs below ~160°K and that raising the temperature to only 173°K gave appreciable hydrogenation.

The rapid self poisoning of tungsten at 300°K results from the first decomposition step of ethylene, reaction 40. From the flash filament data and from adsorption experiments (31) this reaction is known to be complete at 300°K. Flashing the filament after either hydrogenation or self hydrogenation results in just the β_2 or acetylenic peak.

At 195°K where the decomposition of ethylene, reaction 40, is slow and the mobility of hydrogen is still large, the hydrogenation reaction on tungsten does not poison. Hydrogenation runs similar to Figure 27 have been conducted for several hours with a given leak setting by simply opening the valve to the pumps every few minutes to sweep out the products. A shift in the relative activity of tungsten at low temperatures had been reported previously (32). The deuteration rates obtained by Kemball (32) at -100°C and the hydrogenation rates at 0°C reported by Beeck (29) are reproduced in Table 1. The rates are tabulated as the log of the rate relative to Rh. By cooling to the point where we now know ethylene to be stable on tungsten, the spread in the relative rates has decreased drastically with the tungsten rate increasing by two orders of magnitude relative to rhodium. Thus there is a 30° to 40° temperature range where tungsten is a relatively effective catalyst for the hydrogenation of ethylene. This range, however, is between ~160°K and 200°K.

The surface reactions of acetylene and ethylene can be summarized in the following sequence of reactions.

$$C_2H_{4(g)} \rightarrow \overset{*}{C}H_2\text{-}\overset{*}{C}H_2 \tag{69}$$

$$\overset{*}{C}H_2\text{-}\overset{*}{C}H_2 \rightarrow \overset{*}{C}H\text{=}\overset{*}{C}H + 2\overset{*}{H} \tag{70}$$

$$\overset{*}{C}H\text{=}\overset{*}{C}H \rightarrow (\overset{**}{C_2}) + 2\overset{*}{H} \tag{71}$$

$$\overset{*}{C}H_2\text{-}\overset{*}{C}H_2 + 2\overset{*}{H} \rightarrow C_2H_{6(g)} \tag{72}$$

$$H_{2(g)} \rightleftarrows 2\overset{*}{H} \tag{73}$$

A reverse step has been included in Equation 70. The decomposition of ethylene on tungsten is essentially irreversible (29), however the reverse step has been added for those metals that do hydrogenate acetylene (2). The relative importance of these steps, of course, depends on the temperature. Below 200°K, in the case of tungsten, only 69, 72, and 73 need be considered. At 300°K one must consider the whole sequence. However the forward step in 70 would be the predominant reaction.

Reaction 72 probably occurs as a two step reaction similar to the half hydrogenated mechanism of Horiuti and Polanyi (78).

$$\overset{*}{C}H_2\text{-}\overset{*}{C}H_2 + \overset{*}{H} \underset{k_2}{\overset{k_1}{\rightleftharpoons}} \overset{*}{C}H_2\text{-}CH_3 + \overset{*}{H} \tag{74}$$

$$\overset{*}{C}H_2\text{-}CH_3 + \overset{*}{H} \xrightarrow{k_3} C_2H_{6(g)} \tag{75}$$

In the steady state where the surface is predominantly covered with hydrocarbon and the surface concentration of hydrogen is low (31,37), the addition of hydrogen would probably not occur by a concerted attack. Reactions 70 and 71 serve to maintain an effective concentration of associative ethylene on the

surface. Since these reactions soon reach a steady state at a given temperature, the kinetic order should be determined by reactions 74 and 75. With the assumption that the ethyl radical reaches a steady state, the rate of production of ethane should be

$$\frac{d(C_2H_6)}{dt} = \frac{k_1 k_3 \Theta_{(C_2H_4)} \Theta_H^2}{k_2 + k_3 \Theta_H^2} \qquad (76)$$

For tungsten at room temperature, the long term rate of ethylene hydrogenation is severely limited by the initial fast ethylene decomposition. On the major portion of a tungsten surface the rate is zero since the ethylene concentration is zero. For those metals where the reverse of reaction 70 is important, the ethylene concentration will be a constant in the steady state. Since the heats of adsorption of ethylene are uniformly greater than the heats of adsorption of hydrogen, preferential displacement of hydrogen should occur. Then with the assumption that $k_2 > k_3\Theta_H$ Equation 76 becomes:

$$\frac{d(C_2H_6)}{dt} = \frac{k_1 k_3}{k_2} K_H \Theta_{C_2H_4} P_{H_2} = K P_{H_2} \qquad (77)$$

The kinetics are reported to be first order in hydrogen and zero order in ethylene (2).

Measurements of the activation energy, however, reflect changes occurring in the whole sequence of reactions. It is found that a plot of log (rate) *vs.* $\frac{1}{T}$ has a maximum, Tm, where the apparent activation energy goes to zero (2). This

must be due to a shift to the right in either reaction 70 or 71, or to the desorption of hydrogen (37). This shift would be the shift in surface equilibrium postulated by Kemball to explain a drop in the rate of exchange of deuterium and ethane when the temperature of his nickel film was heated from 0°C to 80°C for 5 minutes and then cooled back to 0°C (75). The surface ethylene species were converted to acetylene which had to be slowly converted to surface ethylene before the reaction could resume the normal rate. Although infrared spectroscopy has not been completely successful in determining the surface species, the infrared evidence does support a shift in the surface species which depends on the temperature (39,40,41). The effect of the surface decomposition is also seen in the effect of the order of admitting reactants to a nickel surface. The hydrogenation rate decreases in the following order (29,37).

H_2 first > mixture > ethylene first

When ethylene is admitted first the decomposition reaction occurs giving predominantly acetylene on the surface. This must then be converted to surface ethylene before the rate can recover. The rate over nickel decreases with time, and after several additions of an ethylene-hydrogen mixture, finally reaches the rate obtained after predosing the surface with ethylene (38). For this final rate we then have two possibilities for the rate limiting step. If hydrogen has been preferentially displaced to a large extent, the rate

will be limited by the low hydrogen concentration. On a bare nickel surface ethylene is known to decompose (37,39), but on a hydrogen covered nickel surface Eischens and Pliskin claim that ethylene is mainly in the associative form. This is probably true for the initial adsorption where the rate is high. However, in the long term case, where the rate is equal to the rate obtained after predosing with ethylene, the surface is surely covered with the dissociative form and the rate limiting factor here is the hydrogenation of the acetylenic species.

Beeck in 1945 published a correlation between catalytic activity and lattice distance (79) which can be understood in light of the discussion in the section on ethylene and acetylene decomposition. The metals which show the highest activity are the fcc metals. The bcc metals have uniformly low rates. As already pointed out the fcc, because of their shorter spacings, should favor the associative form of ethylene while on the bcc metals the greater percentage of long spacings should lead to easy decomposition. Since the rate (Equation 77) is proportional to the surface concentration of ethylene, the fcc metals should have a greater rate due to a greater effective ethylene concentration.

Decomposition does occur on both the fcc and bcc metals to give an acetylenic species, not all of which can be removed (29,45). The acetylene bond angles would, however, be highly strained on both the short fcc spacings (2.69 Å,

γ = 109.6°) and the long bcc spacings (4.47 Å, γ = 139°). The corresponding angle strain in small ring compounds suggests that the strain energy would be less than 6 kcal (80) while the heats of adsorption of the hydrocarbons are > 50 kcal (29). However the direction of the strain is informative. On the long bcc spacings the acetylene bond angle is opened by 19°. This should decrease the carbon surface distance and increase the carbon-surface interaction. Thus on the bcc metals one should have a greater probability of rupture of the carbon-carbon bond leading to irreversible poisoning. On the face centered metals, however, the angle would be closed by 10°. This would force the carbon away from the surface and decrease the carbon surface interaction, thus favoring a stable acetylene. Although the rates of acetylene hydrogenation are lower than the corresponding rates of ethylene hydrogenation, the fcc metals are active while the bcc metals are inactive (29).

The low temperature (-100°C) deuteration experiments of Kemball (32) can be understood in terms of the spacings. At -100°C we know ethylene to be stable on W and, we can assume that the same holds for the more active metals Rh, Ni and Fe which were also studied by Kemball. Tungsten gave d_2-ethane as the principle product ($\simeq$ 70%) while Rh, Ni and Fe gave much more extensive deuteration as well as extensive olefin exchanges. At this temperature the deuteration of ethylene must be occurring through reactions 74 and 75 with the reverse

step in 74 giving the multiple exchange. This reverse step must occur through a transition state of the form

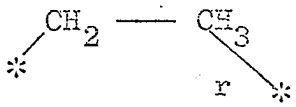

If the distance r is short the reverse reaction will be favored and lead to more extensive exchange. The 4.47Å spacings on tungsten are near the maximum spacings of 4.64Å which could be used for ethylene adsorption. In this case the reverse step should be slow and the reaction over tungsten should give predominantly d_2-ethane.

The deuterium results are clear in this case since the surface species are known. However the interpretation of both kinetic and deuterium exchange experiments at higher temperatures are not as obvious due to the nearly complete lack of knowledge of the surface species. The intermediate reactions 70 and 71 do occur and deuterium experiments might well reflect these reactions as well as 74 and 75. For a discussion of hydrogenation one cannot take the approach that "In order to present a coherent discussion on mechanism ... it will be assumed that it is the associative form of chemisorbed olefin which exists on the surface when both reactants are substantially present in the gas phase ..." (2).

VI. SUMMARY

The surface reactions of methane, ethane, acetylene and ethylene have been studied on tungsten by means of flash filament spectroscopy and rapid scan mass spectroscopy, and the surface reactions of ethylene and acetylene on iridium have been studied by means of flash filament spectroscopy. Ultra-high vacuum techniques were used to prepare clean, reproducible surfaces for these studies.

Flash decomposition of a hydrocarbon monolayer formed at 95°K yields a hydrogen partial pressure spectrum characteristic of the hydrocarbon and a carbon residue on the surface. The decomposition of ethylene on both tungsten and iridium is a two step dehydrogenation reaction yielding two hydrogen peaks in the gas phase. In the case of tungsten adsorption of ethylene is associative below 200°K. On heating decomposition of the associative ethylene starts at 200°K resulting in the first hydrogen peak in the gas phase and an acetylenic residue on the surface. Continued heating decomposes this acetylenic residue giving the second hydrogen peak at 450°K and a carbon residue on the surface. The acetylenic residue from the decomposition of ethylene is identical in both surface stability and amount of hydrogen with the species resulting from the adsorption of acetylene. The first decomposition on tungsten is essentially irreversible and

results in the poisoning of tungsten for hydrogenation. Under the most favorable conditions no hydrogenation of acetylene on tungsten is observed.

Below 200°K where ethylene is stable on tungsten the surface does not poison. However, on tungsten one is limited to an approximately 40°K temperature range for the hydrogenation of ethylene. The lower limit is set by the temperature at which hydrogen is mobile (~160°K) and the upper limit is set by the decomposition of ethylene. Extremely rapid hydrogenation and self hydrogenation reactions have been observed during the formation of the first hydrocarbon monolayer at 300°K. Rapid initial reactions such as this have been observed before and have been used as experimental evidence for the Rideal-Eley type mechanisms. However on the basis of the coverage at the point where self hydrogenation starts the fast initial reaction on tungsten is shown not to occur by a Rideal-Eley mechanism but must occur as a result of a collision between a highly mobile hydrogen adatom and an immobile adsorbed ethylene molecule.

From a knowledge of the surface species and reactions, the surface reactions of acetylene and ethylene can be summarized in the following sequence of reactions:

$$C_2H_{4(g)} \rightarrow \overset{*}{C}H_2\text{-}\overset{*}{C}H_2 \qquad (78)$$

$$C_2H_{2(g)} \rightarrow \overset{*}{C}H{=}\overset{*}{C}H \qquad (79)$$

$$\overset{*}{C}H_2\text{-}\overset{*}{C}H_2 \rightarrow \overset{*}{C}H{=}\overset{*}{C}H + 2\,\overset{*}{H} \qquad (80)$$

$$\overset{*}{C}H=\overset{*}{C}H \rightarrow \overset{**}{(C_2)} + 2\overset{*}{H} \quad (81)$$

$$\overset{*}{C}H_2-\overset{*}{C}H_2 + 2\overset{*}{H} \rightarrow C_2H_{6(g)} \quad (82)$$

$$H_2 \rightleftarrows 2\overset{*}{H} \quad (83)$$

The reverse step in reaction 80 does not occur to any appreciable extent on tungsten but has been included for those metals that hydrogenate acetylene. Since hydrogen is displaced by the hydrocarbons, the concentration of hydrogen in the steady state is low. Thus the probability of a concerted attack in the hydrogenation steps must be low and these reactions undoubtedly occur as two step reactions. The importance of the decomposition reactions is dependent on the temperature. Below 200°K in the case of tungsten one must only consider reactions 78, 79, 82 and 83. At 300°K the ethylene decomposition reaction is rapid and irreversible and is the determining factor in the hydrogenation of ethylene on tungsten.

The decomposition reactions are discussed in terms of the available metal-metal spacings, and the effect of these spacings on the configuration and stability of the adsorbed hydrocarbon molecule. Long metal-metal spacings prevalent on the bcc metals favor irreversible decomposition of ethylene by reactions 80 and 81. Short metal-metal spacings prevalent on the fcc metals favor the stability of ethylene. This is in agreement with the flash filament spectra which indicate that ethylene is stable to 400°K on iridium (fcc) vs. 200°K

on tungsten (bcc), and with the known greater activity of the fcc metals.

Chemisorption of methane and ethane on tungsten at 95°K yields hydrogen and methyl groups in the case of methane, and hydrogen, adsorbed ethylene and ethyl groups in the case of ethane. The main peak in the flash filament spectra of both methane and ethane occurs at 570°K and has been assigned to the decomposition of the methyl and ethyl groups. In the decomposition of both species the rate limiting step is assigned to the removal of the first hydrogen on the carbon bonded to the surface. In the case of ethane the decomposition goes through a transition state where the carbon-carbon bond is being broken and a new carbon-metal bond is being formed.

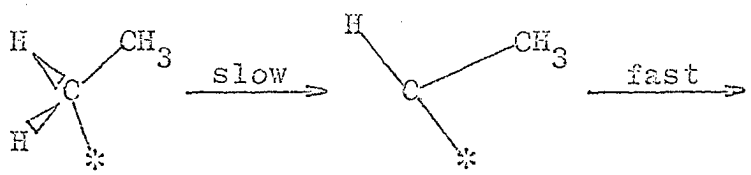

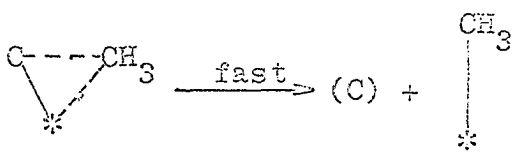

(84)

In hydrocracking experiments where a large excess of hydrogen is present the transition state in 82 would be very liable to attack by hydrogen forming gaseous methane.

VII. SUGGESTIONS FOR FUTURE RESEARCH

Since the great bulk of work in catalysis has been conducted on the more active group VIII metals, the extension of this work to these metals would be desirable. However these metals, with the exception of iridium, have uniformly low melting points and should pose special problems in cleaning. For this reason field emission should be used prior to flash filament spectroscopy. The hexagonal close packed metals ruthenium and rhenium would be interesting and should not present special problems in cleaning.

A geometrical factor in catalysis has been discussed for many years, but has never been experimentally verified. The use of low energy electron diffraction has been so extensive in recent years, that orientated single crystal ribbons are now commercially available. Through a combination of ultra-high vacuum techniques with more conventional catalytic techniques it should now be possible to test for a geometrical factor.

VIII. BIBLIOGRAPHY

1. Rylander, Paul N. Catalytic Hydrogenation over Platinum Metals. New York, N.Y., Academic Press, Inc. 1967.

2. Bond, G. C. Catalysis by Metals. New York, N.Y., Academic Press, Inc. 1962.

3. Rideal, E. C. Advances in Catalysis 9:8. 1957.

4. Redhead, P. A., E. V. Kornelsen and J. P. Hobson. Canadian Journal of Physics 40:1814. 1962.

5. Ehrlich, G. Advances in Catalysis 14:255. 1963.

6. Dushman, Saul. Scientific Foundations of Vacuum Technique. 2nd ed. New York, N.Y., John Wiley and Sons, Inc. 1962.

7. Apker, L. R. Industrial and Engineering Chemistry 40:846. 1948.

8. Nottingham, W. B. and F. L. Torney. Transactions of the National Symposium on Vacuum Technology 7:117. 1960.

9. Schuetze, H. J. and F. Stork. Transactions of the National Sympsoium on Vacuum Technology 9:431. 1962.

10. Bayard, R. T. and D. Alpert. Review of Scientific Instruments 21:571. 1950.

11. Becker, J. A. and C. D. Hartman. Journal of Physical Chemistry 57:153. 1953.

12. Ehrlich, G. Journal of Chemical Physics 34:29. 1961.

13. Redhead, P. A. Transactions of the Faraday Society 57:641. 1961.

14. Eisinger, J. Journal of Chemical Physics 29:1154. 1958.

15. Ehrlich, G. Journal of Chemical Physics 23:1543. 1955.

16. Ehrlich, G. Journal of Physical Chemistry 60:1388. 1956.

17. Hickmott, T. W. and G. Ehrlich. Journal of Physics and Chemistry of Solids 5:47. 1958.

18. Mimeault, V. J. Flash Desorption and Isotopic Mixing of Simple Diatomic Gases on Tungsten, Iridium and Rhodium. Unpublished Ph.D. thesis. Ames, Iowa, Library, Iowa State University of Science and Technology. 1966.

19. Mimeault, V. J. and R. S. Hansen. Journal of Chemical Physics 45:2240. 1966.

20. Redhead, P. A. Vacuum 12:203. 1962.

21. Delchar, T. A. and G. Ehrlich. Journal of Chemical Physics 42:2686. 1965.

22. Rigby, L. J. Canadian Journal of Physics 42:532. 1965.

23. Madey, T. E. and J. T. Yates, Jr. Journal of Chemical Physics 44:1675. 1966.

24. Hickmott, T. W. Journal of Chemical Physics 32:810. 1960.

25. Rigby, L. J. Canadian Journal of Physics 43:1020. 1965.

26. Taylor, T. L. Catalysis 5:257. 1957.

27. Bond, G. C. and P. B. Wells. Advances in Catalysis 15:91. 1965.

28. Brennan, D. Recent Progress in Surface Science 2:57. 1964.

29. Beeck, O. Discussions of the Faraday Society 8:118. 1950.

30. Roberts, R. W. Journal of Physical Chemistry 68: 2718. 1964.

31. Trapnell, B. M. W. Transactions of the Faraday Society 48:160. 1952.

32. Kemball, C. Journal of the Chemical Society 735. 1956.

33. Bond, G. C., J. J. Philipson, P. B. Wells and J. M. Winterbottom. Transactions of the Faraday Society 60: 1847. 1964.

34. Bond, G. C., G. Webb and P. B. Wells. Transactions of the Faraday Society 66:999. 1965.

35. Bond, G. C., J. J. Philipson, P. B. Wells and J. M. Winterbottom. Transactions of the Faraday Society 62:443. 1966.

36. Sato, S. and K. Miyahara. Journal of the Research Institute of Catalysis 13:10. 1965.

37. Jenkins, G. I. and E. Rideal. Journal of the Chemical Society 2490. 1955.

38. Jenkins, G. I. and E. Rideal. Journal of the Chemical Society 2496. 1955.

39. Eischens, R. P. and W. A. Pliskin.. Advances in Catalysis 10:1. 1958.

40. Little, L. H., N. Sheppard and D. J. C. Yates. Proceedings of the Royal Society A259:242. 1960.

41. Little, L. H. Infrared Spectra of Adsorbed Species. New York, N.Y., Academic Press, Inc. 1966.

42. Arthur, J. R, Jr. and R. S. Hansen. Journal of Chemical Physics 362062. 1962.

43. Hansen, R. S., J. R. Arthur, Jr., V. J. Mimeault and R. R. Rye. Journal of Physical Chemistry 70°2787. 1966.

44. Gardner, N. C. A Study of the Surface Reactions of Hydrocarbons on Tungsten by Field Electron Emission Microscopy. Unpublished Ph.D. thesis. Ames, Iowa, Library, Iowa State University of Science and Technology. 1966.

45. Cormack, D., S. J. Thomson and G. Webb, Jr. Journal of Catalysis 5:224. 1966.

46. Cunningham, R. E. and A. T. Gwathmey. Advances in Catalysis 10:25. 1957.

47. Hill, B. J., S. M. A. Lecchini and B. A. Pethica. Transactions of the Faraday Society 62:229. 1966.

48. Schulz, G. J. Journal of Applied Physics 28:1149. 1957.

49. Redhead, P. A. Review of Scientific Instruments 31: 343. 1960.

50. Davis, W. D. and T. A. Vanderslice. Transactions of the National Symposium on Vacuum Technology 7:417. 1960.

51. Todd, B. J. Journal of Applied Physics 26:1238. 1955.

52. Santeler, D. J., D. J. Holkeboer, D. W. Jones and F. Pagano. Vacuum Technology and Space Simulation Washington, D.C., National Aeronautics and Space Administration. 1967.

53. Meaden, G. T. Electrical Resistance of Metals. New York, N.Y., Plenum Press. 1965.

54. Ehrlich, G. Journal of Applied Physics 32:4. 1961.

55. Hickmott, T. W. Journal of Vacuum Science and Technology 2:257. 1965.

56. Yates, J. T. and T. E. Madey. Journal of Chemical Physics 45:1623. 1966.

57. American Petroleum Institute. Mass Spectral Data: Research Project 44. Washington, D.C., National Bureau of Standards. 1949-1959.

58. Rootsaert, W. J. M., L. L. van Reijen and W. M. H. Sachtler. Journal of Catalysis 1:416. 1962.

59. Gomer, R., R. Wortman and R. Lundy. Journal of Chemical Physics 26:1147. 1957.

60. Sachtler, W. M. H. and L. L. van Reijen. Journal of the Research Institute of Catalysis 10:87. 1962.

61. Becker, J. A. Actes du Deuxieme Congress International de Catalyse 2:1777. 1960.

62. Toya, T. Theory of Adsorption of Hydrogen Atoms on Metal Surfaces. Journal of the Research Institute of Catalysis 8:209. 1960. Original not available; abstracted in Chemical Abstracts 55:16075. 1961.

63. Moore, G. E. and F. C. Unterwald. Journal of Chemical Physics 40:2639. 1964.

64. Hayward, D. O. and B. M. W. Trapnell. Chemisorption. 2nd ed. Washington, D.C., Butterworths, Inc. 1964.

65. Stern, R. M. Applied Physics Letters 5:218. 1964.

66. Schlier, R. E. Journal of Applied Physics 29:1162. 1958.

67. Selwood, P. W. Journal of the American Chemical Society 83:2853. 1961.

68. Garnett, J. L. and W. A. Sollich-Baumgartner. Advances in Catalysis 16:95. 1964.

69. Bond, G. C. Discussions of the Faraday Society 41:200. 1966.

70. Halpern, J. Annual Reviews of Physical Chemistry 16: 103. 1965.

71. Condon, James Benton. Field Emission and Flash Filament Studies of Hydrogenation and Decomposition of Cyclohexane and Benzene on a Tungsten Surface. Unpublished Ph.D. thesis. Ames, Iowa, Library, Iowa State University of Science and Technology. 1968.

72. Harris, G. W. Sticking Probability of Hydrocarbons on Tungsten. Dissertation Abstracts 26:3187. 1965.

73. Pauling, L. The Nature of the Chemical Bond. 3rd ed. Ithaca, N.Y., Cornell University Press. 1960.

74. Kemball, C. Proceedings of the Royal Society A217: 376. 1953.

75. Anderson, J. R. and C. Kemball. Proceedings of the Royal Society A223:361. 1954.

76. Anderson, J. R. and B. G. Baker. Proceedings of the Royal Society A271:402. 1963.

77. Bensen, S. W. Journal of Chemical Education 42:502. 1965.

78. Horiuti, J. and M. Polanyi. Transactions of the Faraday Society 30:1164. 1934.

79. Beeck, O. Reviews of Modern Physics 17:61. 1945.

80. Eliel, E. Sterochemistry of Carbon Compounds. New York, N.Y., McGraw-Hill Book Co. 1962.

IX. ACKNOWLEDGMENTS

The author wishes to express his sincere appreciation to Dr. Robert S. Hansen for his encouragement, suggestions and direction during the course of this research. His unique insight will not be forgotten.

To his wife, Rosemary, and children, the author gives special thanks for their love, encouragement and enjoyment.

The stimulating discussion with various members of the group, especially James Gambell, has been both enjoyable and fruitful.